December 2015

Structure, Dynamics and Rheology of Polymer Solutions from Coarse-Grained Molecular Dynamics: Effects of Polymer Concentration, Solvent Quality and Geometric Confinement

Yutian Yang
Syracuse University

Abstract

Understanding flow-microstructure interactions in macromolecular fluids is of great importance in the design and optimization of ubiquitous polymer processing operations. Further, such interactions are routinely encountered in separation of biopolymer mixtures using gel electrophoresis and microfluidic technologies, manufacturing of polymer-based functional nanocomposites and polymer-induced reduction in turbulent friction drag. To date, the vast amount of theoretical/computational modeling efforts on flow-microstructure coupling has focused on continuum-level and stochastic descriptions. Such approaches, while useful in qualitatively predicting polymer dynamics and rheology in model systems, are incapable of describing the effects of polymer-solvent, polymer-polymer and polymer-wall interactions. Further, in the context of polymer solutions, the incorporation of hydrodynamic interaction are often computationally challenging. Hence, the goal of this work has been to investigate the structure, dynamics and rheology of solutions of flexible linear polymers using molecular dynamics (MD) simulations in presence of explicit solvent mediated interactions.

Coarse-grained (CG) molecular models and corresponding force fields are employed to describe the polymer, solvent and the underlying physico-chemical interactions. The CG models are validated against atomistic ones by comparing the predictions of certain structure parameters such as persistence length, radius of gyration and radial distribution functions of the monomeric units. Results are first presented for the dynamics of a single polymer chain in shear flow. The effects of chain length and shear rate on the configuration statistics, e.g. tumbling frequency and orientation distribution of the end-to-

end vector, are presented and compared to experimental observations as well as predictions of mesoscopic stochastic dynamic theories. Further, the effects of solvent-polymer interactions on the configuration dynamics of a single polymer chain under good, theta and poor solvent conditions are discussed. Specifically, the role of solvent quality is shown to have a pronounced effect on coil-stretch transition in shear flow. We also show that in addition to tumbling dynamics, polymer chain may undergo configurational changes through a novel mechanism, namely collapse dynamics. CGMD predictions for the relationship between the zero-shear viscosity and polymer concentration in dilute and semi-dilute regimes are presented and compared to experiment results. Shear thinning behavior is observed in both dilute and semidilute solutions in non-equilibrium molecular dynamics simulations. Possible approaches to parameterizing phenomenological constitutive models using MD simulation data is explored. Subsequently, influence of solvent quality on the rheological properties of dilute and semidilute solutions is discussed. Finally, the effect of geometric confinement on equilibrium configurations as well as shear-induced migration of the polymer chains is described.

STRUCTURE, DYNAMICS AND RHEOLOGY OF POLYMER SOLUTIONS FROM COARSE–GRAINED MOLECULAR DYNAMICS:

EFFECTS OF POLYMER CONCENTRATION, SOLVENT QUALITY AND GEOMETRIC CONFINEMENT

By

Yutian Yang

B.S. Shanghai Jiao Tong University, 2010

DISSERTATION

Submitted in partial fulfillment of the requirements for the degree of

Doctor of Philosophy in Chemical Engineering

Syracuse University

December 2015

ACKNOWLEDGEMENTS

First and foremost, I would like to thank my dissertation advisor, Professor Radhakrishna Sureshkumar, for his great insight, inspiration, guidance and support over the past four years to my dissertation research. I would like to thank my committee members: Professor Shalabh Maroo, Professor Jesse Bond, Professor Ian Hosein, Professor Shikha Nangia and Professor Dacheng Ren for their constructive suggestions and valuable comments to my dissertation.

This dissertation would not have been completed without the support of my family and friends. I would like to take this opportunity to acknowledge my parents who have always supported and believed in every of my decision. I would like to thank Professor Jacques Lewalle for mentoring me and supporting me. I would like to thank Yazhen Xiang, Xiaochuan Zhou, Chongzhe Li, Mike Chen and all other friends who have helped and supported me whenever I need them.

I would like to thank my fellow classmates and group colleagues: Dr. Subas Dhakal, Abhinanden Sambasivam, Bendy Estime, Matthew Ali, Dr. Ashish Sangwai, Dr. Satvik Wani, Kelechi Okwuchi Okoroafor, Theresa Hendrick, Yating Liu, Peter Paynter, Dr. Jennifer Amey, Stephen DeSalvo and Mardochee Reveil for their support and company.

I appreciate the superb support from Dawn Long, Sabina Redington, Kristin Lingo, Barbara Walton and Lynore de la Rosa.

I would like to acknowledge financial support for this work from the National Science Foundation and Syracuse University. I would like to thank the travel grants from the Society of Rheology, Graduate School and Nunan Graduate Travel Fund.

Table of Contents

LIST OF FIGURES

List of Tables

Chapter 1

Introduction

In the last few decades, polymers have emerged as an effective, flexible solution for numerous applications in the multi-billion dollar materials and chemical processing industries. Key to exploiting their many useful properties is to understand the processes by which they are shaped. However, designing these processes is quite challenging since the configuration dynamics[1-4] of polymer molecules is complicated due to hydrodynamic, entropic and stochastic forces experienced by the polymer chains. Such configuration changes can have profound impact on the macroscopic rheological properties of polymeric fluids. Among other phenomena, polymeric fluids exhibit non-Newtonian rheological properties such as shear thinning, shear thickening or yield stress. Further, they tend to be viscoelastic, i.e., their behavior is intermediate to that of a viscous fluids and an elastic solid. Non-Newtonian rheology could lead to instabilities in polymer processing operations such as melt fracture and sharkskin in extrusion processes[5]. For example, the elastic energy stored by the polymer during the flow can be eliminated by the relaxation and creation of new surface at the die exit, if the material is not strong enough, extruding skin fracture such as sharkskin can be discovered[6].

Recently, the advances in distributed computing and development of efficient algorithms have allowed for the use of multiscale models to predict flow behaviors of polymeric fluids. Continuum-level formulations consist of conservation laws mass, momentum and energy coupled with constitutive laws for the spatio–temporal evolution of the polymeric stress tensor, expressed in the form of partial differential or integral equation[7-9]. They can qualitatively

describe rheological properties and viscoelastic flow phenomena in simple geometries. Continuum-level models can be developed based on different approaches. Network theory and phenomenology are used in Giesekus[10], Phan-Thien and Tanner[11-13], and White-Metzner[14] models used to model shear thinning fluids that exhibit normal stresses. For instance, Li *et al.*[9] have predicted shear thinning behavior for moderately concentrated polymer solution and fitted the experimentally measured shear and normal stress data to the predictions of above-mentioned constitutive models in both forward and rear stagnation flows.

Polymer kinetic theory and ad hoc closure approximations can also be used to develop constitutive equations. Purnode and Crochet[15] have characterized the rheological properties of aqueous polyacrylamide solutions in shear and extensional flows using the Finitely Extendible Nonlinear Elastic-Peterlin (FENE-P) constitutive model. Sureshkumar and Beris[16] have performed direct numerical simulation (DNS) of a fully turbulent channel flow of dilute polymer solutions. They represented polymer chains by using the FENE-P model and showed that polymer stresses induce several changes in the turbulent flow characteristics, including reduction in friction drag, which are consistent with experimental results.

However, while continuum-level constitutive models focus on the mathematical representation of the macroscopic viscoelastic stress, they do not attempt to capture the details of the polymer configuration dynamics. Recently, the growth of bio- and nano- technologies has presented novel problems that necessitate the modeling of the effect of flow on the configurational dynamics at the single molecule level. For example, Smith *et al.*[1] have observed the conformational dynamics of individual, flexible DNA chains in steady shear flow using video fluorescence microscopy. Stochastic simulation algorithms have allowed for the predictions of such configurational details and identify the drawbacks of the existing continuum-level models.

Brownian Dynamics Simulations (BDS) are stochastic simulations that use detailed micromechanical models such as bead-rod (e.g., Kramers)[17] or bead-spring (e.g., Rouse-Zimm)[18] representations of polymer chains. The central ideas behind this mesoscopic modeling are shown in Figure 1.1. The most detailed models are the bead-rod model developed by Kramers. One bead represents a collection of atoms, typically 10-20 monomer units whose exerts "concerted motion", i.e., the velocity correlations are sufficiently strong such that the motion of these atoms may be considered to be concerted. The rod length is referred to as the Kuhn length, which is twice the persistence length, which is a length scale over which orientational correlations are lost along the contour of the chain. The rigid rod connecting any two beads of a Kramers chain is hence free to move in any angular direction. At equilibrium the motion of a given bead is influenced by the connecting force with the adjacent beads, Brownian motion and hydrodynamic drag of the solvent molecules. Given number of bead-rod units, the chain has fixed contour length. Doyle and Shaqfeh[19, 20] have applied Kramers bead-rod model and studied the rheology and optical properties during the startup of uniaxial extensional and shear flow using BDS. The bead-spring models, in which the spring has an entropic origin, is a less detailed model, i.e., a bead-spring unit can sample the phase space accessible to several bead-rod units. Bead motion is influenced by hydrodynamic drag and Brownian motions as in the bead-rod models as well as the restoring effect of the spring force. If the springs are represented by a linear Hookean spring, the chain is referred to a Rouse-Zimm chain[21]. However, the linear spring has limited applications in flows that produce large deformation. Several nonlinear models have been proposed such as the FENE spring and the wormlike spring. For example, Fetsko and Cummings[22] have studied the steady state and transient rheological behavior of bead-spring chains with a FENE spring in elongational flow. Larson *et al.*[23] have used a bead-spring model

with the wormlike spring law and predicted the tumbling dynamics of a single DNA chain in extensional flow. They have shown good agreement with experimental results[4] both in the percentages of various unraveling states, and in the ensemble-averaged chain stretch and rate of stretch. Large biopolymers that resist local bond torsion (e.g., duplex DNA) can also be modeled using a wormlike model[24]. The elastic dumbbell is the simplest mechanical model of a polymer chain. Nevertheless, it captures the stretchability and orientability of the chains when subjected to flow. However, the lack of internal degrees of freedom makes it incapable of predicting configurational dynamics at the single molecule level. However, these models offer computational tractability, and it is still widely used as far as obtaining rheological predictions is concerned. For example, Cifre *et al*.[25] have applied the dumbbell model and modeled reversible polymer networks. They have shown that under simple shear, the model is able to predict main characteristics of a reversible network of telechelic chains, e.g., Newtonian plateau, shear thickening and shear thinning.

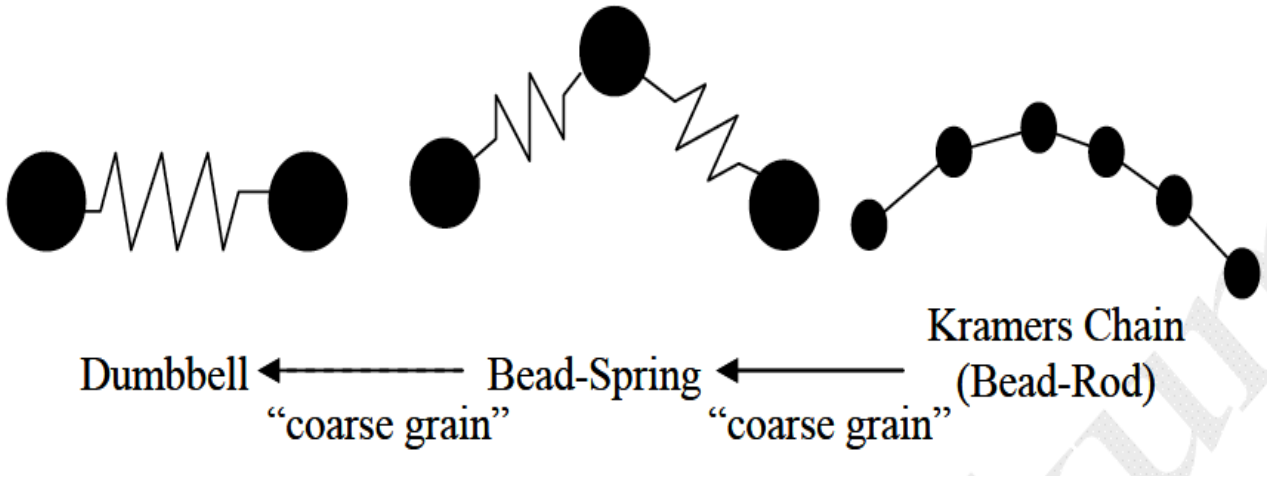

Figure 1.1: Typical mesoscopic polymer models in the stochastic dynamics

Micro-macro models where BDS are self-consistently integrated into continuum-level conservation laws for mass and momentum typically solved using a finite element method have also been developed. For example, Öttinger *et al.*[26] developed the CONNFFESSIT model (i.e., Calculation Of Non-Newtonian Flow: Finite Elements & Stochastic Simulation Techniques) that incorporated coarse-grained molecules into a flow domain of interest. Koppol *et al.* [27] investigated the relationship between friction drag and flow rate of dilute polymeric solutions using a multi-segment bead-spring polymer model and the 4:1:4 axisymmetric contraction and expansion flow geometry. These models take the advantage of using BDS to study the configuration dynamics of polymer chains while drastically suppressing the level of fluctuations in the simulations.

Dissipative particle dynamics (DPD) simulations[28-30] is another kind of mesoscopic simulation method in which a liquid is modeled by coarse-grained particles that carry momentum. Similar to BDS, DPD is governed by stochastic equations of motion. Individual particles are used to represent a large number of atoms or molecules. Polymer chain can also be represented by bead-spring chains as described above. However, unlike most simulations, where solvent exists only through assumed potential of a mean force, DPD represents the solvent as coarse-grained packets. This allows for explicit solvent-polymer interactions that can be applied to study the solvent quality influence on polymer dynamics. For example, Kong *et al.*[31] have modeled solvent quality effects on the equilibrium properties of linear polymer chains using DPD.

While the abovementioned approaches are promising, they do not have the ability to faithfully represent chemical, electrostatic or hydrophilic/hydrophobic interactions that are present in many systems of practical interest. Hydrodynamic interactions (HI), which is a long-

range force acting on solvent and other particles that arises from motion of a particle[32], is often neglected due to computational complexity, which may lead to uncertainty in the prediction of rheological properties[33]. For a dilute polymer solution, HI is very important in predicting the spectrum of polymer sizes and relaxation times of flexible polymer chains. For example, the prediction of polymer's longest relaxation time is shown to scale with number of monomers N as $N^{3\upsilon}$ in presence of HI (Zimm model) and $N^{1+2\upsilon}$ without HI (Rouse model), where υ is the exponent in the power law scaling relationship between N and equilibrium radius of gyration of the polymer chain. Many approaches have been developed to incorporate HI into BD simulations[33-35]. These algorithms utilize HI interaction tensors, such as the Rotne-Prager-Yamakawa tensor[36-38] to represent the hydrodynamic coupling of bead motions. However, the resulting stochastic differential equations are significantly more complicated as compared to those without HI. This leads to excessive computational cost.

Solvent quality affects the polymer configurations, dynamics and hence rheology of polymer liquids. While DPD can explicitly model inter-particle interactions, it is not a straightforward task to calibrate DPD parameters, i.e., to decipher the correlation between the parameters in the DPD model and molecular properties. Polymer dynamics under confined geometries, which is defined as the motion of a polymer chain constrained in spaces comparable to their radius of gyration, is important in fields ranging from enhanced oil recovery to transport of biopolymers through nanopores. However, most of such studies are based on theoretical predictions[39-42] and experimental observations[43-45]. While some simulation approaches[34, 46-48] have been developed to study such phenomena, these simulations do not discuss how conformations of polymer chains change under shear due to confinement.

All-atom (AA) simulations, on the other hand, give detailed atomistic descriptions of the

chemical structure of the monomer. For instance, they have been widely used in the study of protein structure[49-51]. However, such detailed representations are infeasible and unnecessary as far as configurational and rheological predictions for macromolecular fluids consisting of polymer chains with contour lengths that far exceed their persistence lengths. Recently, coarse-grained molecular dynamics (CGMD) approaches, which remove ultrahigh frequency motions within the molecules while preserving essential chemical features, have been developed as a promising simulation platform intermediate to AA and BD simulations. CGMD approaches allow for significant reduction in computational cost while enabling the incorporation of solvent quality, hydrophobicity and HI. This approach is employed in this work. The details are provided in Chapter 2.

A schematic representing a hierarchy of simulation techniques for studying molecular dynamics is shown in Figure 1.2. This figure also represents the typical time and length scales that can be accessed with a given technique. In the upper right side resides the continuum-level or mean field approximations that are often used to study the flow behaviors of polymeric liquids. These techniques as mentioned above focus on modeling mean field quantities such as velocity, pressure and polymeric stress and do not attempt to capture microstructural details. On the other extreme, is the ab-initio quantum mechanical methods, which are limited to systems containing up to several hundred electrons. In between these limits lie AA, CGMD and stochastic simulations discussed previously.

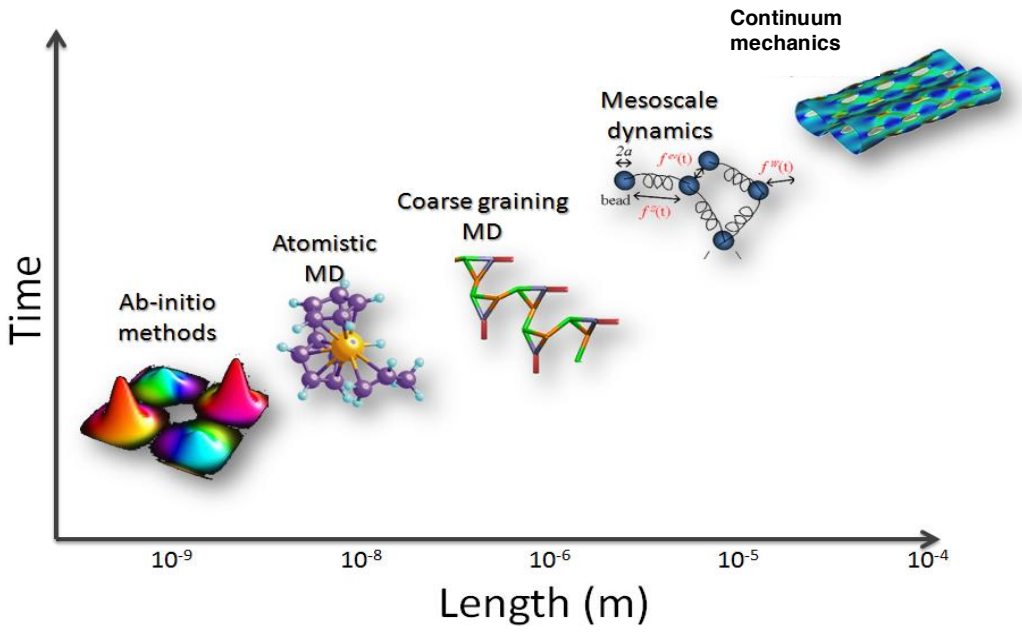

Figure 1.2: A hierarchy of molecular modeling and simulation techniques.

The *focus* of this work is to develop a faithful coarse-grained representation of a typical linear polymer [polyethylene oxide (PEO)] and utilize it to study the structure, dynamics and rheology of dilute and semi-dilute aqueous PEO solutions in presence of explicit solvent-polymer interactions. In Chapter 2, we discuss the CG PEO model and corresponding force fields. CGMD predictions are validated against atomistic MD ones and experimental observations by comparing the predictions of certain structure parameters such as the persistence length and equilibrium properties such as the radius of gyration. We also present the predictions of tumbling dynamics of a single PEO chain under uniform steady shear flow in a "theta" solvent, i.e., a solvent that has neither hydrophilic nor hydrophobic interactions with the polymer, but rather acts as a Brownian bath.

In Chapter 3, we discuss solvent quality influence on the properties and dynamics of a single

PEO chain. We show that solvent quality affects the equilibrium size of polymer as well as the longest relaxation time. We compare CGMD prediction to classical theoretical results of Zimm[32]. Under uniform steady shear, solvent quality is shown to greatly affect the coil-stretch transition of single polymer chain. In poor solvents, we show that a *new* "stretch and collapse" mechanism is a key determinant of polymer configuration dynamics.

Chapter 4 focuses on the rheological properties of PEO solution. We first show the influence of concentration on the zero-shear viscosity. Subsequently, we discuss solvent quality effects on the zero-shear viscosity and its dependence on concentration. In shear flow, CGMD can accurately predicted shear thinning and normal stresses consistent experimental observations. Possible approaches to parameterizing phenomenological constitutive models using MD simulation data are also be discussed. Solvent quality influence on such rheological properties are reported as well.

Chapter 5 will discuss the influence of geometric confinement on the dynamics of a single PEO chain. We first discuss this using CGMD to build a confined system for single polymer chain. We then discuss the predictions of equilibrium configurations of a single PEO chain under confinement. We compare the CGMD results with theory and experimental observations. Further, chain migration under steady shear is described and compared against theoretical and experimental observations. Finally, in Chapter 6 we provide an overall summary of this work and propose directions for future explorations.

Chapter 2

Development and Validation of

Coarse-Grained Molecular Dynamics Simulations

2.1 Introduction

Most CGMD approaches rely on representing collections of atoms as an effective bead. The beads interact through each other through both bonded and non-bonded forces. The non-bonded interactions are typically represented by Lennard-Jones (LJ) potentials. Smit *et al.*[52] used LJ potentials to represent all inter-particle interactions in an oil-water-surfactant system and performed CGMD simulations. They concluded that structure in simple liquids, and even more complex systems such as liquid crystals, can be predicted by using hard-core interactions. Later their techniques have been widely used in simulating lipid systems[53-56]. There are a large variety of CGMD techniques ranging from solvent-free models[57-59] to explicit solvent representations[60-62]. However, these simulations typically require parameterization against atomistic simulations and can only represent a particular state point of a specific system.

Recently, Marrink *et al.*[63] developed the MARTINI force field, which can be applied to a broad range of systems without having to re-parameterizing the force field every time. The model is based on a four-to-one mapping, i.e., on average four heavy atoms are represented by one interaction site. Their approach utilizes LJ potential for non-bonded and harmonic potentials for bonded interactions respectively. Details of the model are described in the next section. This

model has been widely used in various systems. For example, Faller and Marrink[64] have applied MARTINI force field and predicted lamellar phases in lipids. Other applications include peptide-bilayer systems[65], carbohydrates[66] and collagen systems[67]. Recently, Sangwai and Sureshkumar have utilized this approach to simulate self-assembly and shape transitions in cationic surfactant solutions[68, 69]. Further, MARTINI-based CGMD was used by Nangia and Sureshkumar[70] and DeSalvo *et al*.[71] to study transport of nanoparticles and signal factors across lipid membranes. More recently, Sambasivam *et al*[72] used similar coarse-grained representations to study non-equilibrium phenomena, namely shear-induced dynamics and scission of a cationic cylindrical micelle in aqueous solution. Their predictions for micelle tumbling dynamics was consistent with those obtained from mesoscopic theories and BD simulations. Further, they were able to estimate the dispersive forces that hold together the self-assembled micelle and thresholds of the shear rate required to rip such assemblies apart. However, application of such CGMD simulations to the discovery of structure, dynamics and rheology of polymeric fluids is a new frontier of research.

A lucid understanding of the configurational dynamics of polymer chains is essential in achieving quantitative predictions of the polymeric stress. Note that the configuration-dependent stress is elastic, i.e., its origin lies in the loss of translational entropy decreased when the chains are oriented and stretched by an external stimulus such as mechanical shear. In turn, an accurate description of the spatio-temporal evolution of the polymeric stress is required to quantitatively predict rheological behavior such as shear thinning or shear thickening and viscoelastic flow instabilities such as melt fracture and sharkskin. Smith *et al.*[1] observed, using fluorescence microscopy that an individual DNA molecule, when subjected to uniform steady shear, undergoes a *cyclic* motion. A typical cycle is characterized by stretching of a coiled polymer in

the flow direction by shear forces, followed by a loss of alignment of the end-to-end vector from the flow-gradient plane due to thermal (Brownian) fluctuations, referred to as "tumbling", which, in turn causes the stretched chain to relax back to a coiled state. It has been shown[1, 73-76] that there are six primary chain configurations in uniform steady shear flow: stretched, folded, kinked, dumbbell shaped, half-dumbbell shaped and coiled. Further, the tumbling frequency, defined as the reciprocal of the time of a characteristic tumbling cycle, follows a power-law relation with respect to the shear rate with an exponent of 2/3[75, 77]. A rigorous test for the CGMD simulations performed here is to capture quantitatively the signatures of such dynamical phenomena.

We select the MARTINI force field to develop the CGMD PEO model. In this chapter, we first discuss the model parameters and validate the model by comparing structure parameters as well as equilibrium properties against atomistic MD and experimental observations. Single PEO chain dynamics under uniform steady shear is then investigated and compared with the predictions of stochastic dynamics. We show that our model can quantitatively predict the tumbling dynamics of a single polymer chain under steady shear.

2.2 The CGMD polymer model

A linear flexible polymer model that mimics the equilibrium properties of a polyethylene oxide (PEO) molecule in water[63, 78] is used. Figure 2.1 illustrates AA and CG representations of the molecule. Specifically, in the CG model, each $–CH_2-O-CH_2-$ group is represented by one bead, and four water molecules are coarse-grained into a single water bead, both following the standard MARTINI[63] convention.

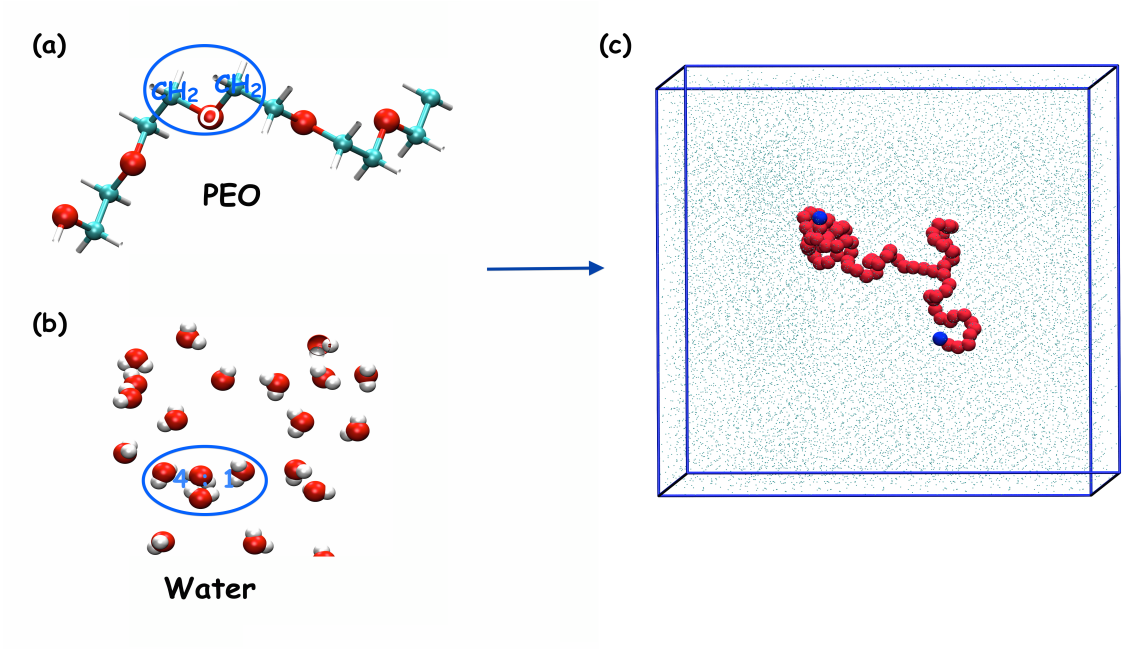

Figure 2.1: All-atom (AA) and coarse-grained (CG) representations of PEO and water molecules: (a) AA representation of part of a PEO chain. The red beads are oxygen atoms, light blue ones are carbons and bonds to hydrogen atoms are shown white; (b) AA representations of water molecules with red and white beads representing oxygen and hydrogen respectively; (c) CG representation of single chain PEO solution. Red beads represent monomers, the two end beads are shown in blue and the light blue dots represent water beads.

Bonded stretching and bending interactions are represented using weak harmonic potentials V_{b} and V_{θ} respectively:

$$V_{\mathrm{b}}(b) = \frac{1}{2}K_{\mathrm{b}}(b - b_0)^2, \qquad (2\text{-}1)$$

$$V_{\theta}(\theta) = \frac{1}{2}K_{\theta}(\cos(\theta) - \cos(\theta_0))^2, \qquad (2\text{-}2)$$

where b_0 and θ_0 are the bond length and bond angle at the minimum energy configuration, respectively, and K_{b} and K_{θ} are constants associated with bond stretching and bending energies respectively.

All non-bonded intramolecular interactions among the polymer beads as well as intermolecular interactions between polymer and solvent beads are represented by a Lennard-Jones (LJ) 12-6 potential. The LJ potential V_{LJ} between beads i and j separated by a distance r_{ij} is given by:

$$V_{\mathrm{LJ}}(r_{\mathrm{ij}}) = 4\varepsilon_{\mathrm{ij}}\left[\left(\frac{\sigma_{\mathrm{ij}}}{r_{\mathrm{ij}}}\right)^{12} - \left(\frac{\sigma_{\mathrm{ij}}}{r_{\mathrm{ij}}}\right)^{6}\right], \qquad (2\text{-}3)$$

where $\varepsilon_{\mathrm{ij}}$ is the minimum in V_{LJ} and σ_{ij} is the distance at which the V_{LJ} vanishes. The values of these parameters are adopted from the work of Lee *et al.*[78] with minor modifications to obtain a closer agreement between the predictions of the AA and CGMD simulations for the persistence length, as well as a better agreement between the CGMD predictions and experimental observations for the power law exponent in the radius of gyration vs. molecular weight

relationship. These parameters are reported in Table 2.1 where subscripts *p* and *s* denote the polymer and solvent, respectively.

Table 2.1: Bonded and non-bonded interaction parameters

Non-bonded interaction				**Bonded interactions**			
σ_{ps}(Å)	ε_{ps}(kJ/mol)	σ_{pp}(Å)	ε_{pp}(kJ/mol)	b_0(Å)	K_b(kJ/mol)	θ_0(°)	K_θ(kJ/mol/nm^2)
4.7	4.05	4.3	3.29	3.3	17000	130.0	50.0

Approximately 10 percent of total solvent beads are "antifreeze" particles as prescribed by the MARTINI model in order to prevent artifacts arising from solvent solidification[79]. All simulations are performed using the GROMACS simulation software[80]. The LJ potential is smoothly shifted to zero between 9 and 12 Å and a cutoff is set at 12 Å. Cubic boxes of linear dimension b with periodic boundary conditions (PBC) in all three orthogonal spatial coordinates are used in simulations. Each system is equilibrated in an isothermal-isobaric (NPT) ensemble using Berendsen pressure coupling with pressure maintained at 1 bar for 100 ns. Temperature is maintained at 296 K by a velocity-rescaling coupling algorithm. Product runs are carried out in Canonical (NVT) ensemble. A time step of 10 fs is used in simulations. Simulations span up to two microseconds, which is approximately 1000 times the longest relaxation time of the fluids studied.

Non-equilibrium molecular dynamics (NEMD) simulations are performed by applying velocity deformations of u and $-u$ at the top and bottom of the box respectively along the flow direction (x). The corresponding shear rate ($\dot{\gamma}$) is given by:

$$\dot{\gamma} = \frac{2u}{b} \qquad (2\text{-}4)$$

The Weissenberg number Wi, which is the ratio of the characteristic relaxation time τ_{R} (see section 2.3.1 below) to the inverse shear rate is defined as:

$$Wi = \tau_{\mathrm{R}}\dot{\gamma} \qquad (2\text{-}5)$$

2.3 Results and Discussion

2.3.1 Model verification

Polverari and van de Ven[81] have used light scattering studies to ascertain that water is a good solvent to PEO. Flory theory[82] predicts that the equilibrium radius of gyration R_{g} of a flexible polymer chain obeys a power law relationship with respect to number of monomers N, i.e.,

$$R_{\mathrm{g}} \propto N^{\nu} \qquad (2\text{-}6)$$

where the power law coefficient $\nu = 0.588$ in good solvent. R_g is calculate through Eq. (2-7):

$$R_{\mathrm{g}}{}^2 = \frac{1}{N}\sum_{i=1}^{N}(\boldsymbol{R}_{\mathrm{i}} - \boldsymbol{R}_{\mathrm{cm}})^2 \qquad (2\text{-}7)$$

where $\boldsymbol{R_i}$ and $\boldsymbol{R_{cm}}$ denote the position vectors of bead i and the center of mass of the chain respectively. The coefficient ν in Eq. (2-6) is ½ for a theta solvent in which case the chain essentially undergoes a random walk subject to Brownian forces imparted by the solvent and hydrodynamic drag force. In a good solvent, favorable solvent-polymer interactions cause the chain to swell. Consequently, $\nu > \frac{1}{2}$, and equals $\frac{3}{5}$ according to Flory theory and 0.588 based on experimental observations. In this work, the equilibrium properties of PEO chains in solution were studied using CGMD simulations for $10 \leq N \leq 91$. In this work, the equilibrium properties of PEO chains in solution were studied using CGMD simulations for $10 \leq N \leq 91$. Figure 2.2 plots R_g predicted by CGMD simulations of PEO in water vs. N. The exponent $\nu = 0.588 \pm 0.008$ is in very good agreement with experimental results[81].

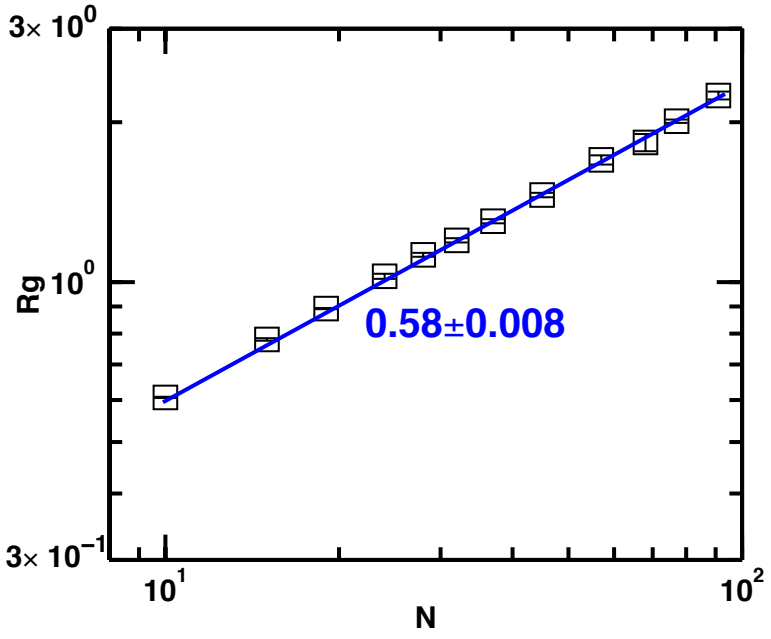

Figure 2.2: Radius of gyration $\boldsymbol{R_g}$ dependence on number of monomers $\boldsymbol{N}$

The inter-bead interactions between polymer chain monomers and solvent beads allow the polymer to drag some solvent beads with it, which in turn, affects the polymer's motion. The long-range force from the polymer chain that acts on the solvent beads is called hydrodynamic interaction (HI). Zimm model[83] predicts that when HI is included, the relaxation time follows a power law relationship with *N* as well:

$$\tau_{\mathrm{R}} \propto N^{3\nu} \qquad (2\text{-}8)$$

where ν relates to the R_{g}-N relationship described previously.

The longest relaxation time of the chain τ_{R}, is calculated by fitting the autocorrelation function (ACF) of R_{g} at equilibrium to an exponential form:

$$ACF = Kexp(-\frac{t}{\tau_{\mathrm{R}}}) \qquad (2\text{-}9)$$

where K is a fitting constant and t is the time.

Figure 2.3 shows a power law relationship between τ_{R} vs. N. The corresponding exponent is 3ν, which is consistent with the prediction of Zimm model, which incorporates the effect of long range intra-chain hydrodynamic interactions on polymer configuration. In CGMD simulations, such interactions are incorporated by virtue of having an explicit representation of the solvent.

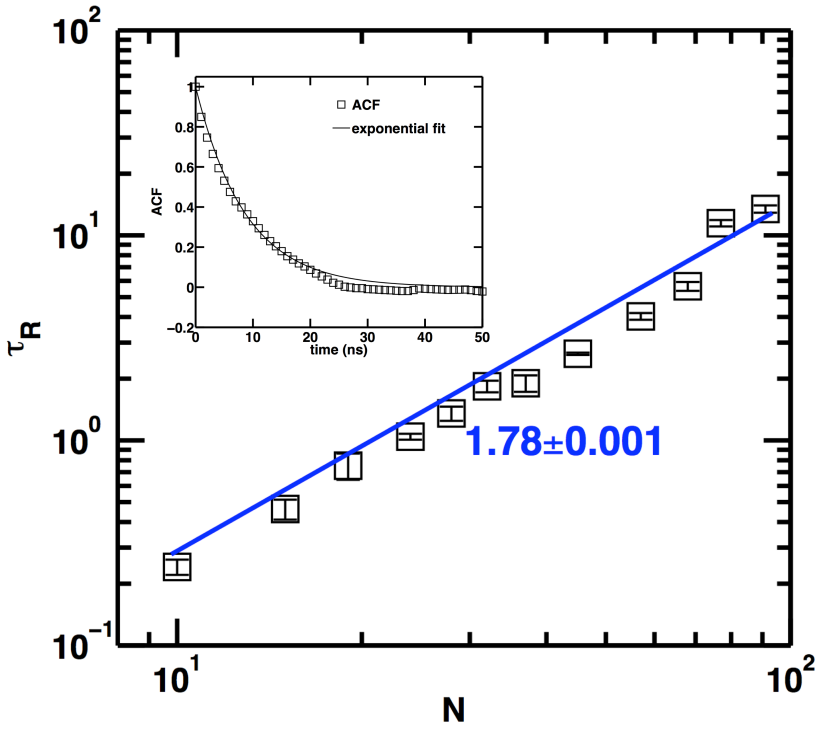

Figure 2.3: Longest relaxation time $\boldsymbol{\tau_R}$ and $\boldsymbol{N}$ follows a power-law relationship, the exponent shows to be triple of the one in $\boldsymbol{R_g}$-$\boldsymbol{N}$ relationship. The inlet plots the ACF of PEO with $\boldsymbol{N = 91}$, which shows a good exponential fit

The persistent length P of the polymer chains was also computed by quantifying the orientational correlations between the bonds. Specifically, the ensemble average of the cosine of the bond angle was fitted to an exponential function as:

$$< cos\theta >= e^{-(\frac{L}{P})} \qquad (2\text{-}10)$$

where L is the distance measured along the contour of the chain. As shown by figure 2.4, P converges to 0.42 nm with increasing N, which is in good agreement with the predictions of recent atomistic MD simulations[84, 85]. Note that $P \approx 1.27b_0$ signifying that the polymer chain is flexible for $N \gg 1$.

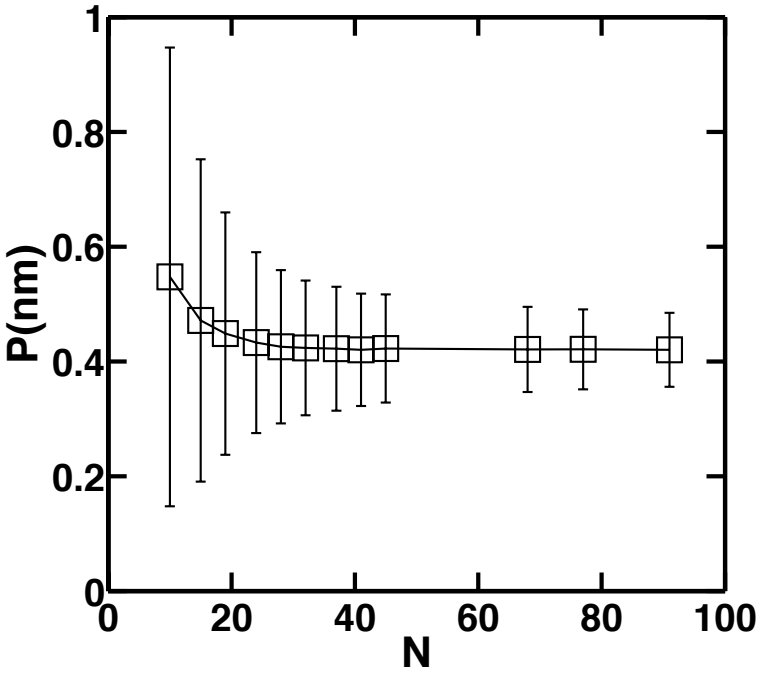

Figure 2.4: Persistence length P versus chain length N**.**

2.3.2 Single chain dynamics in steady shear flow

In this section we investigate whether CGMD simulations are capable of quantitatively predicting the configurational dynamics of a single polymer chain in shear flow. Towards this

end, CGMD predictions are compared with those obtained from stochastic theories and simulations as well as experimental measurements[73, 75, 77, 86, 87]. Flow-induced configuration changes become prominent for $O(1)$ values of Wi. When subjected to a uniform shear flow, hydrodynamic forces cause a coiled chain to extend in the flow direction. Such a chain can lose its flow-alignment by the action of Brownian forces which could tip the end-to-end vector to the vorticity-flow gradient plane, thereby causing the chain to collapse into a coiled state. This cyclic process, characterized by flow-induced extension, tumbling and collapse, is a signature of the configuration dynamics of a single macromolecule in shear flow. Further, a variety of configurations are observed[1, 73, 87] including coiled, fully extended, dumbbell, half-dumbbell, knotted (kinked) and hairpin-shaped or folded.

Figure 2.5 shows the instantaneous end-to-end distance Q and orientation angle θ subtended between the projection of the end-to-end vector onto the flow (x)-gradient (y) and the flow direction[75] defined as:

$$\tan(2\theta) = \frac{2G_{xy}}{G_{xx}-G_{yy}} \qquad (2\text{-}11)$$

where G_{ij} is the the ij component of the radius of gyration tensor of the chain, defined as

$$G_{ij} = \sum_{n=1}^{N} <\Delta\, r_{n,i} * \Delta\, r_{n,j}>/N \qquad (2\text{-}12)$$

with $i, j = x, y, z$ and $\boldsymbol{r}_n \equiv \boldsymbol{R_n} - \boldsymbol{R_{cm}}$. The angle θ is defined positive when measured from x toward y in the x-y plane. Note that $\theta = 0°$ and $90°$ correspond to configurations aligned and orthogonal to the flow respectively. Snapshots of various configurations of the polymer chain are

also provided in Figure 2.5. It is evident that CGMD simulations capture the stretching-tumbling cycles as well as the configurational diversity observed in experiments. Specifically, Q increases when polymer extends and decreases when it tumbles and coils; θ approaches zero with a stretched conformation while it has a larger value when the chain tumbles.

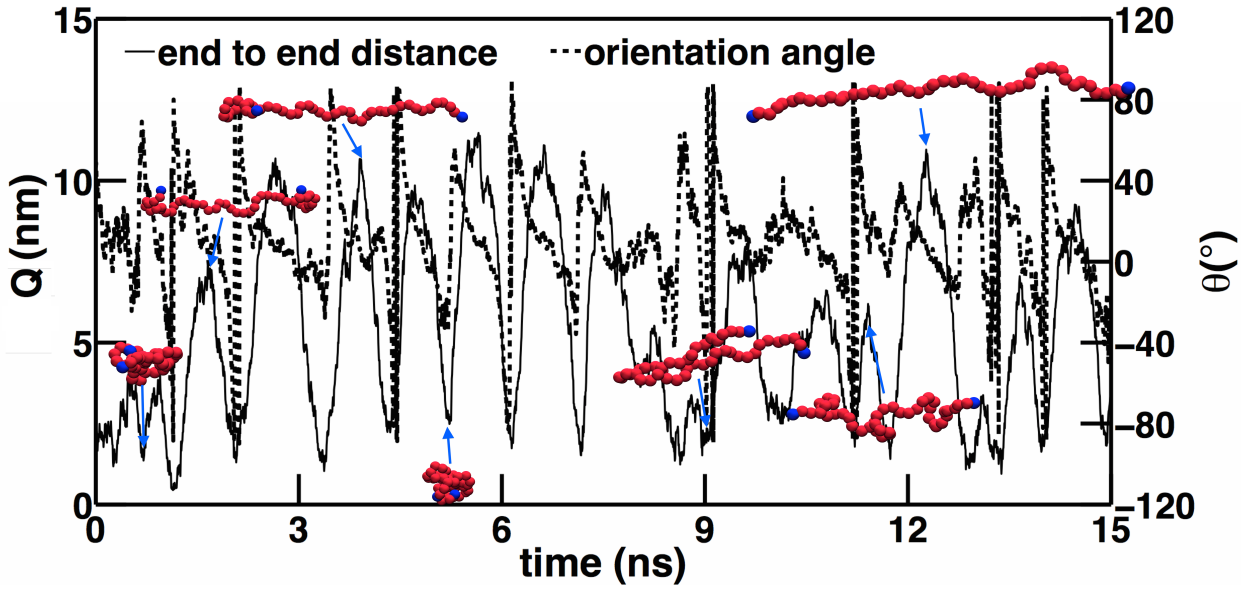

Figure 2.5: Instantaneous behaviors of polymer with $\boldsymbol{N = 45}$ at $\boldsymbol{Wi = 37.5}$. $\boldsymbol{Q}$ increases and $\boldsymbol{\theta}$ tends to align to the flow direction when chain stretches and $\boldsymbol{Q}$ decreases while $\boldsymbol{\theta}$ approaches 90 degree when chain tumbles and coils.

It can be seen that change of the configurations correspond to the change of Q and θ: Q increases when polymer extends and decreases when it tumbles and coils; θ approaches to zero with a stretching conformation while has a larger value in magnitude when it tumbles.

Schroeder *et al.*[4] have shown that the frequency of the stretching-tumbling-coiling cycle follows a power law relationship with respect to Wi, i.e.,

$$f \propto Wi^{\alpha} \qquad (2\text{-}13)$$

The exponent α, has been determined to be 0.66 for 80 μm DNA in experiments and 0.62 in Brownian Dynamic simulations[74]. Winkler studied the dynamics of the semiflexible polymers under uniform steady shear analytically and showed that the exponent α equals 2/3 for $Wi \gg 1$[88]. In what follows, a quantitative analysis of the cyclic configuration dynamics obtained from the CGMD simulations is presented.

The temporal cross correlation function between G_{xx} and G_{yy}, C_{xy},[86] can be used to calculate the duration of tumbling events. This function is defined as

$$C_{\mathrm{xy}}(t_{\mathrm{d}}) = \frac{\sum_{t_{\mathrm{i}}}({G_{\mathrm{xx}}}'(t_{\mathrm{i}}) * {G_{\mathrm{yy}}}'(t_{\mathrm{i}}+t_{\mathrm{d}}))}{\sqrt{\sum_{t_{\mathrm{i}}}({G_{\mathrm{xx}}}'(t_{\mathrm{i}})^2} * \sqrt{\sum_{t_{\mathrm{i}}}({G_{\mathrm{yy}}}'(t_{\mathrm{i}}+t_{\mathrm{d}})^2}} \qquad (2\text{-}14)$$

where t_{i} is the instantaneous time and t_{d} is the delay time. A primed variable denotes deviation of its instantaneous value from its time-averaged stationary value. Figure 2.6 shows a typical C_{xy} curve during a tumbling event. The peak at the negative time lag reveals the polymer extension in the y-direction is on average followed by its extension in the x-direction. Similarly,

the large valley at the positive time lag indicates that positive deviations in G_{xx} are followed by negative fluctuations in G_{yy}.

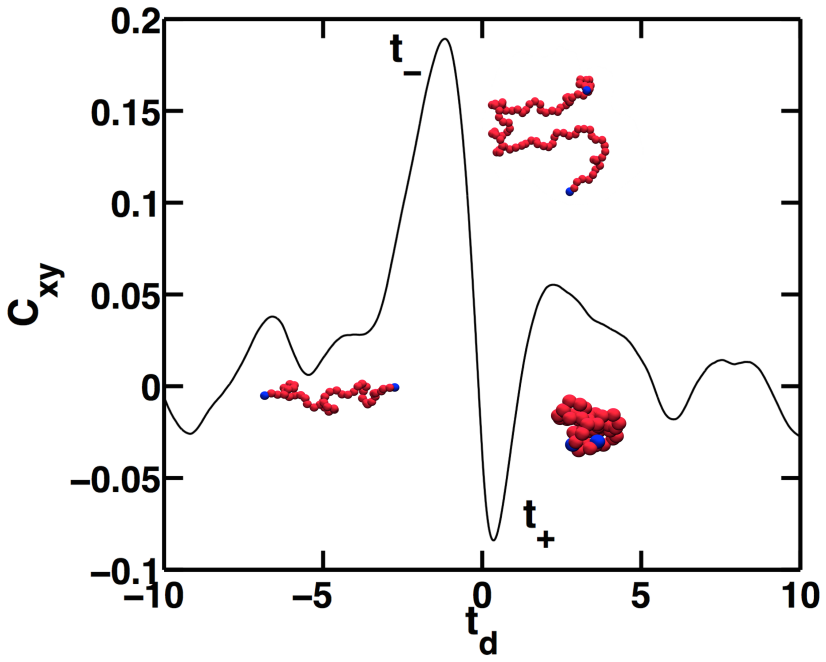

Figure 2.6: Cross correlation function $\boldsymbol{C_{xy}}$ between $\boldsymbol{G_{xx}}$ and $\boldsymbol{G_{yy}}$ of polymer with $\boldsymbol{N = 68}$ at $\boldsymbol{Wi = 49.1}$. $\boldsymbol{t_-}$, $\boldsymbol{t_+}$ denotes for the delay time when $\boldsymbol{C_{xy}}$ reaches for the peak and valley, respectively.

As shown by Huang *et al.*[86], the tumbling time can be calculated as twice the difference between the valley (t_+) and peak (t_-) locations as

$$\tau_t = 2(t_+ - t_-) \quad (2\text{-}15)$$

Further, a dimensionless tumbling frequency can be defined as

$$f = \tau_R/\tau_t \qquad (2\text{-}16)$$

Figure 2.7 shows the variation in f with increasing Wi for N = 91. A power law behavior with an exponent $\alpha = 0.67$ is observed, consistent with predictions of the stochastic dynamics theory/simulations and experimental measurements.

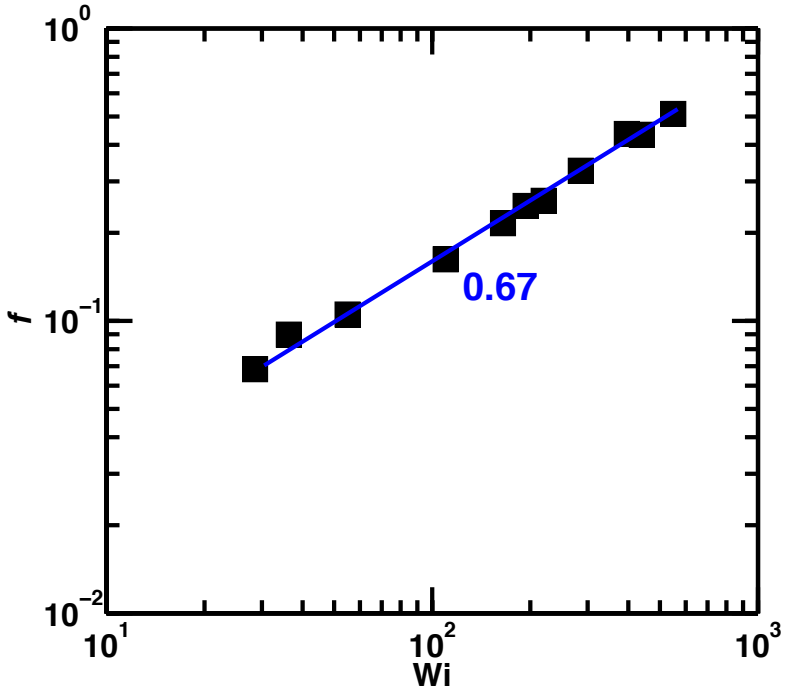

Figure 2.7: Tumbling frequency dependence on $\boldsymbol{Wi}$ for polymer with $\boldsymbol{N = 91}$.

Figure 2.8 shows the probability distribution function (PDF) of θ for N = 91 at various values of Wi. The PDF is uniform for $Wi = 0$ suggesting the absence of any preferred

orientation. As Wi is increased, the effect of flow on chain orientation becomes progressively more prominent and the PDF approaches a Gaussian function for $Wi \gg 1$:

$$PDF = Aexp[-\frac{1}{2}\left(\frac{\theta-\theta_0}{b}\right)^2] \quad (2\text{-}17)$$

where A, b and θ_0 are fitting parameters.

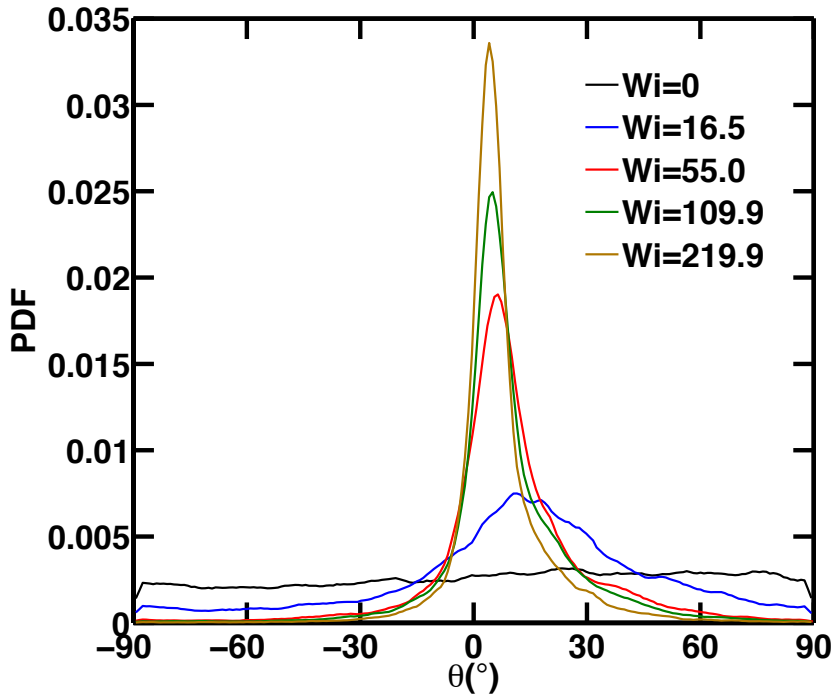

Figure 2.8: PDFs of $\boldsymbol{\theta}$ with different $\boldsymbol{Wi}$ for polymer with $\boldsymbol{N = 91}$. The mean value is slightly positive and approaches 0 with increasing $\boldsymbol{Wi}$.

However, even at large Wi, the mean orientation is slightly biased to positive θ values. This can be attributed to frequent tumbling events during which the chain orientations are misaligned with the flow. Figure 2.9 shows the full width at half maximum (FWHM), defined as:

$$FWHM = 2\sqrt{2}b \quad (2\text{-}18)$$

versus Wi for $N = 91$ along with a power law fit with an exponent $\beta = -0.33$. This result agrees well with the theoretical predictions by Gerashchenko and Steinberg[89].

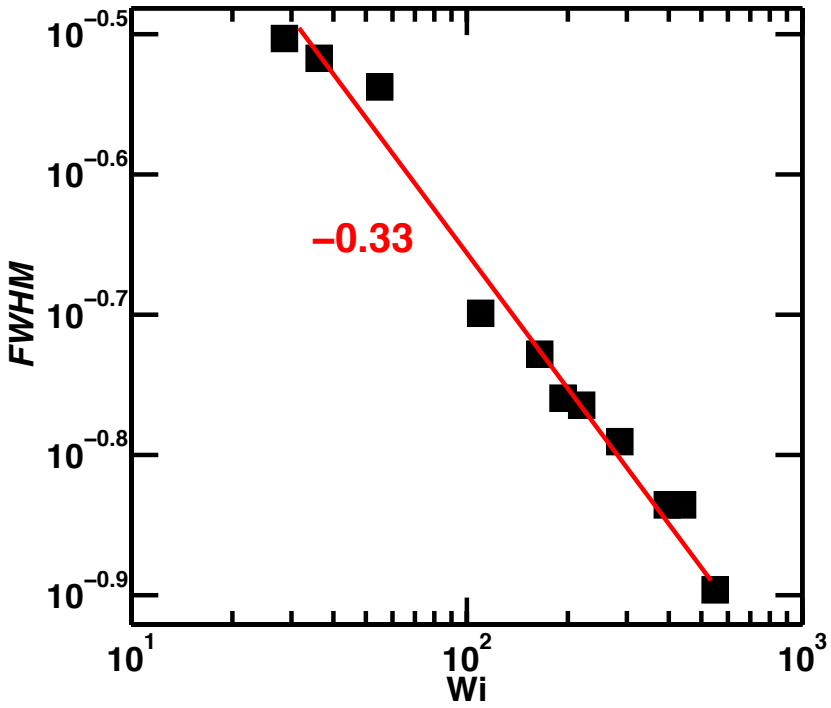

Figure 2.9: Full width at half maximum ($FWHM$) of the shifted Gaussian fitting for the probability distribution function of polymer with $N = 91$ vs. Wi.

Figure 2.10 shows α and β, the exponents in the power law relations of f and FWHM with Wi respectively, the coefficient between $FWHM$ and Wi, as a function of N. Both coefficients approach the predictions of mesoscopic theory/simulation with increasing N. Hence, it is clear that CGMD simulations performed here are capable of reproducing not only the equilibrium properties of the chain but also asymptotic scaling laws that govern its configurational dynamics. Further, CGMD framework allows for the incorporation of the effects of finite polymer concentration as well as polymer-solvent and polymer-wall interactions. In the next section, we explicitly demonstrate the extension of the effect on polymer concentration on the rheological properties under uniform shear flow.

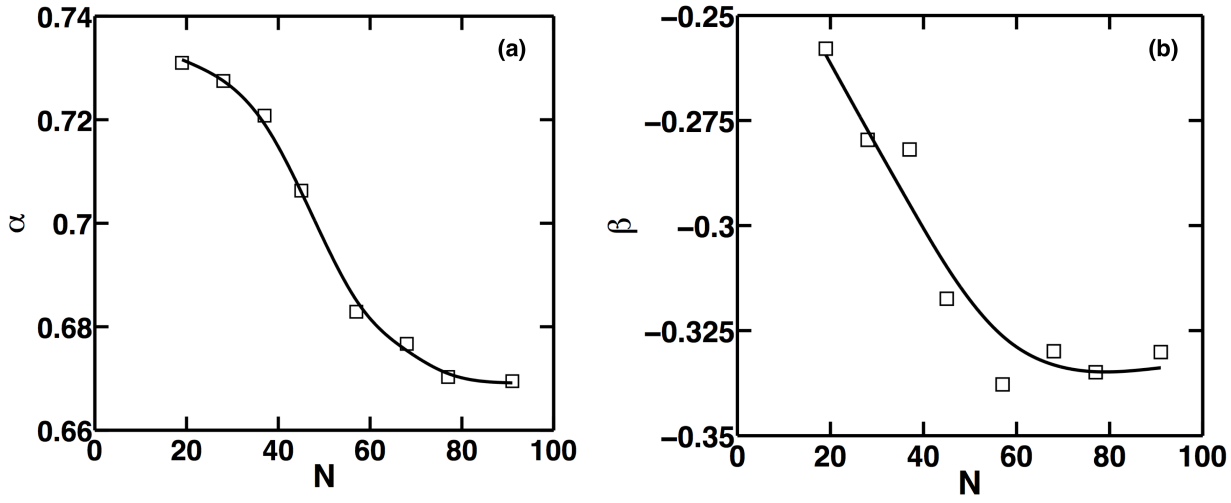

Figure 2.10: Tumbling dynamic characteristics dependence on number of monomers: (a) power law coefficient α of tumbling frequency f; (b) power law coefficient β of FWHM of the Gaussian fitting for PDFs of the orientation angle θ

2.3.3 Effect of Torsional Motion

In lots of systems, dihedral angle potentials are used for complicated geometries to prevent out of plane distortions. An illustration of the torsional angle for the dihedral angle potentials can be seen in Figure 2.11. The torsional angle ϕ_{ijkl} is defined as the angle between the plane that beads i, j, k lie on and the plane that beads j, k, l lie on.

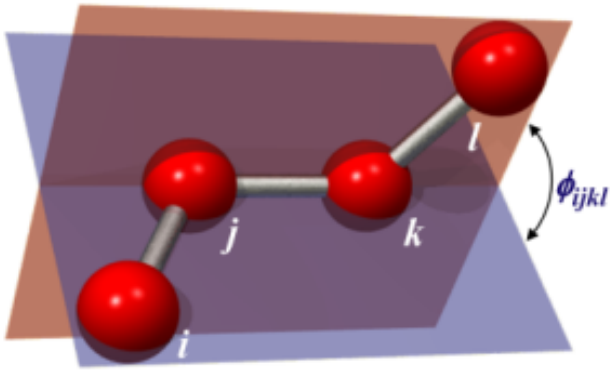

Figure 2.11: An illustration of the torsional angle.

Dihedral angle potentials are used to represent torsional forces in molecules with complicated nonlinear chemical architectures. The specification of a dihedral angle requires four adjoining beads which corresponds to a contour length of $3b_0$. As shown in section 2.3.1, the persistence length of the linear PEO chain considered in this work is $1.27b_0$. Hence, dihedral potentials are unlikely to have an appreciable effect on polymer properties for $N >> 1$. We verify this rigorously by performing CGMD simulations in which dihedral potentials are included and

comparing the predictions of such simulations with those obtained in the absence of torsional effects. In MARTINI force field, the dihedral angle potential is defined as

$$V_{\text{dihedral}}(\phi) = \sum_{i=1}^{m} K_{\phi,\text{i}}(1 + \cos(n_{\text{i}}\phi - \phi_{\text{i}})) \quad (2\text{-}19)$$

where n_{i} and ϕ_{i} are the multiplicities and offsets, and $K_{\phi,\text{i}}$ is the corresponding potential constant for i-th bead. Lee *at al*.[78] have included proper dihedral angle potential in their CG PEO parameterization. These parameters are reproduced in Table 2.2.

Table 2.2: Parameters for dihedral angle potential

$\boldsymbol{\phi_0}$(°)	$\boldsymbol{K_\phi}$**(kJ/mol)**	**n**
180	1.96	1
0	0.18	2
0	0.33	3
0	0.12	4

Figure 2.12 shows the scaling relation between R_{g} and N and Figure 2.13 shows the tumbling frequency f dependence on Wi with and without dihedral potential. It is evident that incorporation of torsional forces has negligible effect on R_{g} and f.

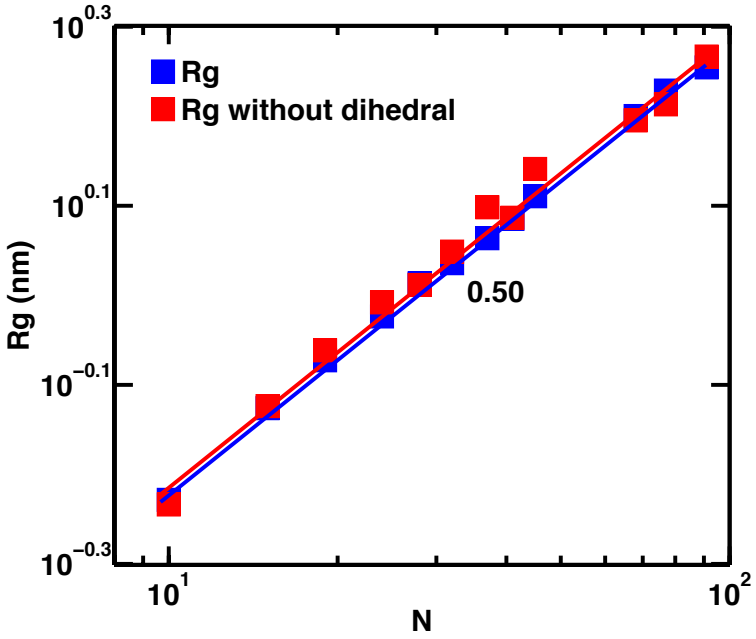

Figure 2.12: R_g vs. N in theta solvent with and without dihedral angle potential

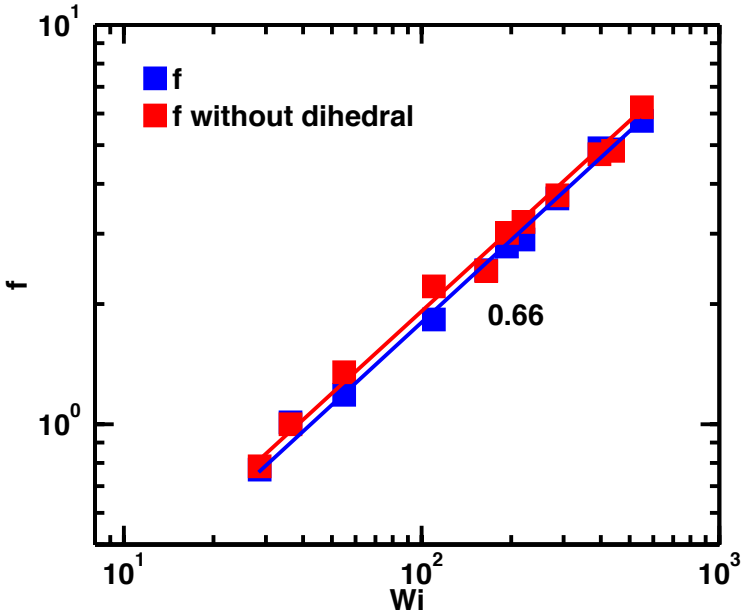

Figure 2.13: Tumbling frequency $\boldsymbol{f}$ vs. $\boldsymbol{Wi}$ of $\boldsymbol{N = 91}$ with and without dihedral angle potential

2.4 Conclusion

Configuration dynamics and rheology of solutions of linear flexible polymers have been studied using coarse-grained molecular dynamics (CGMD) in presence of explicit solvent-polymer interactions subjected to MARTINI force field. Equilibrium properties in solution such as radius of gyration, relaxation time and structure properties such as persistent length have shown that current CG model takes in to account hydrodynamic interactions of polymer chain subjects in solution. The dynamics of a single polymer chain has been studied by using non-equilibrium molecular dynamics (NEMD). The simulations are capable of accurately predicting stretch-tumbling cycles of a single polymer chain subjected to steady uniform shear flow. Different configurations, i.e., extended, half-dumbbell, dumbbell, kinked, folded and coiled configurations, of a polymer chain have been observed in the simulations. Tumbling frequency has been found to follow a power law relation with the increasing Weissenberg number (Wi), a dimensionless number used to characterize the flow behavior. The power law exponent has been found to approach 0.67 with the increasing chain length, which corresponds to experimental observations and predictions of stochastic dynamics theory/simulations. We have also analyzed the orientation distribution of the end-to-end vector, which is characterized by the orientation angle θ, defined as the angle between the projection of the end-to-end vector onto the flow-gradient plane and the flow direction. The mean orientation angle has been discovered to be slightly biased to positive θ values and the probability distribution function (PDF) of θ could be approximated by a shifted Gaussian for $Wi > 1$. Full width at half maximum (FWHM) of PDF of θ follows a power law relation with Wi, and the coefficient approaches to -1/3 with the

increasing chain length, which is in good agreement with mesoscopic theories. Dihedral potential is shown to have no significant influence on the equilibrium properties and single chain dynamics of dilute PEO solution. This is because the persistent length is less than the length scale where dihedral potential affects the chain configuration.

Chapter 3

Solvent quality influence on dilute polymer solution

3.1 Introduction

The configuration dynamics of polymer chains has been widely studied for more than a decade. As discussed by previous chapters, it has been observed in experiments and predicted by the simulations that such conformation changes may have profound impacts on the macroscopic rheological properties[1, 73, 86, 90]. Moreover, solvent quality has a pronounced effect on the equilibrium properties (e.g. radius of gyration) and configuration dynamics of polymer chains in solution[82]. When a polymer chain is in a theta solvent, the steric repulsions among monomers are annulled by the solvent-chain attractions, thus the equilibrium configuration is dictated by a balance between Brownian fluctuations and dissipation caused by hydrodynamic drag. In a poor solvent, the net repulsive interaction between polymer and solvent molecules causes the chain to form a dense globular shape. Various studies have been performed on the coil-globule transition of a polymer chain, i.e., the transition of a flexible macromolecular chain from random coil conformation in θ-state to a compact globule in a collapsed state. These studies include phenomenological models such as the one predicted by de Gennes[91], in which collapsing chain is viewed as "sausage" of collapsed blobs, models based on Langevin equations[92-94], experimental studies on the configurational entropy of the coil-globule transition[95], and so on. However, these studies fail to show how solvent quality affects the globule-coil transitions.

Single chain dynamics have been widely studied over the past decades. Schroeder *et al.*[74, 75] have used Brownian Dynamics Simulations (BDS) and predicted the tumbling dynamics of single DNA chain under simpler shear flow. Other groups have also used BDS and predicted the solvent quality influence on the coil-stretch transition of polymer in elongation flow[96, 97]. Several studies have been focused on the solvent quality influence on the single chain dynamics. For example, Lee and Muller[98] conducted light scattering experiments to study the effect of solvent quality on configurational dynamics of polymer chains in shear flow. They analyzed angular dissymmetry of the scattered light intensity to determine polymer chain alignment in the flow direction and showed that flow alignment of the chain increases with decreasing solvent quality. Alexander-Katz and Netz[99] performed Langevin dynamics simulations to study the effect of shear flow on a collapsed polymer chain and predicted that polymer chain remains as a globe below a critical shear rate which depends on the globule size. Above the critical shear rate, the chain undergoes repeated globe-stretch transitions. However, non-equilibrium molecular dynamics studies of shear-induced configurational transitions in polymer chains in presence of explicit solvent-mediated interactions are still lacking.

Recently, the advances in distributed computing and development of efficient algorithms have allowed for the use of multi-scale models to predict dynamics of polymeric fluids. Besides those that have been mentioned in the previous two chapters, several new techniques have been emerged to study the solvent quality influence. Dissipative particle dynamics (DPD) is another mesoscopic simulation method in which a liquid is modeled by coarse-grained particles that carry momentum. DPD have been widely used to study solvent quality effects in dilute polymer solutions[31, 100-102]. Pan and Manke[100] have used DPD and studied the rheology and configurational properties of dilute polymer solutions in steady shear flow. Opps *et al.*[103] have

also showed the coil-globule transition phase diagram using Discontinuous Molecular Dynamics. Although DPD can explicitly model inter-particle interactions, it is not a straightforward task to calibrate DPD parameters, i.e., to decipher the correlation between the parameters in the DPD model and molecular properties.

In this chapter, we first describe the determination of appropriate polymer-solvent interactions and validation of CGMD predictions. The model is validated by comparing equilibrium properties of the polymer chain under different solvent condition against Flory theory. Next, solvent quality effects on the equilibrium properties of dilute PEO solutions are discussed. A linear relationship is discovered between the polymer size as well as the longest relaxation time of the chain and the solvent quality tuning parameter. Solvent quality influence on the single chain dynamics in steady shear flow is then investigated. We show that, in a poor solvent, a "stretch and collapse" mechanism is a key determinant of polymer configuration dynamics. Weissenberg number Wi (defined in Chapter 2), at which the chain starts to stretch, increases when the solvent quality gets poorer.

3.2 Simulation method

A linear flexible polymer chain that mimics the equilibrium properties of polyethylene oxide (PEO) molecule is placed in a cubic box with explicit polymer-solvent interactions. Bonded stretching and bending interactions are represented by weak harmonic potentials, as introduced in Chapter 2.

All non-bonded intramolecular interactions among the polymer beads as well as intermolecular interactions between polymer and solvent beads are represented by a LJ 12-6 potential:

$$V_{\mathrm{LJ}}(r_{\mathrm{ij}}) = 4\varepsilon_{\mathrm{ij}}\left[\left(\frac{\sigma_{\mathrm{ij}}}{r_{\mathrm{ij}}}\right)^{12} - \left(\frac{\sigma_{\mathrm{ij}}}{r_{\mathrm{ij}}}\right)^{6}\right] \quad (2\text{-}3)$$

where ε_{ij} is the potential well and σ_{ij} is finite distance at which the inter-bead potential is zero. The values of these parameters are adopted from previous work in Chapter 2. From Eq. (2-3) and Figure 3.1, we can see that increasing ε_{ij} will increase the attraction between two beads while reducing ε_{ij} will decrease the attractive interactions between two beads. Thus, ε_{ij} can be served as a tuning parameter for different solvent qualities when used for intermolecular interactions. As described in Chapter 2, subscripts *pp* indicate polymer-polymer intramolecular non-bonded interactions and *ps* indicate polymer-solvent intermolecular interactions.

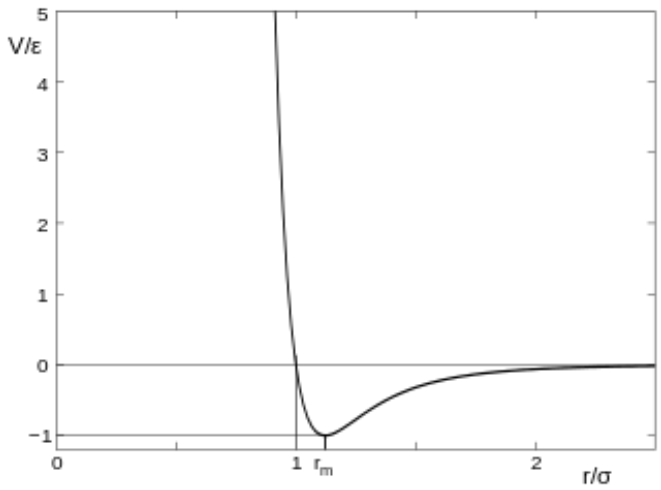

Figure 3.1: A typical scheme of LJ potential

Each single chain system is equilibrated in an isothermal-isobaric (NPT) ensemble using Berendsen pressure coupling with pressure maintained at 1 bar for 100 ns. Production runs are carried out in an NVT ensemble. A time step of 10 fs is used in the simulations. Temperature is maintained at 296 K by a velocity-rescaling algorithm. The LJ potential is smoothly shifted to zero between 0.9 and 1.2 nm and a cutoff is set at 1.2 nm. Cubic boxes with periodic boundary conditions (PBC) in all dimensions are used in simulations. The dimensions of the boxes are chosen as the same as those in Chapter 2. Approximately 10% of the solvent beads are "antifreeze" particles as prescribed by the MARTINI model in order to prevent artifacts arising from solvent solidification[104].

Non-equilibrium molecular dynamics (NEMD) simulations are performed by applying velocity deformations on top and bottom of u and $-u$ at the top and bottom of the box respectively along the flow direction (x). The shear rate is calculated as in Eq. (2-4) and Wi is used to characterize the flow behavior:

$$\dot{\gamma} = \frac{2u}{b} \qquad (2\text{-}4)$$

$$Wi = \tau_{\mathrm{R}}\dot{\gamma} \qquad (2\text{-}5)$$

To make the variables constants, we normalize all energy terms by RT, where R is the gas constant and T is the temperature of the system. Polymer properties are normalized by their equilibrium properties in theta solvent. For example, R_g and τ_R are normalized by the ones in theta solvent, R_{g_0} and τ_{R0}, and ε_{ps} is normalized by RT.

3.3 Results and Discussion

3.3.1 PEO in different solvent systems

When polymer chain is in a theta solvent, the solvent mediated attractions between monomers and solvent beads cancel the steric repulsions among monomers, thus the net excluded volume is zero. When the polymer-solvent attractions increase, the polymer chain has positive net excluded volume, and the polymer starts to swell. On the contrary, when the polymer is in a poor solvent, the polymer - solvent repulsions lead to a negative excluded volume, the polymer chain collapses and behaves as a dense globe[32, 105]. Flory theory[82] predicts that the size of the polymer chain under different solvent conditions follows a power law relationship with the number of monomers:

$$R_{\mathrm{g}} \propto N^{\nu} \qquad (2\text{-}6)$$

The power law exponent ν in good, θ and poor solvents are 0.588, 0.5 and 0.33, respectively.

The inter-bead interactions between polymer chain monomers and solvent beads allow the polymer to drag some solvent beads with it, which in turn, affects the polymer's motion. The long-range force from the polymer chain that acts on the solvent beads is called hydrodynamic interaction (HI). Zimm model[83] predicts that when HI is included, the relaxation time follows a power law relationship with N as well:

$$\tau_{\mathrm{R}} \propto N^{3\nu} \qquad (2\text{-}8)$$

where ν relates to the R_{g}-N relationship described previously.

The parameters of each polymer-solvent interaction are shown in Table 3.1.

Table 3.1: Parameters of different solvent-chain interactions

Solvent	$\boldsymbol{\varepsilon_{ps}}$**(kJ / mol)**	$\boldsymbol{\sigma}$ **(nm)**
Poor solvent	2.7	0.47
Theta solvent	3.96	0.47
Good solvent	4.05	0.47

Figure 3.2 plots the scaling relation between R_{g}-N (a) and τ_{R}-N (b) of PEO in different solvent systems. τ_{R} is calculated by fitting the autocorrelation function (ACF) of R_{g} to an exponential form:

$$ACF = Kexp(-\frac{t}{\tau_{\mathrm{R}}}) \qquad (2\text{-}9)$$

The predicted scaling exponents in the R_g vs. N relationships in all three solvent types are in good agreement with Flory theory and DPD simulations[31, 101]. Moreover, the power law exponent between τ_R and N, are approximately three times the ones between τ_R and N, in accordance with Zimm theory.

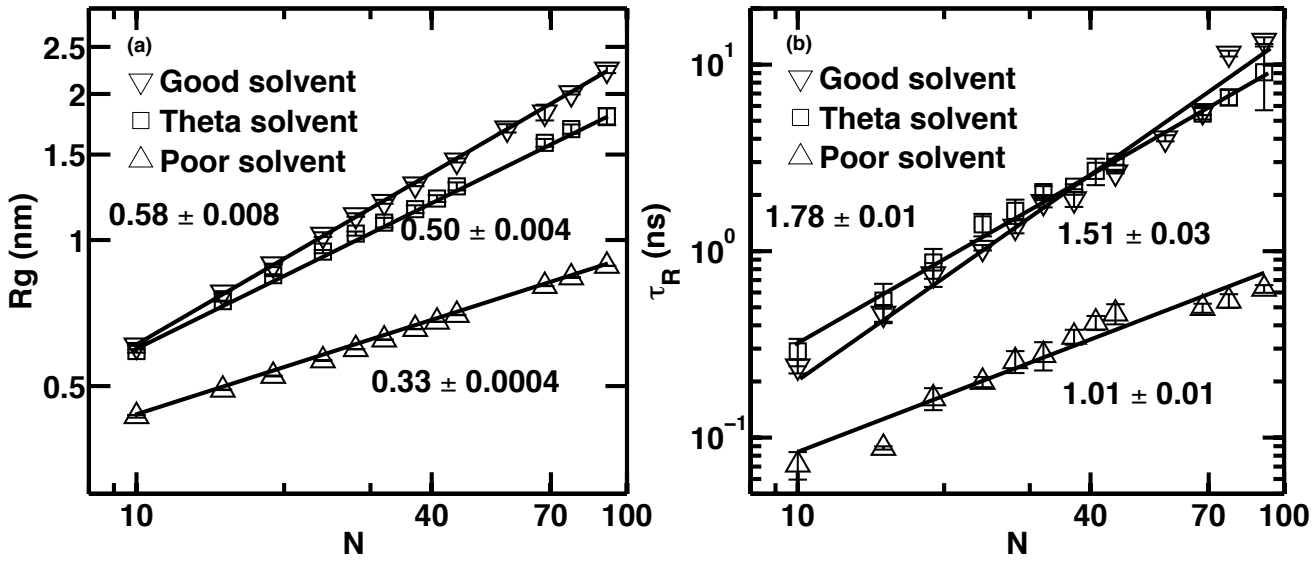

Figure 3.2: Scaling relation between (a) $\boldsymbol{R_g}$ and (b) $\boldsymbol{\tau_R}$ vs. N in different solvent conditions. The power law exponent of $\boldsymbol{R_g}$ vs. N corresponds the prediction by Flory theory. The exponent of $\boldsymbol{\tau_R}$ vs. N is approximately triple of that of $\boldsymbol{R_g}$ vs. N, which corresponds to Zimm model prediction and shows HI is included in the model.

3.3.2 Solvent quality influence on the size and relaxation of single polymer chain

Figure 3.3 shows R_g and τ_R as a function of the solvent quality parameter ε_{ps}. Both R_g and τ_R are nearly constant when $\varepsilon_{ps} < \varepsilon_{pp}$. They gradually increase when $\varepsilon_{ps} > \varepsilon_{pp}$, and exhibit sharp linear increases close to theta solvent conditions.

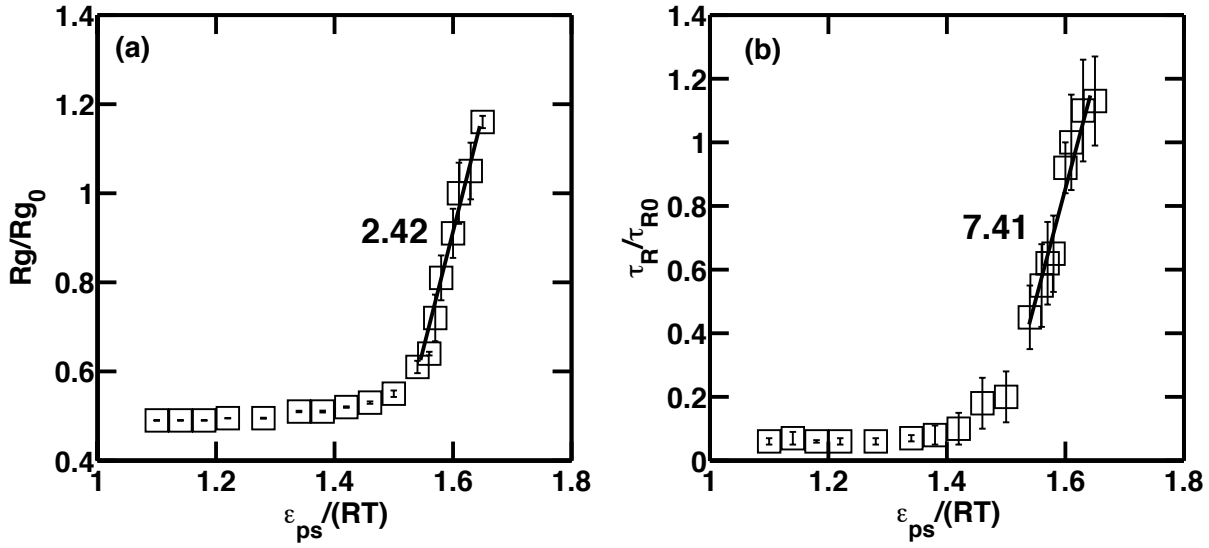

Figure 3.3: (a) $\boldsymbol{R_g}$ and (b) $\boldsymbol{\tau_R}$ versus $\boldsymbol{\varepsilon_{ps}}$, the tuning parameter that indicates solvent quality. Both properties are nearly constant when $\boldsymbol{\varepsilon_{ps} \sim \varepsilon_{pp}}$, where $\boldsymbol{\varepsilon_{pp}}$ is the potential well of LJ potential among polymer beads, and $\frac{\boldsymbol{\varepsilon_{pp}}}{\boldsymbol{RT}} = \mathbf{1.33}$. They start to increase when $\boldsymbol{\varepsilon_{ps} > \varepsilon_{pp}}$, and show rapid linear increment at near theta condition ($\frac{\boldsymbol{\varepsilon_{ps}}}{\boldsymbol{RT}} = \mathbf{1.61}$ at theta condition).

Models developed by de Gennes[91, 106, 107] predict a two-stage coil–to–globule transition when polymer is quenched from a theta-temperature: in the first stage the polymer size will decrease dramatically from an unknotted chain to a "sausage" like blobs. The chain then would gradually rearranges to form a compact globule in the second stage. The analogy here is that if we view it reversely, when intra-chain interactions are greater than polymer-solvent interactions, monomers

would remain in close proximity to one other due to strong attractive forces, and the size of the polymer would not vary appreciably with an increase with $\varepsilon_{\mathrm{ps}}$. Moreover, the configuration dynamics is expected to be slow for large collapsed chains, thus the relaxation time would remain nearly constant. When polymer-solvent interactions increase, the solvent molecules start to "pull" the chain, and chain would form a loose blob. For ε_{ps} values near the theta solvent condition, the chain would expand rapidly due to favorable solvent-polymer interactions, and becomes a random coil.

3.3.3 Solvent quality effects on coil-stretch transition in shear flow

It is well-known that when a flexible polymer chain initially at equilibrium is subjected to a simple shear flow, it would tend to flow align stretch as Wi becomes O(1), i.e., when the hydrodynamic forces overcome the conformational entropy of the chain[1, 73, 75, 77, 86, 87, 108]. However, when the polymer is in a poor solvent, the polymer assumes a dense globular shape and the net attraction among polymer monomers makes it harder for the hydrodynamic force to deform the chain. Thus, in order to stretch the chain, the work performed by hydrodynamic force needs to be larger (compared to that in theta solvents) enough to offset the effect intramolecular attractions. Here, we quantify the intramolecular net attraction by the variable δ:

$$\delta = V_{\mathrm{LJ\_ps}} - V_{\mathrm{pp}} \quad (3\text{-}1)$$

which is the difference between polymer-solvent ($V_{\mathrm{LJ\_ps}}$) and total polymer-polymer interactions (V_{pp}). V_{pp} is the sum of bonded and non-bonded interactions among all polymer beads and $V_{\mathrm{LJ\_PS}}$

is the polymer-solvent LJ potential. The hydrodynamic drag force is calculated by Stokes-Einstein relationship[32] and the work done by the drag force is characterized by:

$$W_{\mathrm{D}} = F_{\mathrm{D}} Q = 6\pi\eta u Q^2 \quad (3\text{-}2)$$

where Q is the end-to-end distance of the polymer chain at the given u, and η is the equilibrium viscosity of the solution, which is calculated by Green-Kubo relation[109, 110].

Figure 3.4 plots W_{D}, δ and Q versus Wi of a single PEO chain in a solvent system with $\frac{\varepsilon_{\mathrm{ps}}}{RT} = 1.38$. The end-to-end distance Q does not show significant increment until W_{D} and δ intersect. We use the corresponding Wi value to characterize the onset Wi (Wi_0) for coil-stretch transition.

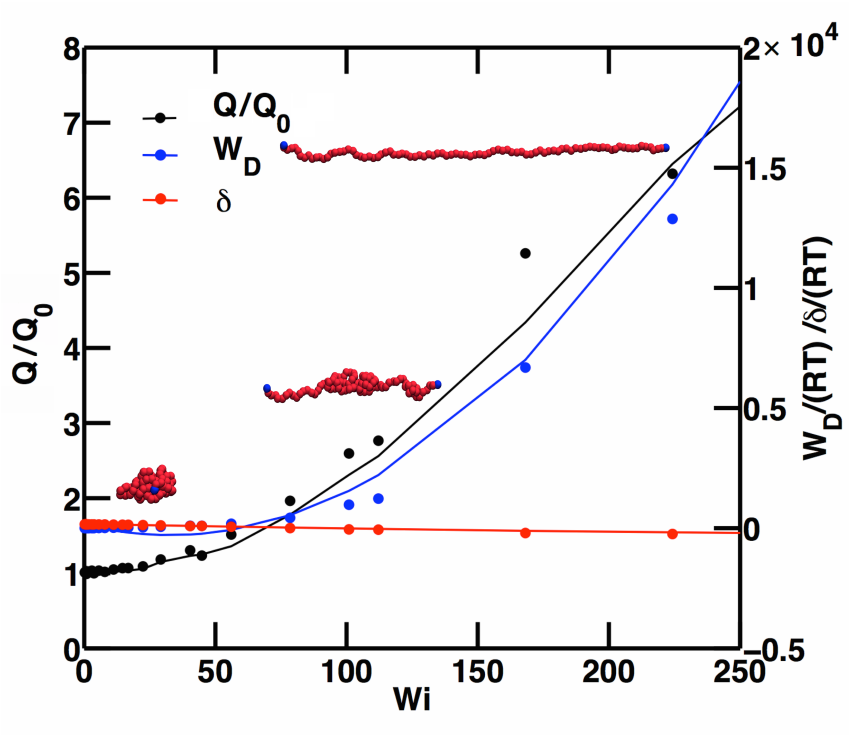

Figure 3.4: W_D, work done by the hydrodynamic drag force, δ, the intramolecular net attraction, and Q, end-to-end distance of the chain versus Wi. The chain doesn't show significant increment until W_D surpasses δ. At low Wi, the chain cannot be fully stretched, when $Wi > Wi_0$, the chain starts to stretch and at high Wi, the chain can be fully extended.

It is evident from Figure 3.4 that the end-to-end distance Q also increases sharply for $Wi > Wi_0$. For the case reported in Figure 3.4, $Wi_0 = X(\gg 1)$ as compared to ~1 for a theta solvent. Figure 3.5 shows that when solvent quality improves, i.e., when ε_{ps} increases, Wi_0 decreases *linearly* before converging to a value close to unity.

The linear dependence of Wi_0 on ε_{ps} can be rationalized as follows. For a given V_{pp}, the net attractive intra-chain interactions, and consequently the hydrodynamic work required to unravel the chain, increase linearly with decreasing ε_{ps}. Eq. (2-4) and Eq. (3-2) imply that:

$$W_D = \frac{3\pi\eta b Q^2}{\tau_R} Wi \propto Wi \quad (3\text{-}3)$$

For a given chain length, for $Wi < Wi_0$, chains exist in a coiled state. Hence, Q^2 at $Wi = Wi_0$ may be treated as a constant. Therefore, a linear increase in W_D requires a commensurate increase in the applied shear rate, or equivalently, in Wi. This is reflected in the linear increase in Wi_0 with decreasing $\varepsilon_{\mathrm{ps}}$.

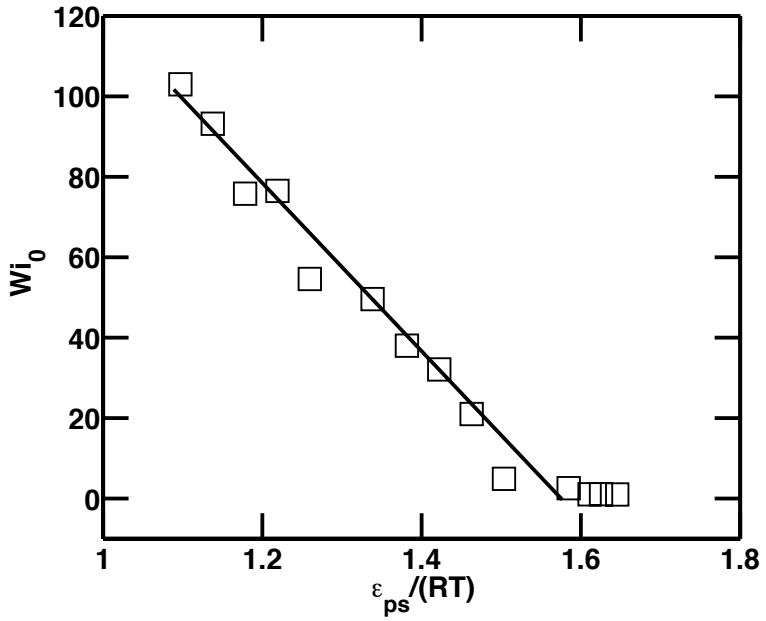

Figure 3.5: Wi_0, the onset Wi at which the chain starts to stretch, follows a negative linear relationship with $\varepsilon_{\mathrm{ps}}$, the solvent quality indicator. Wi_0 converges to 1 in theta and good solvent conditions.

3.3.4 Solvent quality influence on tumbling dynamics

A simple shear flow can be decomposed to a rotational component and an elongation component with equal magnitude. Thus, it is understandable that polymer chain will not sustain in a stretched configuration in such case. Smith *et al.* [1] has first discovered that in a theta solvent, single polymer chain goes cyclic motion. When the polymer chain is subjected to the shear flow, while the hydrodynamic drag force stretches the chain, the solvent molecules, which undergo Brownian motion[111], perturb the chain. Together with the entropic restoring force among beads, the polymer chain tumbles and coils. Followed research[73-75, 87, 108] has shown that the polymer chain has six different configurations, i.e., coil, fold, dumbbell, half dumbbell, kinked and stretched.

In a poor solvent, due to the repulsion between the chain and the solvent molecules, the dynamics become more complicated as compared to those in a theta solvent. Figure 3.6 shows the instantaneous Q and orientation angle θ of a single polymer chain subjected to a poor solvent at different Wi. The orientation angle θ is defined in Chapter 2:

$$\tan(2\theta) = \frac{2G_{xy}}{G_{xx}-G_{yy}} \qquad (2\text{-}11)$$

where G_{ij} is the radius of gyration tensor of the chain with $i, j = x, y, z$, as defined in Chapter 2:

$$G_{ij} = \sum_{n=1}^{N} <\Delta r_{n,i} * \Delta r_{n,j} >/N \qquad (2\text{-}12)$$

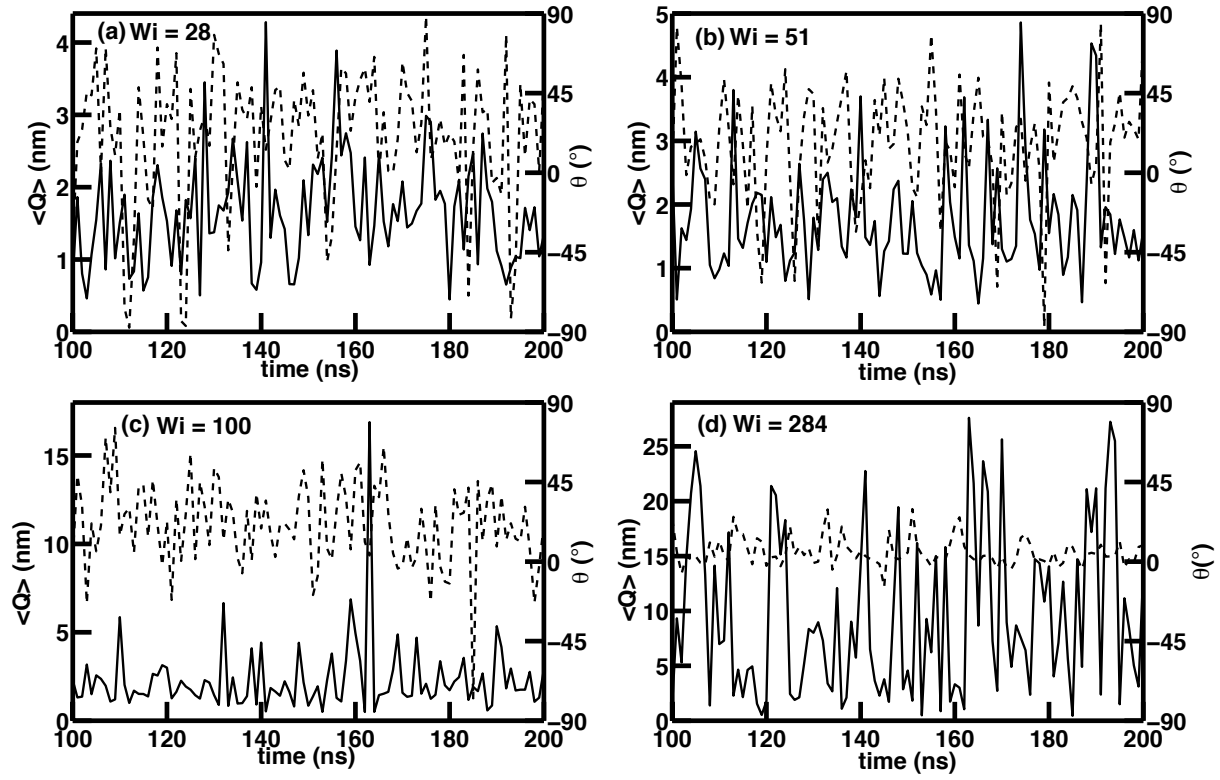

Figure 3.6: Instantaneous Q and orientation angle θ at $\frac{\varepsilon_{\mathrm{ps}}}{RT} = 1.38$ at (a) $Wi = 28$, (b) $Wi = 51$, (c) $Wi = 51$ and (d) $Wi = 284$. $Wi_0 = 43$ at this solvent condition. When $Wi < Wi_0$, the chain cannot extend due to the strong net intramolecular attraction, but it is still subjected to the rotational component of the flow, thus tumbling dynamics dominates. The chain starts to stretch at $Wi \sim Wi_0$. When $Wi > Wi_0$, the chain may stretch and collapse without tumble, Q decreases while the chain still aligns to the flow, which is defined as collapse dynamics. At $Wi \gg Wi_0$, the chain tends to stay in extended configuration due to large hydrodynamic drag force, but net attraction among beads also "pushes" the chain and the chain is dominated by the collapse dynamics.

As expected, with increasing Wi, Q attains progressively larger values. Simultaneously, the fluctuations in θ decreases with its mean value getting close to zero, which shows that on average, the chain is better aligned to the flow. Moreover, at high values of Wi, as shown schematically in Figure 3.7, after the chain is fully stretched, it can collapse directly (i.e., without tumbling) due to repulsive solvent-polymer interactions, while θ remains close to zero (Figure 3.7).

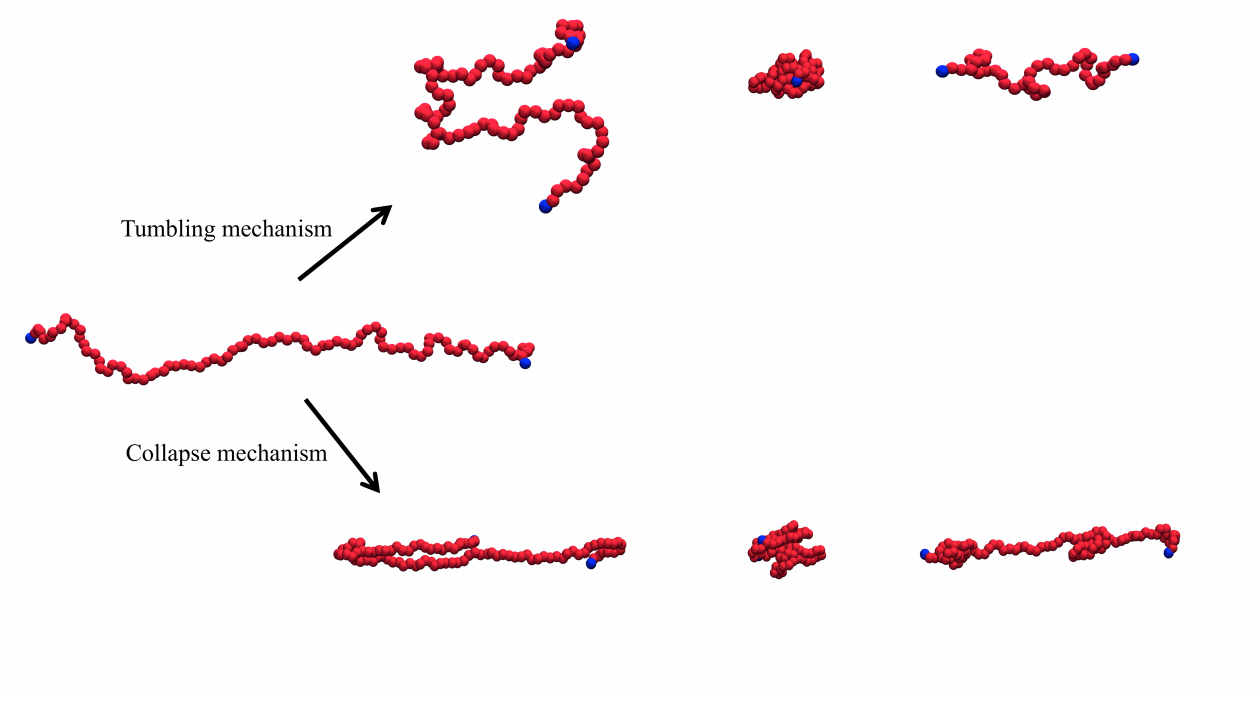

Figure 3.7: At $Wi > Wi_0$ in poor solvents, after fully stretched, the chain may tumble and rotates, which follows the tumbling mechanism, or it may collapse without tumbling.

When Wi is less than Wi_0, even though the chain cannot be fully stretched, it is still subjected to the rotational component of the flow, thus the chain maintains the tumbling motion. When Wi is much greater than Wi_0, due to the strong hydrodynamic drag force, which is much larger than the entropic restoring force, the chain is prone to stay at the stretched configuration. However, due to the strong net attraction among polymer beads, the chain may collapse directly without tumbling. We define this mechanism as the collapse mechanism. At $Wi \sim Wi_0$, the chain is able to be fully stretched, but the hydrodynamic force is not too large that the chain is still able to rotates and tumbles, the chain is subjected to both mechanisms.

Further insight on the coexistence of two mechanisms is acquired by examining the probability distribution function (PDF) of θ. Figure 3.8 shows the PDF of θ in flows with different Wi and different solvent conditions. In a theta or good solvent, the predicted PDFs are in agreement with the experiment observations and Brownian Dynamics simulations[75, 86], i.e., the PDFs can be fit to asymmetric Gaussian functions that are biased to positive mean values. A positive mean θ signifies tumbling and rotation of the chain. In poor solvents, double peaks are observed when Wi is greater than Wi_0. The peak at positive θ is a signature of tumbling events while the sharp peak at zero can be attributed to collapse events. At low Wi ($Wi < Wi_0$), mean θ is prone to a larger positive value in poor solvents than that in theta and good solvents. This result agrees with the experimental observations by Lee and Muller[98]. At very high Wi, mean θ is close to zero in all solvent conditions. This is because the chain is temporarily "locked" by the strong hydrodynamic drag force and approximately one-dimensional[112].

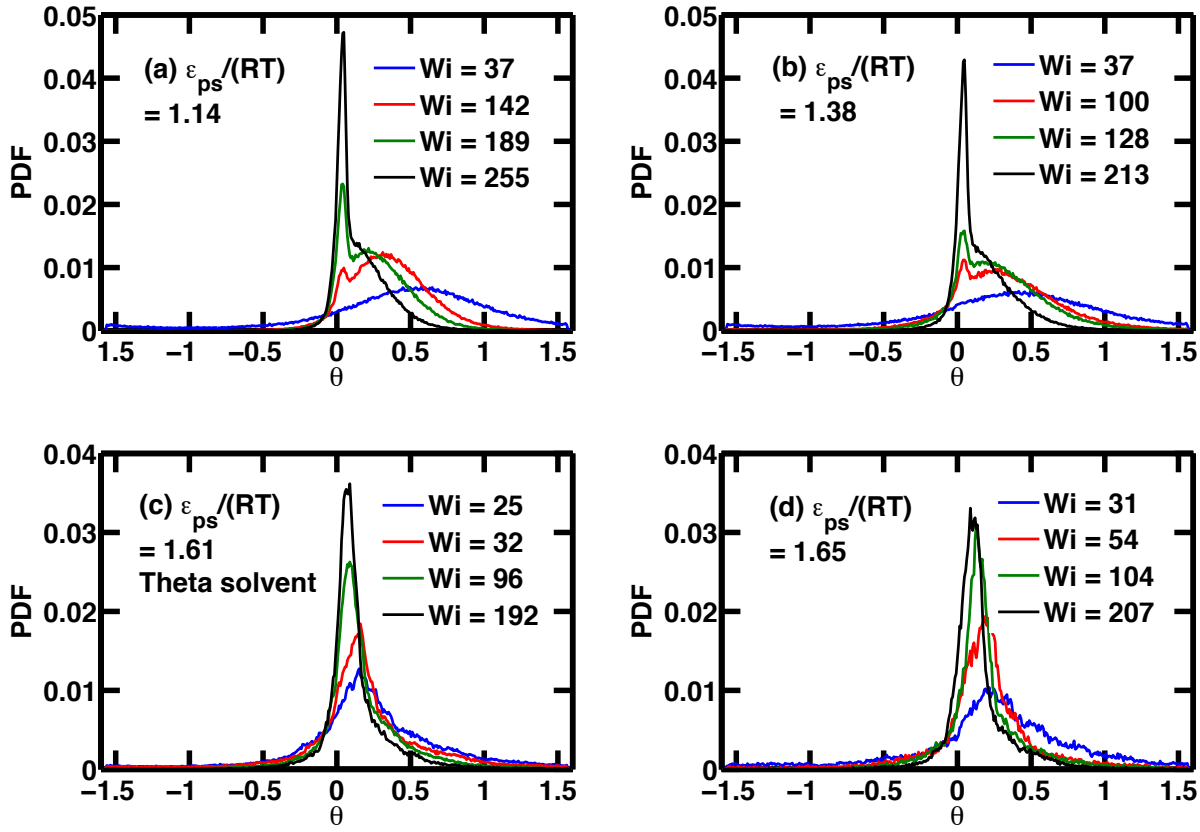

Figure 3.8: Probability distribution function (PDF) of orientation angle θ at (a) $\frac{\varepsilon_{ps}}{RT} = 1.14$, (b) $\frac{\varepsilon_{ps}}{RT} = 1.38$, (c) $\frac{\varepsilon_{ps}}{RT} = 1.61$, a theta solvent condition, and (d) $\frac{\varepsilon_{ps}}{RT} = 1.65$, a good solvent condition. In poor solvents, double peaks are observed at $Wi > Wi_0$, (a) $Wi_0 = 93$ and (b) $Wi_0 = 43$. The peak at positive θ indicates the chain tumbles and rotates and the peak at $\theta = 0$ shows the chain tends to stay in extended condition, which proves that the chain may collapse without tumbling.

In a theta and good solvent, the tumbling frequency, which is used to characterize the tumbling dynamics, follows a power-law relation with Wi, with the power-law exponent discovered to be 0.66 in experiments[74].

In this chapter, we calculate the characteristic frequency of orientational fluctuations ω_0, by fitting the x component of the radius of gyration tensor, G_{xx}, to the position autocorrelation function $C(t)$ of a damped linear oscillator[113]:

$$C(t) = A^2 \cos(\omega_d t + \psi) \exp(-\Gamma t) \quad (3\text{-}4)$$

In the above equation, Γ is the damping rate, ω_d is the damped frequency, ψ is the phase lag, and the tumbling frequency ω_0 is calculated by:

$$\omega_d{}^2 = \omega_0{}^2 + \Gamma^2 \quad (3\text{-}5)$$

The motion of the chain is dissipative and a consequence of external forcing, which features shared by narrow band processes. This provides the rationale for evaluating ω_0 by invoking the analogy to a damped oscillator.

In a theta and a good solvent, the predicted ω_0, follows a power–law relationship with Wi, with a power–law exponent of 0.67, which is in agreement with experiments[74]. Figure 3.9 shows the variation in ω_0 as a function of Wi at different solvent conditions. In a poor solvent, when $Wi < Wi_0$, the chain dynamics is dominated by tumbling events. Hence, ω_0 obeys a power-law relationship with respect to Wi. The power law exponent is the same as the one predicted for a

theta solvent. At higher Wi, the abovementioned collapse mechanism becomes the prominent determinant of chain dynamics. Consequently, ω_0 decreases as a function of increasing Wi_0.

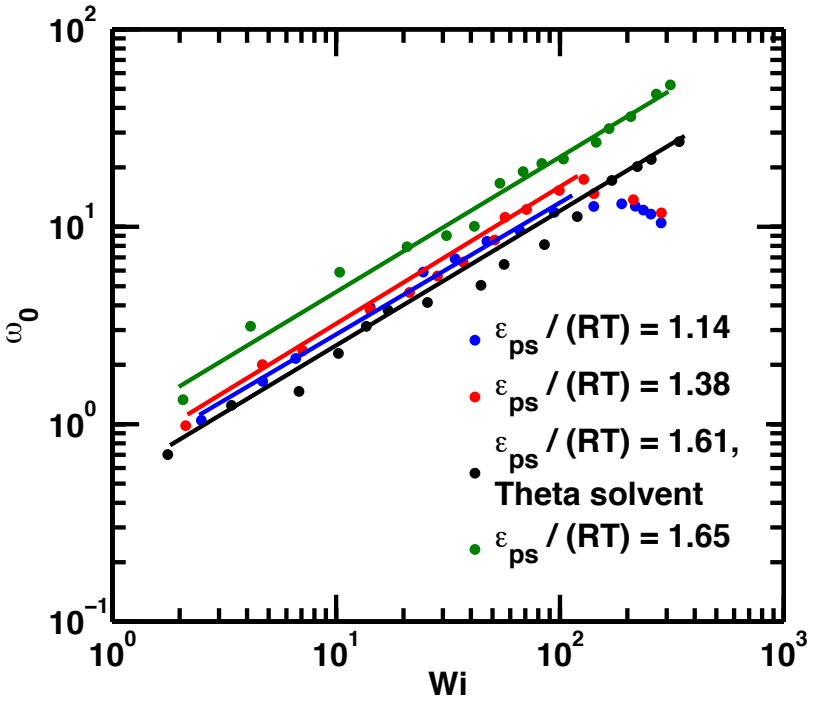

Figure 3.9: Tumbling frequency ω_0 vs. Wi at different solvent conditions. In theta and good solvents, ω_0 and Wi follows a power law relation with the theoretical exponent at 2 / 3. In poor solvents, below Wi_0, ω_0 and Wi also follows a power law relation with the exponent converges to the one predicted to the theta solvent. At $Wi > Wi_0$, the collapse dynamics inhibits the tumbling dynamics, thus the tumbling frequency decreases. The power law exponents γ predicted from the simulations are: $\frac{\varepsilon_{ps}}{RT} = 1.14$, $\gamma = 0.68$; $\frac{\varepsilon_{ps}}{RT} = 1.14$, $\gamma = 0.68$ $\frac{\varepsilon_{ps}}{RT} = 1.38$, $\gamma = 0.69$; $\frac{\varepsilon_{ps}}{RT} = 1.65$, $\gamma = 0.67$.

3.4 Conclusions

In this work we use coarse-grained molecular dynamics (CGMD) simulations with MARTINI force field and built polymer-solvent systems with explicit solvent mediated interactions. Lennard-Jones (LJ) potential is used to represent polymer-solvent interactions. The potential well depth, ε_{ps}, of the LJ potential has been used as a parameter to tune polymer-solvent interactions. We have shown that our simulations are capable of accurately predicting the equilibrium properties of polymer chains in good, theta and poor solvents, consistent with Flory theory[82].

Polymer size and relaxation time are influenced by solvent quality. When $\varepsilon_{\mathrm{pp}}$, which is the potential well of LJ potential describing attractive intrachain interactions, is greater than $\varepsilon_{\mathrm{ps}}$, the polymer assumes as a dense globular shape. When $\varepsilon_{\mathrm{ps}} \sim \varepsilon_{\mathrm{pp}}$, solvent molecules start to "pull" the monomers apart from one another and the size of the chain begins to increase. When $\varepsilon_{\mathrm{ps}}$ is close to theta condition, the attraction between the solvent molecules and the polymer chain leads to a sharp linear increase in the chain size.

The polymer chain starts to stretch at $Wi = 1$ in a theta or good solvent. In a poor solvent, the net attractions among polymer beads prohibit the chain from stretching until sufficient hydrodynamic work is expended to overcome the attractive interactions. Thus, it requires larger hydrodynamic force for the chain to stretch. The coil-stretch transition occurs at a critical Weissenberg number, Wi_0 follows an inverse linear relationship with respect to $\varepsilon_{\mathrm{ps}}$ and converges to unity in theta and good solvent condition.

Orientation fluctuations of polymer chains have been extensively studied in both experiments and simulations. In theta and good solvents, when polymer is subjected to a simple shear flow with $Wi > 1$, the chain goes repeated coil-stretch transitions. In poor solvents,

the chain cannot be fully extended when $Wi < Wi_0$ due to the strong repulsion with the solvent molecules. However, the chain is still able to partially extend, tumble and rotate because of the rotational component in the shear flow. When $Wi > Wi_0$, the chain aligns to the flow and stretches, but the attractive forces among the monomers "push" the chain and make it collapse without tumbling. We have quantified the orientation fluctuations by analyzing the PDFs of chain orientation. Finally, the orientational fluctuations ω_0 has been shown to follow a power-law relationship with Wi at different solvent conditions. The power-law exponent converges to the one predicted for theta-solvent conditions by experiments and BD simulations[1, 74, 75]. At $Wi \gg Wi_0$ in poor solvents, ω_0 decreases because the chain may also collapse without tumbling.

Chapter 4

Multi-chain system

4.1 Introduction

When multiple polymer chains are present in the solution, a given chain does not only interact with the solvent molecules around it, but it may also interact with neighboring chains. At very low concentrations, each polymer chain is well separated and acts as a random coil. When the concentration increases to a threshold one, the chains start to interact among one another, this concentration is defined as the overlapping concentration c^*[32]. Solutions with concentration $c < c^*$ are considered dilute under equilibrium conditions while those with $c > c^*$ are termed semidilute. In the dilute regime, a polymer chain cannot "feel" the presence of other polymer chains and intra-chain hydrodynamic interactions are important.

The properties and dynamics of multi-chain system have a wide range of applications ranging from transport of biological cells[114] to turbulent drag reduction in fluid flows. Moreover, the viscoelastic behaviors of polymer chains in equilibrium and non-equilibrium conditions play important roles in polymer processing. For example, the elastic energy stored by the polymer during the flow can be eliminated by the relaxation and creation of new surface at the die exit, if the material is not strong enough, extruding skin fracture such as sharkskin can be discovered[6].

The basic physics of dilute and semidilute polymer solutions in equilibrium has been widely studied in theory and experiments. In the dilute regime, a polymer chain cannot "feel" the

existence of other polymer chains, hydrodynamic interactions (HI) are important, so the scaling law is characterized by Zimm model. The scaling relation between zero-shear viscosity of the polymer solution and the polymer concentration can be predicted by Eq. (4-1):

$$\eta_0 = 1 + k'[\eta]C + \cdots \quad (4\text{-}1)$$

where k' is the Huggins' constant and $[\eta]$ is the intrinsic viscosity. In semidilute regime, the dynamics becomes more complex due to the intermolecular excluded volume interactions. de Gennes[115] describes polymer chains in this regime using the concept "blobs". A polymer chain is consisted of a number of blobs each has g monomers and a radius of ξ. Inside each globe, the dynamics follows the predictions of the Zimm model. On length scales larger than ξ, due to the chain overlap, the hydrodynamic interactions and excluded volume effects are screened, thus Rouse model is applied. The scaling relation between zero-shear viscosity η_0 and the polymer concentration C is shown to follow a power-law relation[32, 116, 117]:

$$\eta_0 \propto C^{1/(3\upsilon-1)} \quad (4\text{-}2)$$

where υ is the same exponent between the polymer size and number of monomers N, i.e., $\upsilon = 0.5$ for theta solvent and $\upsilon = 0.588$ for good solvent.

In poor solvents, the repulsion between polymer chain and the solvent molecules lead the chain to form a dense globe, as has shown in Chapter 3. In dilute regime, HI is important and the scaling relations can still be predicted by Zimm model. Takahashi *et al.*[118] have observed in experiment that a linear relation between η_0 and C of poly(α-methylstyrene) in a poor solvent,

which corresponds to Zimm model prediction for scaling law of polymer solution in theta and good solvents. In semidilute regime, since the polymer chains start to interact and they like each other better than they like solvent molecules, phase separation may be observed. Gandhi and Williams[119] have observed that η_0 increases faster in poor solvent systems than that in good solvent systems and eventually η_0 becomes much greater in poor solvent systems. They believe this behavior is due to the polymer aggregation in poor solvents. Other literatures[118, 120] have also mentioned power-law relations between η_0 and C in semidilute regime. While experimental approaches are promising, it is harder to visualize how chains interact with each other and with solvent molecules, thus provide theory to explain the data acquired. Moreover, few literatures have quantitatively examined the exponent of the power-law relation. Thus applying MD techniques to study such topic becomes critical.

Most polymeric fluids exhibit non-Newtonian rheological properties such as shear-thinning, shear-thickening or yield stress in non-equilibrium conditions. Non-Newtonian rheology could lead to instabilities in polymer processing operations such as melt fracture and sharkskin in extrusion processes[121]. Most polymer solutions show shear - thinning in uniform steady shear flow, i.e., the effective viscosity of polymer solution reduced upon shear. Many phenomenological models have been used to describe the shear - thinning behaviors of polymer solutions. The power-law model, which predicts that the apparent viscosity η follows a power-law relation with Wi, the Weissenberg number defined in the previous chapters, with the exponent between-0.4 to-0.9 for a typical polymeric liquid[122]. The Carreau-Yasuda model[122], which takes into account η_0 and the viscosity at shear rate approaches infinity (η_∞), can be represented by Eq. (4-3):

$$\eta = \eta_\infty + (\eta_0 - \eta_\infty)(1 + (Wi)^a)^{\frac{n-1}{a}} \quad (4\text{-}3)$$

where η_∞ is set to be equal to η_{solvent} and $a = 1.2$[123] is a dimensionless parameter that describes the width of transition between zero-shear region and the power law region.

While this topic has been widely studied in experiments for different polymeric liquids. Fewer studies have applied simulation methods on the topic. Likhtman *et al.*[124] have used molecular dynamics (MD) and studied the stress relaxation for polymer melts. Baig *et al.*[125] have applied non-equilibrium molecular dynamics (NEMD) and presented results about the structural and topological properties of linear polyethylene melt. They have also observed shear-thinning behavior at high shear. However, these literatures fail to provide details on the rheological properties of polymeric liquids. Moreover, polymer solutions, where different solvent-chain interactions may affect the properties, have not been studied widely.

In this chapter, we examine the concentration influence on the dynamic and rheological behaviors of polymer chains. We show that our simulations can correctly predict the scaling relations between η_0 and polymer concentration C. Solvent quality influence on the exponents of the scaling relation is also reported. By using non-equilibrium molecular dynamics, we show that our simulations can accurately predict shear-thinning behaviors. Phenomenological constitutive models are parameterized using simulation data and the results are compared with experimental observations.

4.2 Simulation method

Multiple PEO chains with $N = 45$ are placed in simulation boxes to model PEO solutions with different concentration. Figure 2.4 has shown that persistent length P converges at $N = 45$,

thus it is safe to assume the polymer chains are linear flexible polymers. MARTINI force field is applied with the detail described in Chapter 2.

The overlapping concentration c^* is calculated by Eq. (4-4):

$$c^* = M_{\mathrm{w}}/[\left(\frac{4\pi}{3}\right) {R_{\mathrm{g}}}^3 N_A] \quad (4\text{-}4)$$

where M_{w} is the molecular weight, R_{g} is the radius of gyration of the chain at equilibrium, and N_{A} is the Avogadro number. A dimensionless polymer concentration $C = c/c^*$is used below to report results. To study polymer concentration c influence on zero-shear viscosity η_0, shear viscosity η, first and second normal stress coefficients Ψ_1 and Ψ_2, c ranges from 0.06 to 3.87. To study the influence of solvent quality, c ranges from 0.36 to 2.24. The solvent quality tuning parameter, i.e., $\varepsilon_{\mathrm{ps}}$ in the LJ potential between polymer chain and the solvent, is modified according to Table 3.1 to mimic different solvent conditions. Details can be found in Chapter 3. Periodic boundary condition PBC is applied to all dimensions with the size of each dimension large enough to avoid simulation artifacts.

Zero-shear viscosity η_0 is calculated by computing the temporal autocorrelation of the shear stress τ_{xy} using Green-Kubo formula[126]:

$$\eta_0 = \frac{V}{kT}\int_0^\infty dt < \tau_{\mathrm{xy}}(0)\tau_{\mathrm{xy}}(t) > \quad (4\text{-}5)$$

where *V*, *k* and *T* denote the volume of the simulation box, Boltzmann constant and the absolute temperature respectively. Further, the specific viscosity η_{sp} is defined as

$$\eta_{\mathrm{sp}} = \frac{\eta_0 - \eta_{\mathrm{solvent}}}{\eta_{\mathrm{solvent}}} \quad (4\text{-}6)$$

where η_{solvent} is the solvent viscosity determined from simulations of a pure solvent.

Shear viscosity η and first and second normal stress difference N_1 and N_2 are defined as:

$$\eta = \frac{\tau_{\mathrm{xy}}}{\dot{\gamma}} \quad (4\text{-}7)$$

$$N_1 = \tau_{\mathrm{yy}} - \tau_{\mathrm{xx}} = \Psi_1 \dot{\gamma}^2 \quad (4\text{-}8)$$

$$N_2 = \tau_{\mathrm{zz}} - \tau_{\mathrm{yy}} = \Psi_2 \dot{\gamma}^2 \quad (4\text{-}9)$$

τ_{ij} are components of stress tensor with $i, j = x, y, z$, $\dot{\gamma}$ is the shear rate defined in the previous chapters, Ψ_1, Ψ_2 are first and second normal stress difference coefficients, respectively.

4.3 Results and discussion

4.3.1 Zero-shear viscosity dependence on the concentration

Figure 4.1 shows the variation of η_{sp} with increasing C in a theta solvent. A linear relationship is observed in the dilute regime. In the semi-dilute regime (C > 1), η_{sp} increases more rapidly with increasing C with a power law exponent of 1.94 ± 0.01. These results are consistent with the abovementioned theoretical predictions[32] and experimental observations by Ebagninin *et al*[127] for aqueous PEO solution. They measured η_{sp} of PEO solution at different molecular weight and showed that the exponents in the η_{sp}- C power-law relationship are 1 and 2 for the dilute and semi-dilute regimes, respectively.

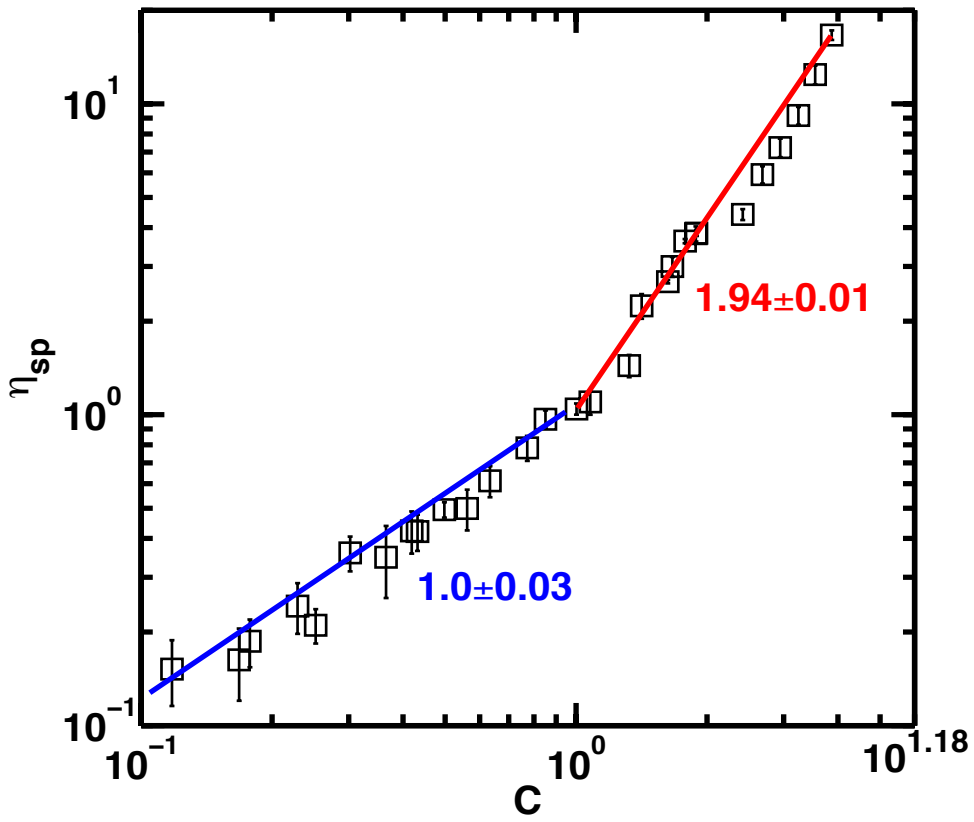

Figure 4.1: Specific viscosity $\boldsymbol{\eta_{sp}}$ dependence on concentration. A linear relation can be found in dilute regime and a power relation is shown in semidilute regime

Figure 4.2 shows the results of a linear regression analysis of η_0 vs. C in the dilute regime. The value of η_0 extrapolated to $C = 0$, i.e., η_{solvent}, equals one half of $\eta_0(c^*)$, consistent with the theoretical prediction that $\eta_0(c*) = 2\eta_{\text{solvent}}$.[128]

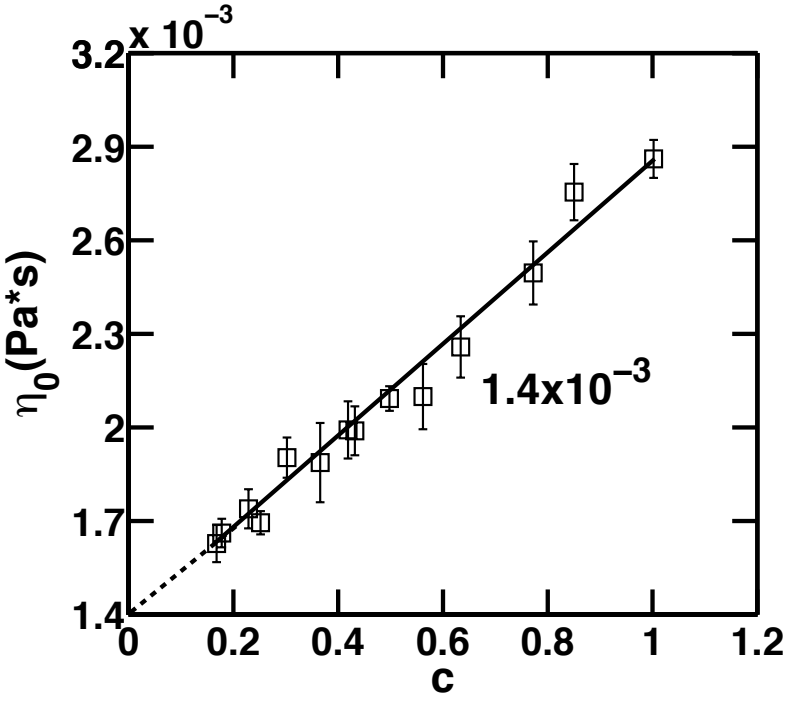

Figure 4.2: Linear regression of $\boldsymbol{\eta_0}$ and $\boldsymbol{c}$ shows equal slope and intercept, which proves that $\boldsymbol{\eta_0 = 2\eta_{solvent}}$ at $\boldsymbol{c}^*$.

4.3.2 Solvent quality influence on zero-shear viscosity

As described in Chapter 3, when polymer chain is in different solvent medium, the configurations are affected by the solvent quality. In theta solvents, the polymer chain behaves like a random coil. In good solvents, the polymer chain swells due to positive excluded volume effects. In poor solvents, the chain acts as a globe. The size of the globe depends on the extent of the repulsion between the chain and the solvent molecules. When there is more than one chain in the system, the chains interact with each other. As mentioned in the introduction, in the dilute regime, the chain each acts as a random coil that does not interact with other chains. In semidilute regime, polymer chains interact with each other, thus HI and excluded volume effects

are screened. In poor solvents, due to the repulsion between the chain and the solvent molecules, the chains tend to aggregate together, thus phase separation may be observed. Figure 4.3 shows systems of PEO in different solvent conditions with $c = 0.98$. In a poor solvent, all the chains aggregate together and a clear phase separation is observed. In a theta solvent, the chain acts as random coils and start to interact with each other. In a good solvent, chains extend more than that in the theta solvent.

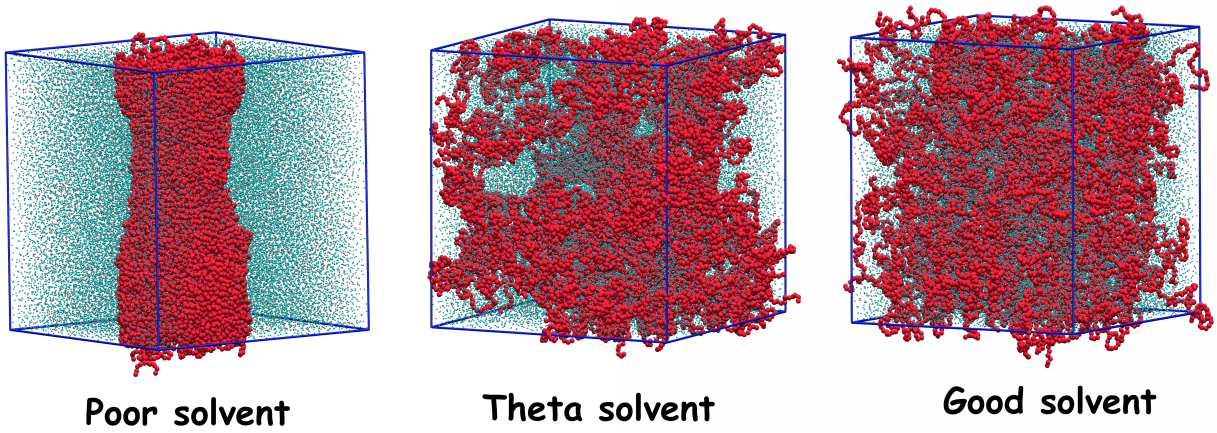

Figure 4.3: Systems of PEO in different solvent at $c = 0.98$. The red chains are PEO and blue dots are water beads. In a poor solvent, all PEO chains aggregate together due to repulsion between PEO and solvent, thus we observe phase separation. In theta solvent, the chains act as random coil. In good solvent, the chains swell due to the attraction between PEO and solvent.

η_0 versus c of PEO in different solvent systems in the dilute regime is plotted in Figure 4.4. η_0 converges to the one predicted by Zimm model for theta solvent, as shown in Eq. (4-1). The

result is understandable for PEO in good solvent: the chain each forms a swelled globe with the size slightly larger than that in theta solvent, yet there is no polymer-polymer interactions in the solution.

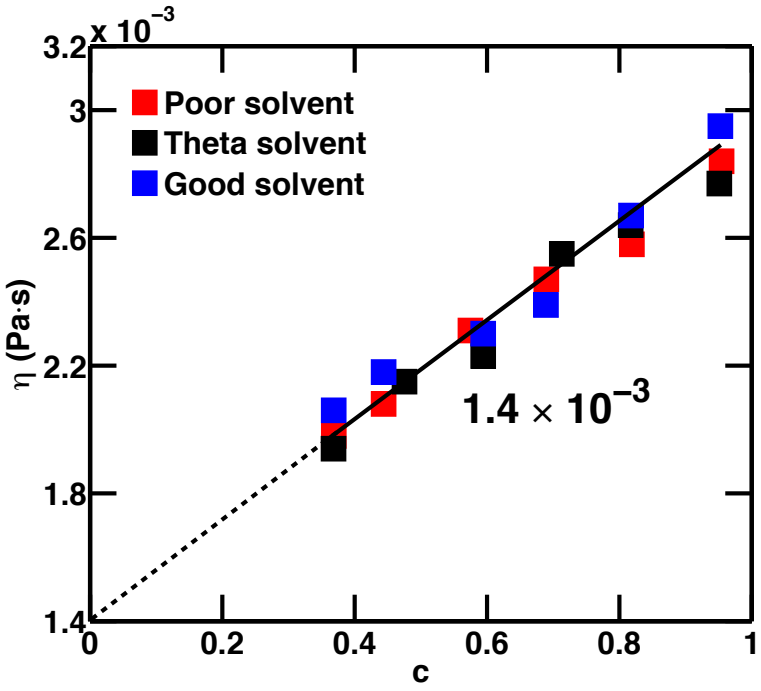

Figure 4.4: Zero shear viscosity η_0 vs. c for PEO at different solvent conditions in dilute regime, linear regression converges to the one predicted at theta solvent

In poor solvent, since aggregation may occur, each aggregated clusters may be viewed as one large globe (Figure 4.5), with length scale larger than the globe, HI still plays an important role, thus the Zimm model is still applicable.

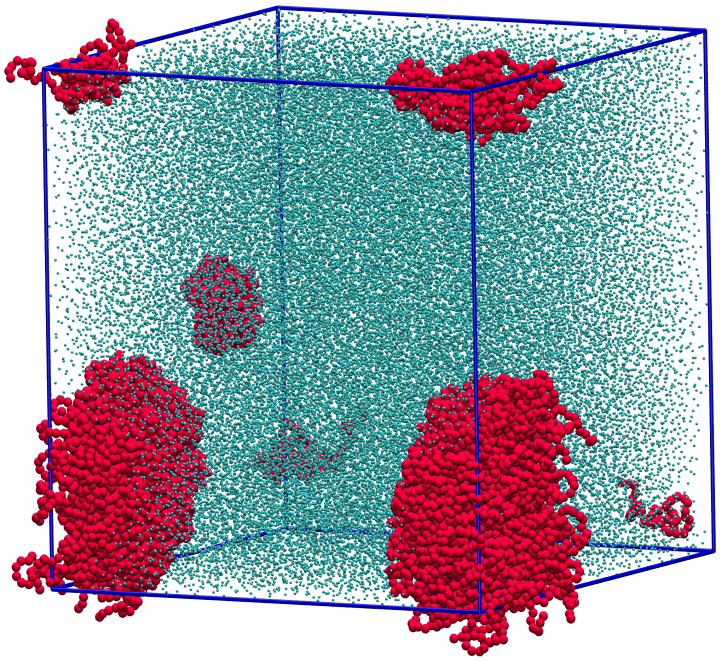

Figure 4.5: PEO in poor solvent at $\boldsymbol{c = 0.54}$

In semidilute regime, de Gennes[32, 115] predicts a power law relation between η_0 and c (Eq. (4-2)), for polymers in theta and good solvents. In poor solvents, Gandhi and Williams[119] observed that η_0 increases faster than that in good solvent. Figure 4.6 plots log (η_0) and log (c) of PEO in different solvent systems. Power law relations can be discovered for all three solvent systems. The power law exponent decreases with the improvement of solvent quality, i.e., smallest for PEO in good solvent and largest for PEO in poor solvent. The exponent for PEO in good solvent is slightly overpredicted in simulation than from Eq. (4-2). However, Pan *et al.*[129] have conducted experiments on DNA chains and shown that the exponent in good solvent ranges from 1.5 to 1.9 depending on different solvent quality. Thus our prediction is still in the reasonable range. In poor solvent, the exponent is shown to be larger than that in theta solvent,

but we didn't observe significant increment in the exponent. This may because $N = 45$ is still considered as short polymer chains, and the chain may not form entanglements[123, 130], thus significant viscosity increment is not observed.

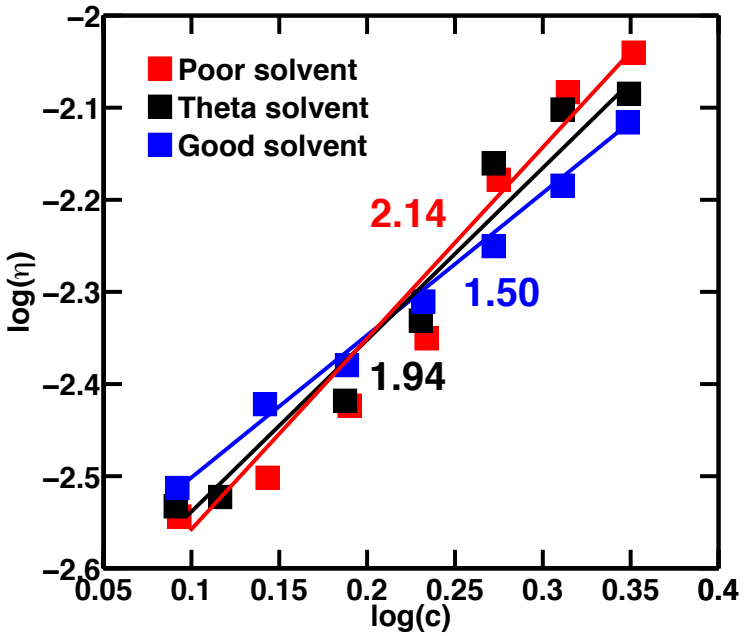

Figure 4.6: Zero shear viscosity η_0 vs. c for PEO at different solvent conditions in semidilute regime. Power law relation can be observed in all three conditions.

4.3.3 Shear thinning of PEO in uniform steady shear

PEO has been observed to exhibit shear-thinning behaviors[131]. While the dynamics of single polymer chain has been widely studied, few simulations studies have been carried on the

rheological properties of polymeric liquids. Figure 4.7 shows the material functions of PEO solution for $C = 1.54$. At low Wi, shear stress τ_{xy} increases linearly. At higher shear rate, η decreases with increasing Wi. The magnitudes of N_1 and N_2 increases with increasing Wi while those of Ψ_1 and Ψ_2 decreases. The magnitudes of N_1 and Ψ_1 are orders larger than those of N_2 and Ψ_2, respectively, which is quite typical for polymeric liquids [122].

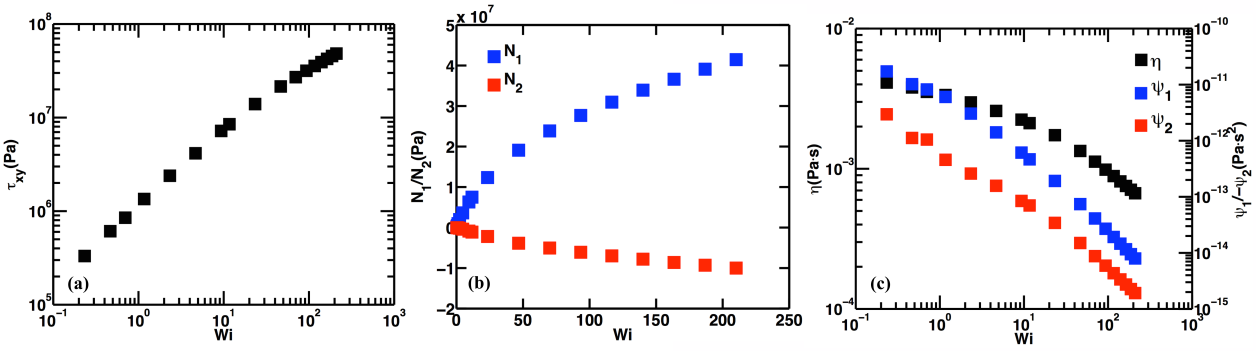

Figure 4.7: Material functions of polymer solution at $\boldsymbol{c = 3.87}$: (a) Shear stress (b) First and second normal stress difference (denoted as $\boldsymbol{N_1}$, $\boldsymbol{N_2}$, respectively); (c) shear viscosity $\boldsymbol{\eta}$, first and second normal stress difference coefficients $\boldsymbol{\Psi_1}$ and $\boldsymbol{\Psi_2}$, respectively.

It is interesting to explore whether CGMD simulation data could be parameterized using simple phenomenological models utilized in rheological characterization in industry. Plots of log (η) vs. log (Wi) are shown in Figs. 4.8(a) and 4.8(b) along with fits to the power law and Carreau-Yasuda models for $Wi > 1$ for three different concentrations. The latter model is given by Eq. (4-3). Both models fit the simulation data well. Ebagninin et al.[127] observed that for PEO aqueous

solution with molecular weight $4\times10^6 g/mol$, the extent of viscosity decrease increases with increasing PEO concentration. The magnitude of the slope in the power-law model decreases with increasing C signifying that shear thinning is more pronounced at higher polymer concentrations, which agrees with the abovementioned experimental observations. Heo and Larson[123] fitted rheological data for λ-phage DNA solution to Carreau-Yasuda with $a = 1.2$ and obtained n ranges from 0.15 to 0.6 for different λ-phage DNA concentration. The parameterization from our simulation data has shown a similar range of n, which indicates that CGMD can reliably predict shear rheology of linear flexible polymer solutions.

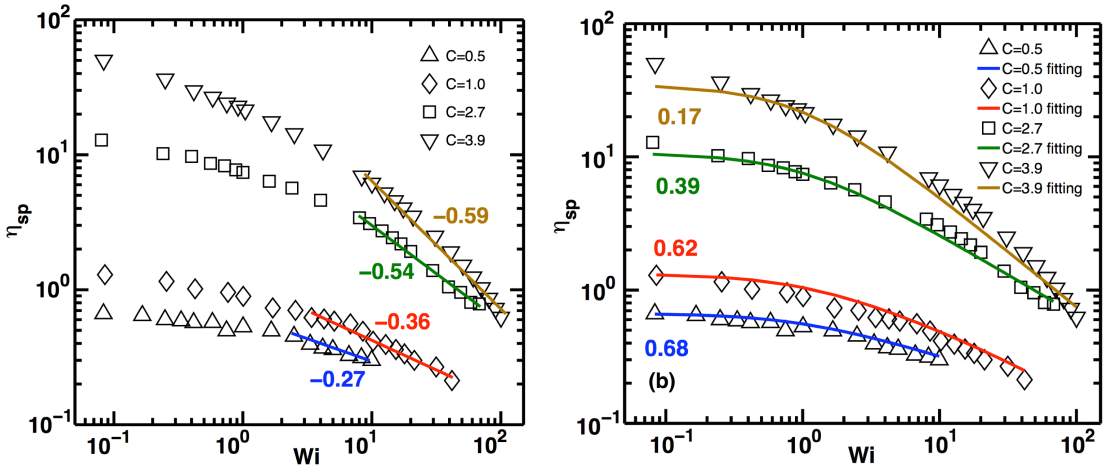

Figure 4.8: (a) log-log plot of shear viscosity and Wi at $Wi > 1$ for c = 0.50, 1.08, 2.68 and 3.87. The magnitude of the power law coefficient increases with the increases concentration and approaches experimental value; (b) Parameterization of Carreau-Yasuda model. The curve at each concentration is the fitted curve. n for each curve is labeled and is decreasing with the increasing concentration

4.3.4 Solvent quality influence on shear-thinning behaviors of polymer solutions

Figure 4.9 plots η versus Wi of PEO in different solvent conditions at different concentrations. In all three concentrations, the poor solvent cases have shown to have lowest η_0 values, while the good solvent cases have shown to have highest η_0 values, which corresponds the result from Green-Kubo relations explained in Section 2. It is noticeable that η_0 in theta and good solvents only show slight difference in log plots. This is because η_0 in good solvents does not increase as faster as that in theta solvents, thus the difference of η_0 between good solvents and theta solvents is not significant in semidilute regime (Figure 4.6), and is further diminished by the log plots.

The Newtonian plateau is shown to be wider in a poor solvent than that in a theta and a good solvents. This is because the chain will not extend if $Wi < Wi_0$, as explained in Chapter 3. The exponents of the power-law regime converge in different solvent systems. Pan and Manke[100] have used dissipative particle dynamics (DPD) and predicted the similar results.

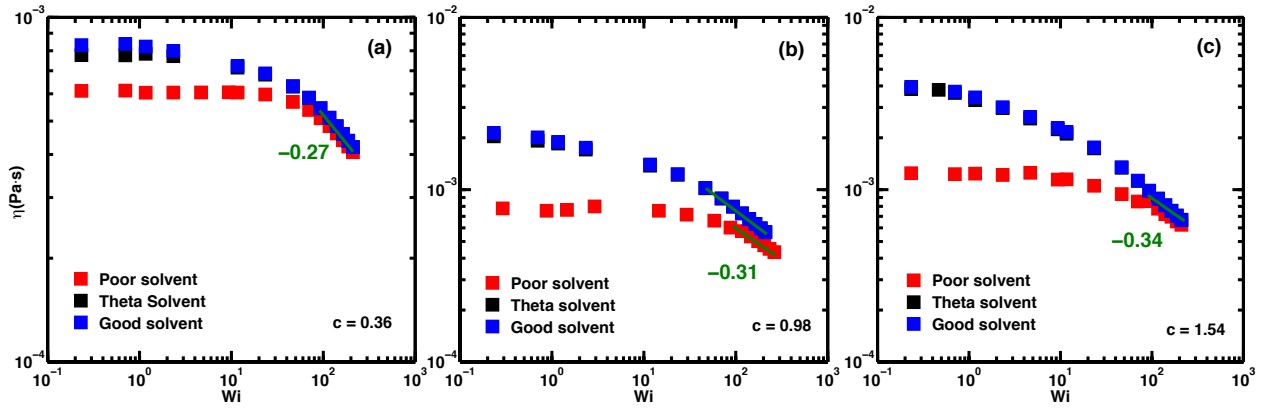

Figure 4.9: Viscosity η of PEO in different solvent condition at c =0.36, 0.98 and 1.54. η converges in theta and good solvent. η in all three conditions show lower values in poor solvent

Figure 4.10 shows the snapshots of PEO in different solvent conditions at $c = 0.98$ and $Wi = 210$. In all three conditions, the chains are fully extended. It is interesting to notice that the systems look alike for PEO in theta and good solvent conditions, while in poor solvents, aggregation can still be observed. It is possible that the power law exponent is more related to the degree of extension of the chain rather than the solvent quality at $Wi > Wi_0$.

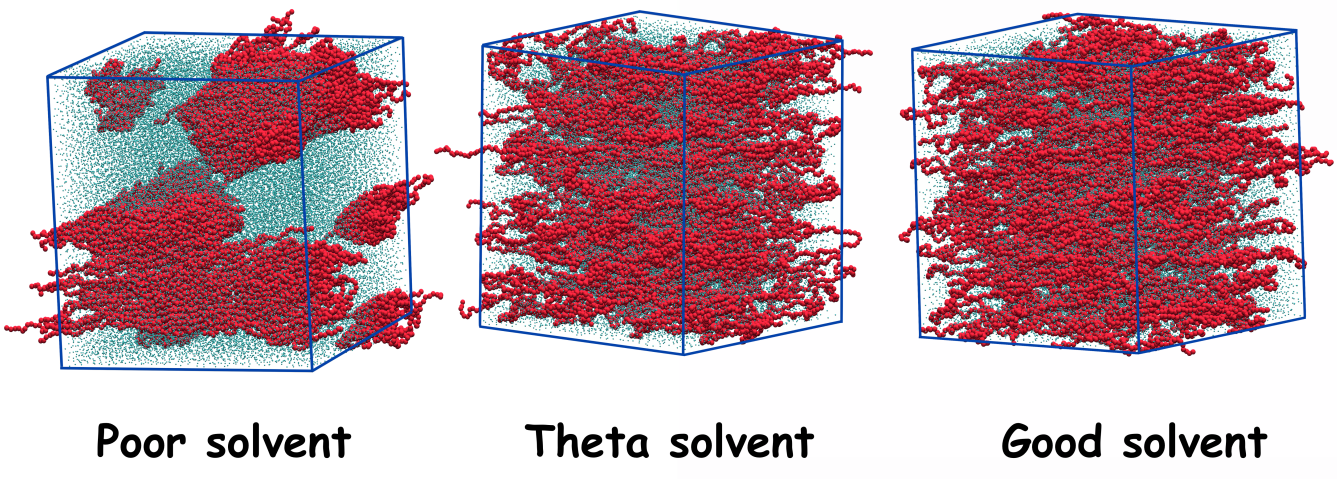

Figure 4.10: Snapshots of PEO in different solvent conditions at $\boldsymbol{c = 0.98}$ and $\boldsymbol{Wi = 210}$.

Figure 4.11 and 4.12 plot first normal stress coefficient Ψ_1 and second normal stress coefficient Ψ_2 of PEO in different solvent systems. Both Ψ_1 and Ψ_2 are shown to decay faster in poor solvent than in theta and good solvent systems. Ψ_2 seems to converge at high shear. This result corresponds to Pan and Manke's[100] predictions using DPD.

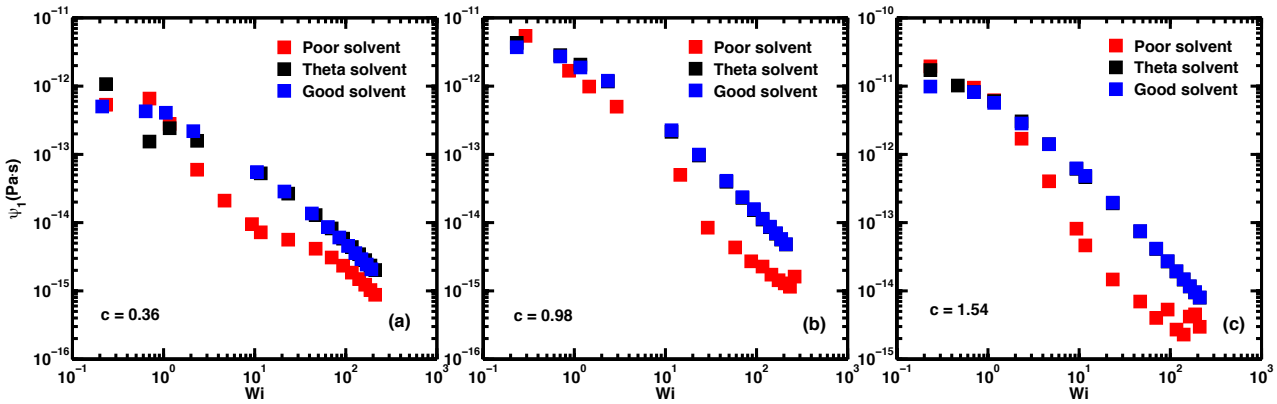

Figure 4.11: First normal stress coefficient Ψ_1 of PEO solutions with different concentration at different solvent conditions

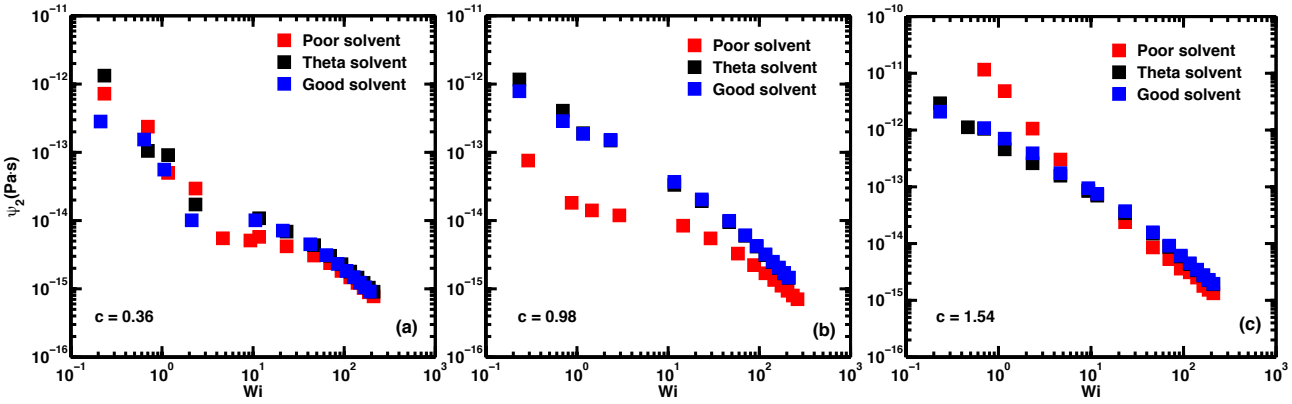

Figure 4.12: Second normal stress coefficient Ψ_2 of PEO solutions with different concentration at different solvent conditions

4.4 Conclusion

In this chapter, we have studied the rheological properties of PEO solutions. We have first examined the zero-shear viscosity dependence on polymer concentration. A linear relationship is predicted for polymer in dilute solutions and linear regression predicts $\eta_0 = 2\eta_{solvent}$ at overlap concentration c^*. This result agrees with the Zimm model prediction for the dilute solution. In the semidilute regime, polymer chains interact with each other, at length scale greater than the pervaded volume of the chain, HI and excluded volume effects are screened. Rouse model predicts that η_0 follows a power law relation with c, with the power-law exponent equals to 2 for theta solvent, which is accurately predicted by our model.

Next, we discuss the solvent quality influence on the scaling relation between η_0 and c. Linear relations can be observed in poor solvent and good solvent systems as well. Linear regression to both systems have shown to converge to the one predicted for the theta solvent. In

good solvents, polymer chains have larger pervaded volume, but each chain still acts as random coil thus Zimm model is still applicable. In poor solvents, several chains aggregate to a large globe, and for length scales larger than the globe sizes, chains don't interact with other chains so HI still plays an important role. In the semidilute regime, η_0 and c follows power-law relations for all three solvent conditions. The power-law exponent increases when the solvent quality changes from poor to good. In good solvent condition, the predicted exponent is slightly larger than the prediction from Rouse model (Eq. (4-2)). However, our prediction is in good agreement with the experiment results by Pan *et al.* [129]. In poor solvent, polymer aggregation may be the reason that the exponent is larger than that in the theta solvent.

Shear-thinning phenomenon is observed by applying non-equilibrium molecular dynamics (NEMD). Fitting the simulation data to phenomenological models have shown to be in good agreements with experimental results. The exponent in the power-law model and the coefficient n in the Carreau-Yasuda model both increase in magnitude with the increasing polymer concentration.

In poor solvent, a wider plateau is observed. This is because the chain will not extend when $Wi < Wi_0$, as explained in Chapter 3. Power-law region has been shown to converge in different solvent systems at high shear. It is possible that the power law exponent is more related to the degree of extension of polymer chains then to the solvent quality. First and second normal stress coefficient Ψ_1 and Ψ_2 collide in theta and good solvent. In poor solvent, both Ψ_1 and Ψ_2 decay faster.

Chapter 5

Polymer chain dynamics under geometric confinement

5.1 Introduction

Configuration dynamics of macromolecules in confined geometries, e.g., a flexible polymer of equilibrium radius of gyration R_{g0} transported through a tube diameter ~ R_{g0}, have generated much interest among scientists and engineers. in fluids in confined geometries have been in great interest in industry Much of the excitement in this area in the past two decades have been sparked by the emergence of microfluidics and "lab on a chip" technologies in which biological macromolecules such as DNA and proteins are routinely processed for assays[132, 133]. Moreover, many physiologically relevant transport and signaling processes involve the diffusion of biomacromolecules across porous membranes, tissues and biofilms[71, 134]. Furthermore, nanoparticle-polymer complexes are being developed as means for targeted drug delivery and biomedical imaging for treating diseases ranging from cancer to Alzheimer's[135, 136]. Such nanocarriers often have to navigate pores/channels in the vasculature or tumors. The pore/channel diameters are often comparable to the characteristic size of the macromolecule itself. Such geometric confinement reduces the number of accessible configurations compared to those available for a polymer in bulk solution, thereby decreasing the conformational entropy of the polymer chain.

For decades, various theories have been developed to understand the behavior of polymer chains under confinement. "Confinement" implies that the motion of the chain is constrained in at least one spatial dimension. A typical example is a slit in which the polymer chain is constrained between two parallel walls in one dimension and if free to move in the other two[137]. The equilibrium configurations of the chain have been shown to be affected by the confinement. If the confinement length scale H (e.g., the distance between two walls of the slit) is larger than the equilibrium polymer size R_{g0}, the confinement has no effect on the configurations of the chain[138]. If H is comparable than R_{g0}, the chain expands in the unconfined dimensions due to the excluded volume interactions[40, 41, 137].

Flow deformation introduces an additional fascinating facet to the configurational dynamics of confined chains. Experiments show that when no-slip walls are present, confinement can amplify the influence of hydrodynamic lubrication forces, resulting in chain migration and the formation of depletion layers. Agarwal *et al.* [39] have discovered that flexible polymer chains migrate away from single wall under shear and lead depletion layers close to the wall. Later other groups have also observed apparent depletion layers of confined dilute polymer under uniform steady shear[44, 138]. Seo *et al*.[45] have observed concentration depletion near the capillary wall when water-soluble polymers are under pressure driven flow. Zheng and Yeung[139] have discovered that when external force field is added, the polymer will move towards the wall in a pressure-driven flow. Modeling and simulation studies s have also predicted migration of flowing polymer chains under confinement. Usta *et al.* [47]have used lattice-Boltzmann method (LBM), which also incorporated a DLVO-like repulsion between the polymer chain and the wall. They predicted that when the ratio of the channel height H to R_{g0}, denoted by H_0, is greater than 5, i.e., $H_0 > 5$, the chain migrates towards the centerline of the flow. However, for $H_0 < 5$, the

chain was observed to move in the opposite direction, i.e., towards the wall. Hernandez-Ortiz *et al.* [138] have used Brownian dynamics simulations (BDS) and predicted FENE dumbbell polymer chain migrating away from single wall under steady shear. Jendrejack *et al.*[46] have simulated dilute DNA solution in pressure-driven flow in square microchannels using BDS and shown that polymer chains move towards centerline and the depletion layer increases with increasing average axial velocity. They have also shown that when hydrodynamics interactions between wall and polymer are neglected, the simulations predict that the chain moves towards the wall.

Many theories have been developed to explain such phenomena[48, 140, 141]. For example, Park *et al.*[42] have used kinetic theory and predicted that rigid polymer chains migrate away from the wall in rectilinear flow. They have also shown that a depletion layer is created in the flow and the thickness of which increases with the increasing shear rate. Recently, Ma and Graham[142] have developed a theory based on a dumbbell representation of polymer chain in which each moving bead is treated as a point force acting on the flow, and showed that the force generated by one bead of the dumbbell results in an upward motion of the other bead, and vice versa. This means that each bead will move away from the wall due to the velocity perturbation by the other bead. They have also mentioned that if the dumbbell's initial orientation is perpendicular to the wall, it continues to move towards the wall.

While the experimental as well as theoretical and computational studies mentioned above provide valuable insights into the mechanisms dictating the dynamics of polymer chains under confinement and/or in proximity to a solid wall, certain unresolved questions still remain. For instance, the effect of H_0, the ratio of R_{g0} to channel height H, seen in LBM studies have not been reproduced by BD simulations which utilize bead-spring or bead-rod models with sufficient degrees of freedom and incorporate HI. Moreover, chain dynamics is likely to be influenced by

solvent quality and polymer-wall interactions. Motivated by this, we have developed a CGMD simulation platform to study the dynamics of flexible polymer chains confined between two solid walls. The discussion in this chapter is limited to theta solvent conditions; however the simulations can be extended to incorporate explicit solvent quality effects, as demonstrated in Chapter 3 for bulk systems.

In this chapter, the effects of confinement on the equilibrium configurations of single flexible polymer chain in theta solvent are first examined. We show that polymer-wall repulsion increases in magnitude with the increasing degree of confinement. We will also show that increase in repulsion lead to the increment of chain size. The dynamics of the single polymer chain under uniform steady shear is then discussed. We show that the polymer chain tends to move toward areas with higher velocity, and the tendency of moving increases with the increasing shear rate. The mechanism of the migration of polymer chain under uniform steady shear is then explored.

5.2 Simulation method

A CG polymer model mimicking a PEO chain is used: see Table 2.1 for the model parameters. The simulation system consists of a single PEO chain with $N = 91$ immersed in an explicit solvent mediation that is confined between two walls separated by a gap H. The solvent-polymer interactions are parameterized to mimic a theta solvent condition (see Chapter 2). Periodic boundary conditions are applied only in the x (flow) and y (neutral) directions. The wall is simulated by a plane of LJ beads that is perpendicular to the z direction. As defined in Section 5-1, this can be treated as a slit-like confinement[137, 143]. The periodic lengths in x and y direction

are sufficiently large that interactions between distant images are negligible[47]. A schematic of a typical system is shown in Figure 5.1.

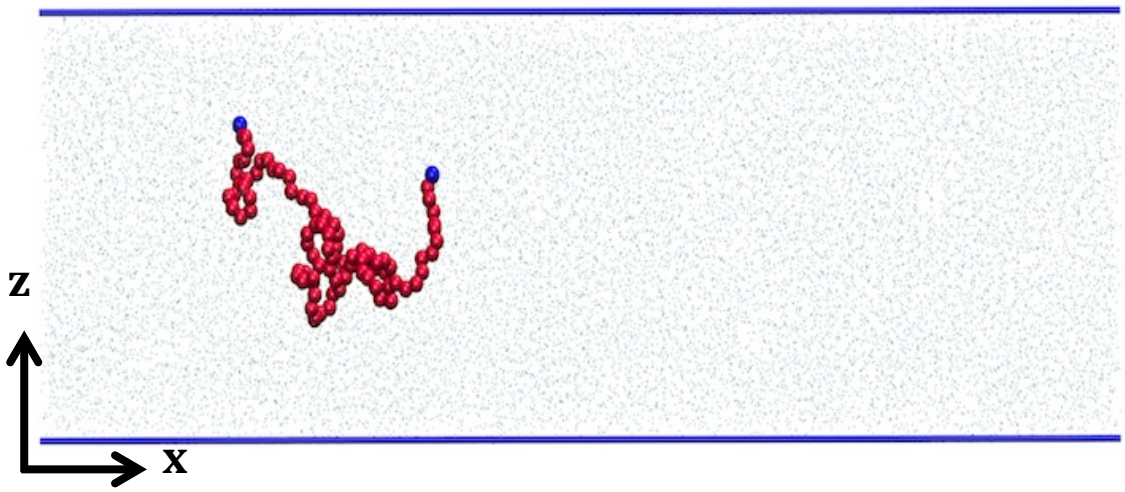

Figure 5.1: Single PEO chain with $N = 91$ confined in two parallel plates with $H_0 = 4$, which is categorized as a moderate confinement

Distance H between two walls is normalized by the radius of gyration R_{g0} of the chain at unconfined conditions, i.e., $H_0 = H/R_{g0}$. For $H_0 > 4$, the confinement effects are relatively weak, i.e., at equilibrium, $R \equiv R_g/R_{g0}$ is ~1. For $H_0 < 2$, confinement effect are sufficiently strong to cause significant chain extension in the $x - y$ plane. The moderate confinement regime corresponds to $2 \leq H_0 \leq 4$.

The polymer-wall (*pw*) and solvent-wall (sw) interactions are represented using LJ potential. The corresponding parameters are shown in Table 5.1. The parameters are chosen in such a way

to mimic a wall with almost no interaction other than excluded volume interactions with the polymer chain.

Table 5.1: LJ parameters for non-bonded interactions in the confined system

	ε(kJ / mol)	σ (nm)
Polymer - wall	0.001	0.15
Solvent - wall	0.001	0.15
Polymer - solvent	3.96	0.47

5.3 Results and discussion

5.3.1 Polymer-wall interactions

Figure 5.2 shows the average polymer-wall interaction V_{pw} versus H_0. V_{pw} is averaged over all beads. It is clear that when $H_0 > 4$, V_{pw} practically vanishes. However, when H_0 decreases, V_{pw} shows slightly positive value and increases with the decreasing H_0. This is expectable since the smaller the H_0, the higher the probability of finding polymer beads in the vicinity of the wall; thus the stronger the repulsion due to excluded volume effects.

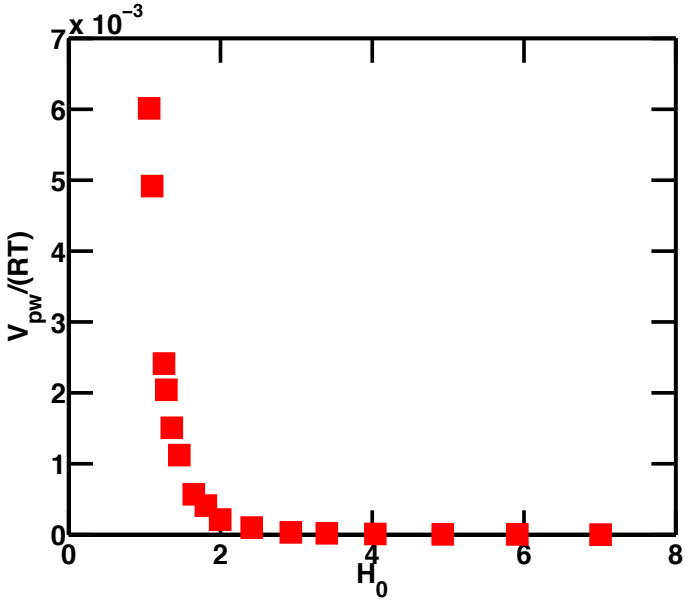

Figure 5.1: Average polymer-wall interaction V_{pw} vs. H_0. In weak confinement, i.e., $H_0 > 4$, V_{pw} is close to zero. V_{pw} starts to increase at moderate confinement regime and show sharp increment at strong confinement.

5.3.2 The chain configurations under confinement

We have shown that the repulsive interactions between the chain and wall increase with the decreasing gap H_0. Thus, the chain tends to stay away from the wall for small H_0. Figure 5.3 shows the configurations of the chain under different levels of confinement.

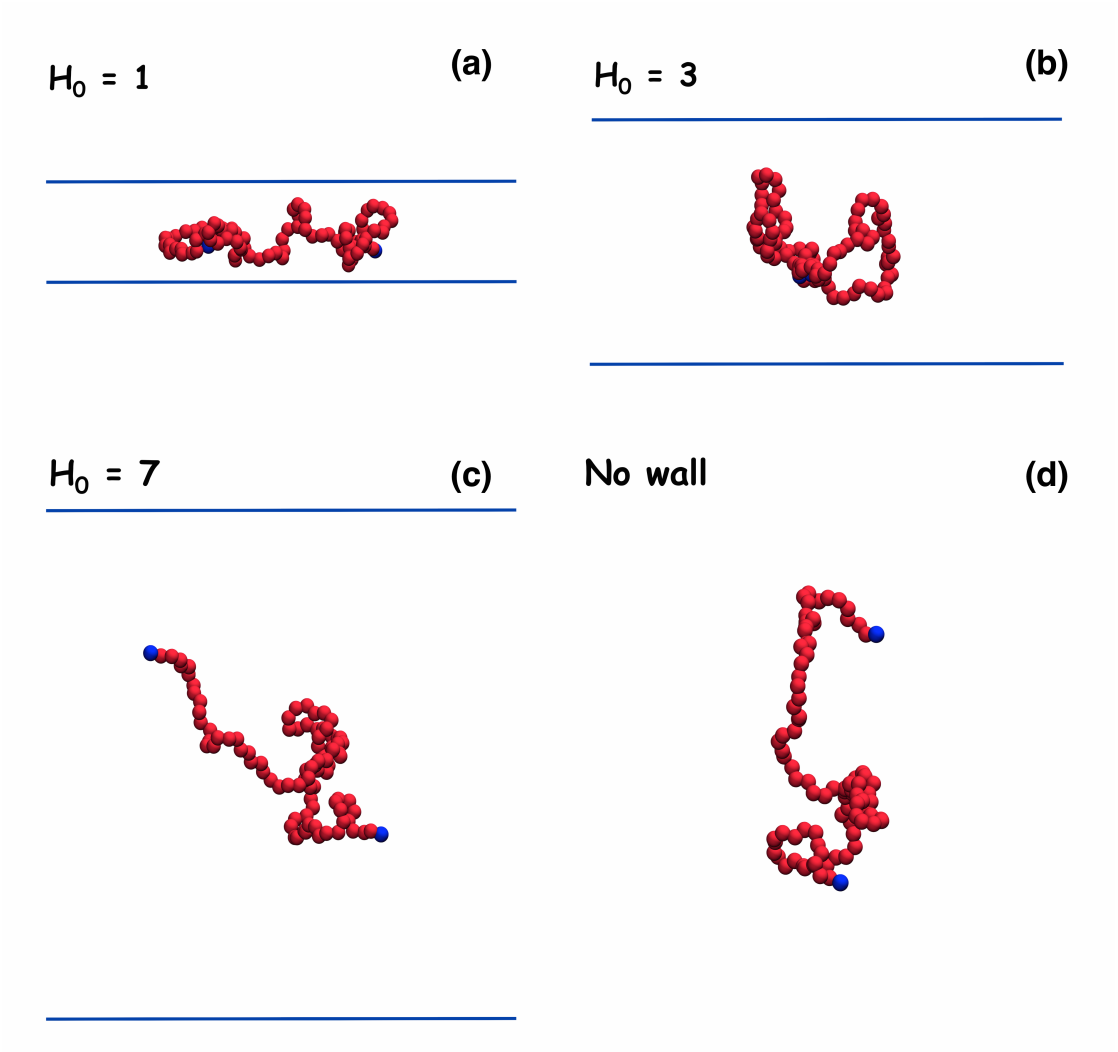

Figure 5.2: Configurations of PEO chain under different degree of confinement: (a) at a strong confinement, polymer motion on z-direction is restricted, thus extends on x and y direction; (b) moderate confinement, polymer is slightly compressed on z direction; (c) weak confinement, no significant influence is shown on the configuration; (d) no confinement

In an unconfined system, the chain behaves as a random coil and can move itself in any spatial direction through self-avoiding random walk. In confined systems, when $H_0 \gg 1$, the configurations of the chain are largely unchanged because the polymer-wall interactions are close to zero. When H_0 decreases, repulsive interactions between the wall and the chain increases, hence the chain is slightly compressed in the z -direction. When H_0 is close to one, the chain is highly constrained in the z-direction, due to the excluded volume effect, hence the chain will expand in the x or y direction[41, 47, 137].

Figure 5.4 shows the relation between the normalized radius of gyration $R_{gN} \equiv R_g/R_{g0}$ and H_0. R_{gN} does not change appreciably for $H_0 > 2$, and exhibits a power law relationship with H_0 for $H_0 < 2$. The inlet shows a plot log (R_{gN}) vs. log (H_0) in this power law range.

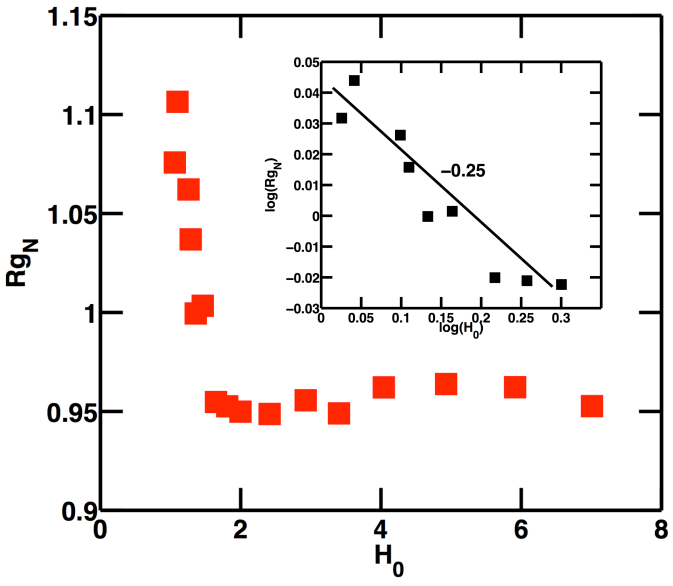

Figure 5.3: Normalized radius of gyration R_{gN} vs. H_0. No significant increment is shown when $H_0 > 2$. At $H_0 < 2$, R_{gN} and H_0 follows a power law relationship. The inlet shows log (R_{gN}) vs. log (H_0) at $H_0 < 2$

Daoud and de Gennes[40] predict that when $H_0 < 1$, the scaling coefficient is -¼. Our result corresponds to this theoretical prediction, but H_0 at which the chain starts to expand is larger. This could be attributed to the differences in polymer-wall interaction potentials: theoretical excluded volume potential used has a sharp cut off whereas the LJ potential used in the present simulations decreases smoothly to zero.

5.3.3 Dynamics of confining polymer chain under uniform steady shear

Uniform steady shear is performed by applying velocity deformation on the two walls and Weissenberg number Wi, defined in Eq. (2-5), is used to characterize the shear rate. Since interactions between the wall and the flow are included, it is worthwhile to examine the velocity profile of the system. Figure 5.5 shows the velocity profile of a confinement system with $H = 15nm$ ($H_0 = 6$) of MARTINI water[63] under shear. A clear straight line indicates a constant velocity gradient, which shows that the simulation is able to predict steady shear under confinement without slip.

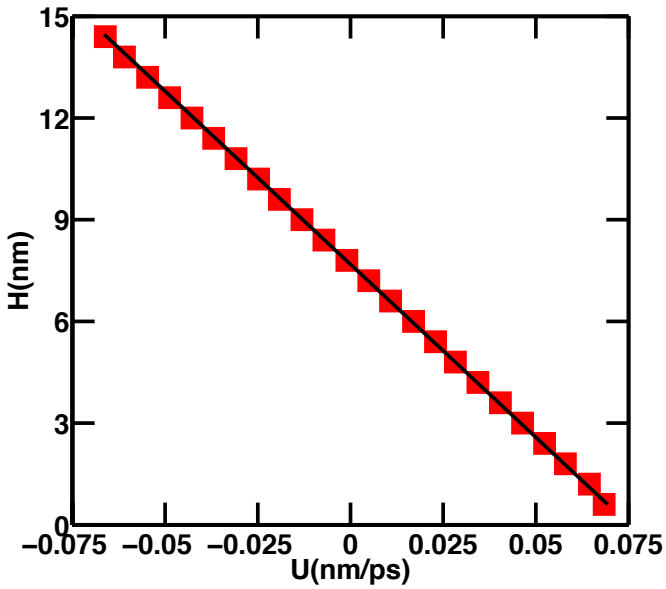

Figure 5.4: Velocity profile of a confinement system of MARTINI CG water at $\boldsymbol{H = 15nm}$

We first examine the polymer migration under shear. Figure 5.6 shows the concentration profile on z - direction of the polymer chain under different degrees of confinement.

In weak confinement, e.g., $H_0 = 6$, the chain tends to stay in the centerline, and the tendency increases with the increasing Wi, however, at very high Wi, the chain tends to stay in the vicinity of the wall. In moderate confinement, e.g., $H_0 = 4$, the chain clearly migrates towards the wall as the shear rate is increased. However, with increasing strength of the confinement, i.e., decreasing of H_0, the tendency of migrating towards wall decreases. Finally, in strong confinement, e.g., $H_0 = 1$, the chain stays in the centerline, and Wi has no influence on the concentration profile of the chain. Moreover, we observe from the simulations that, in all cases, the chain migrates towards the wall at some point during the simulation time, but it may

migrate back to the flow or stay close to the wall, hence the overall time-averaged concentration profile depends on the time the chain spends in these two states.

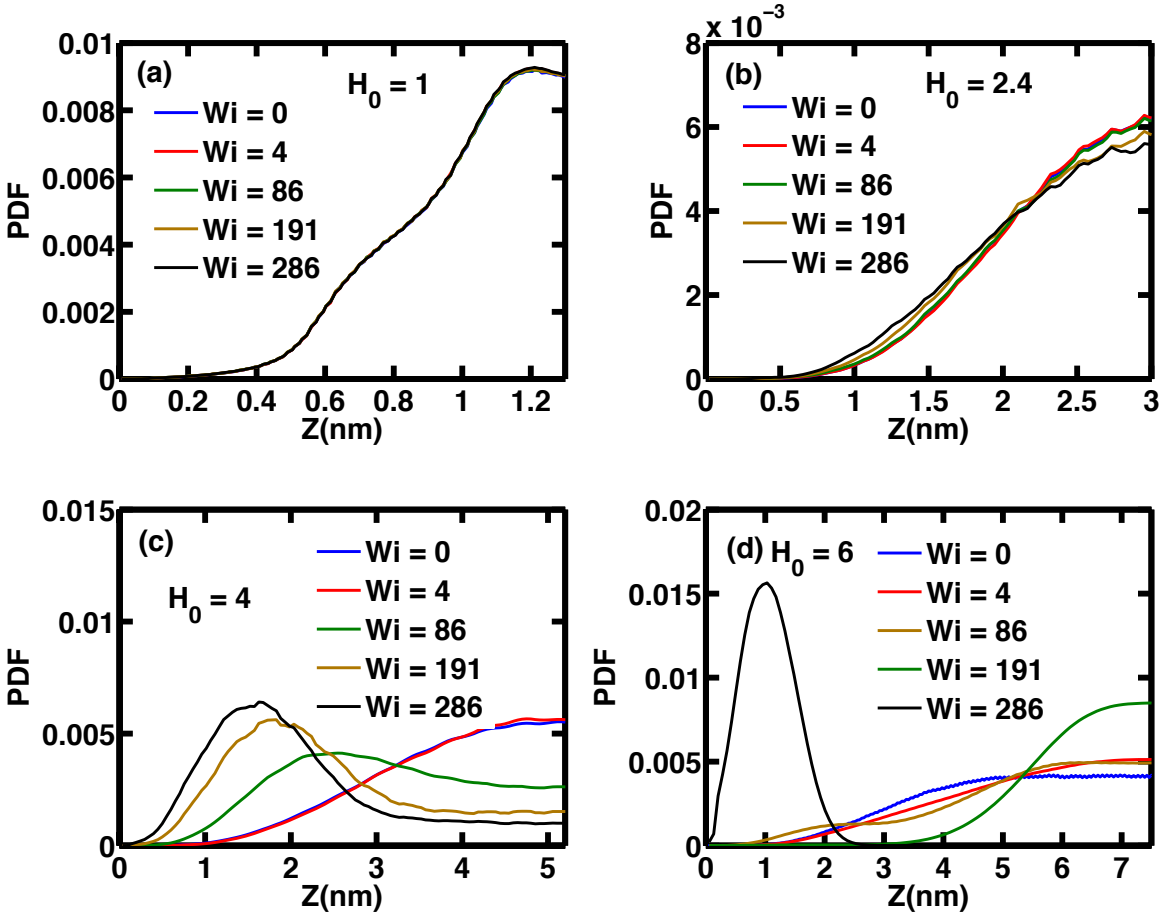

Figure 5.5: Concentration profiles, i.e., the probability distribution function (PDF) of finding a bead at certain z coordinate: (a) $H_0 = 1$, a strong confinement case, where the chain's motion is restricted on z-direction and stays at the centerline; (b) $H_0 = 2.4$, a moderate confinement case, the chain starts to show slightly tendency of migrating towards wall; (c) $H_0 = 4$, the chain shows strong tendency of migrating towards wall at high shear; (d) $H_0 = 6$, a weak confinement example, migration towards center is observed at moderate confinement. At very high confinement, migration towards wall is observed.

Under strong confinement, the movement on z-direction is constrained due to the repulsion between the chain and the wall, hence the concentration profiles at different Wi are identical.

Usta *et al*.[47] have used LBM simulations and predicted that when $H_0 > 5$, the polymer chain migrates towards centerline in uniform steady shear. They have also mentioned that when $H_0 < 5$, the chain migrates towards wall, but they failed to provide a convincing explanation on that. de Pablo *et al*.[144] have predicted that moderately confined chains at very high shear may migrate towards the wall. They suggested that hydrodynamic interactions on the polymer chain from the two walls cancel out, and the chain is slightly compacted in the wall-normal direction, hence allowing it to be closer to the wall.

On the other hand, Fang *et al.*[43, 44] have observed that when place λ-stage DNA near a glass surface in torsion shear flow, the thickness of depletion layer increases with increasing Wi, i.e., the chain migrates away from the wall. Kohale and Khare[145] have also predicted using MD that at weak confinement in a nano-channel, the chain would migrate towards centerline due to lubrication forces.

Under moderate and weak confinement, the polymer is not affected by the wall when it is close to the centerline, and is subject to stretching-tumbling-coiling cycles. The larger the Wi, the higher the tumbling frequency, thus the higher the probability that the chain is not aligned to the flow. Figure 5.7 shows two possible scenarios. In either case, each bead in the chain experiences different velocities, which can be decomposed to one part that leads the chain to align to the flow and the other part that gives the chain a downward momentum. Thus, the chain moves towards area with larger velocity, or towards the wall. In experimental studies where polymer is observed to migrate away from wall, velocity is larger in the centerline then in the vicinity of the wall where the polymer was initially placed. For example, in the experiments by

Fang, *et al.*[43, 44], the upper plate was rotated by a motor while the lower plate was a replaceable glass coverslip. λ-DNA particles was initially settled to the bottom surface. They found that the thickness of the depletion layer increases with increasing Wi. Thus, polymer migration to a region of high velocity is realizable.

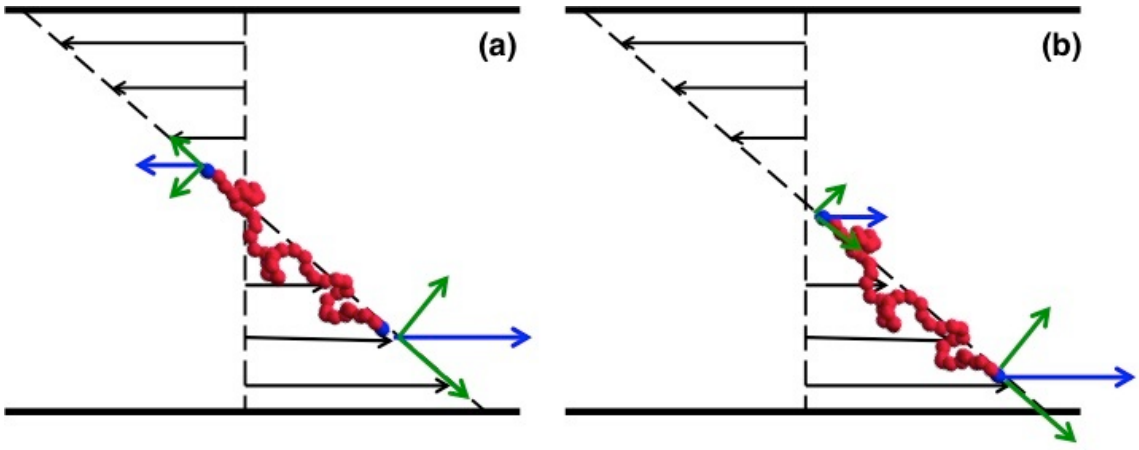

Figure 5.6: Two possible schematics of the chain in a confinement system under shear: (a) Two ends of the chain are advected in opposite directions; (b) Two ends of the chain are advected in the same direction.

In the vicinity of the wall, the chain still has wall-bound momentum yet the motion normal to the wall is restricted. On the other hand, hydrodynamic drag force gives the chain a momentum parallel to the flow. Hence, the chain collapses and forms more compacted configurations (Figure 5.8). This is consistent with the predictions of de Pablo *et al.*[144].

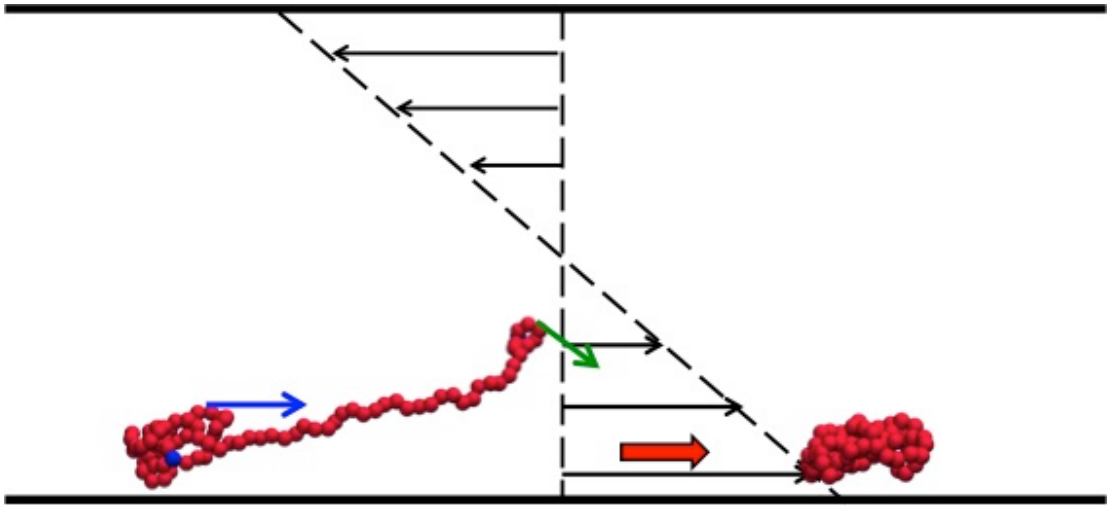

Figure 5.7: Schematic of the chain at the vicinity of the wall. The motion normal to the wall is restricted. Hydrodynamic drag force gives the chain a momentum parallel to the flow, thus the chain rotates and forms a compact globule.

Since the chain is subjected to both the hydrodynamic drag force as well as the repulsion from the wall, the chain is then "pushed" back to the flow, together with the hydrodynamic force that rotates the chain, the chain migrates back to the flow (Figure 5.9). This corresponds to the theoretical and simulation predictions mentioned above. It is noticeable that in Fang *et al.*[43, 44]'s experiments, they place the DNA chain on the vicinity of lower plate while moving the upper plate, so the velocity profile is similar to the upper half of the one from our simulations. The chain moves away from the wall due to the repulsion from the wall and the hydrodynamic drag force that lead it to the larger velocity region.

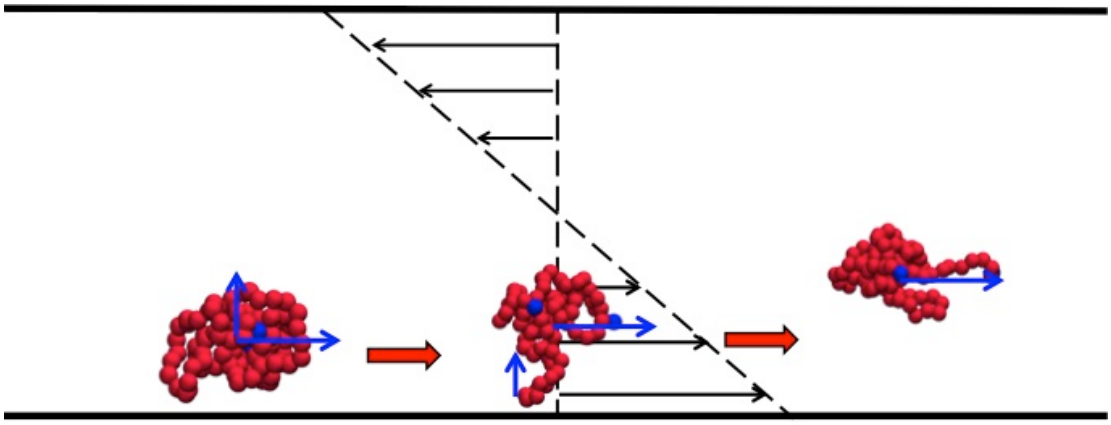

Figure 5.8: The chain is "pushed" back to the flow by the wall

At very high Wi, the chain is quickly stretched by the flow once it collapses at the vicinity of the wall, and it is entropically unfavorable for the chain to move upward. The larger the Wi, the more frequently the chain is stretched, the higher the chance it stays close to the wall, hence the overall concentration profile moves towards the wall with increasing Wi. With the increasing strength of confinement, migration towards the wall is restrained due to the repulsion from the wall, i.e., the chain is "pushed" back by the wall once it deviates from the centerline, so migration towards the wall decreases with decreasing H_0.

Figure 5.10 shows the instantaneous end-to-end distance Q and z coordinate of the center-of-mass of the chain at different Wi in a weakly confined system ($H_0 = 6, H = 15\,nm$). At $Wi = 206$, the chain tends to stay in the centerline with rather coiled configurations while at $Wi = 286$, the chain tends to stay close to the wall with more extended configurations. Dalal *et al.*[112] have used Brownian Dynamics simulations and predicted multiple regimes of polymer chain dynamics under steady shear. In the first regime, the tumbling frequency increases with the

increasing Wi, which corresponds to our simulations in Chapter 2. In the second regime, the chain tends to stay in the extended configuration and the tumbling frequency may decrease. This may explain why we have observed migration towards wall at very high Wi while migration towards the centerline in in weakly confined systems. At very high Wi, the chain tends to stay in extended configurations more often and migrates towards the wall more frequently. At moderate Wi, the probability of the chain staying in extended configurations is lower, and the distance from the centerline to the wall is relatively larger. Hence, an extended chain can tumble and coil before it reaches the wall.

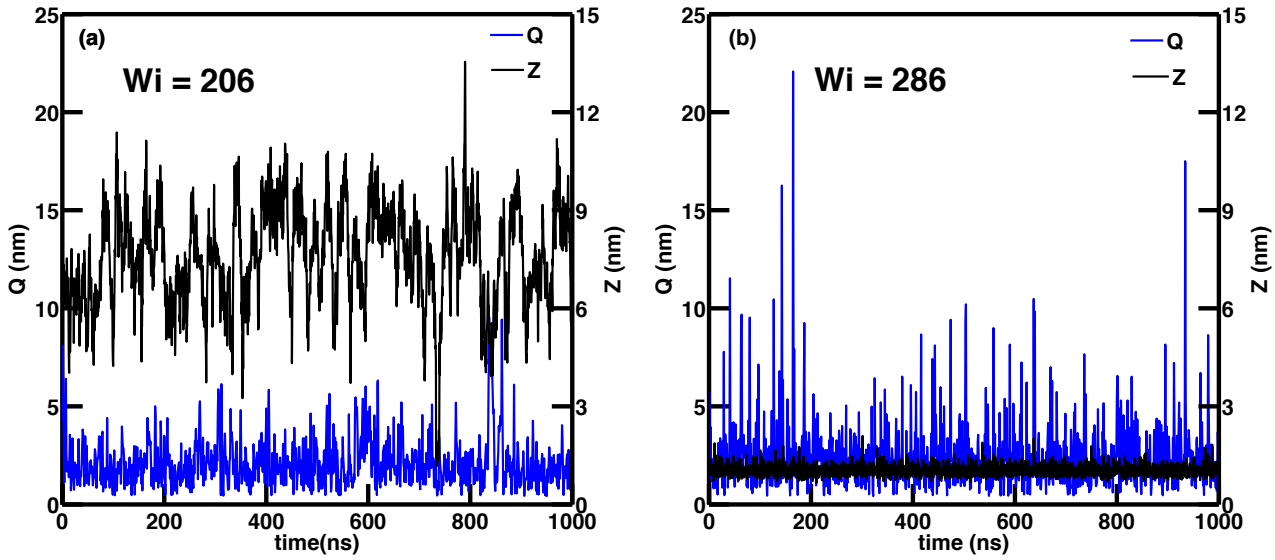

Figure 5.9: Instantaneous end-to-end distance Q and center-of-mass position on z-direction of the chain at $H_0 = 6$ ($H = 15nm$) at (a) $Wi = 206$ and (b) $Wi = 206$

5.4 Conclusion

In this chapter, we have examined influence of confinement on the configurations and dynamics of single polymer chain. The confinement is modeled by placing two walls normal to z-direction so that the PBC is only applied on x- and y- directions. The polymer-wall and solvent-wall interactions are represented using LJ potential with $\varepsilon_w = 0.001$ and $\sigma_w = 0.15$ in order to model a wall with no significant interaction with the flow. For $H_0 > 2$, no strong interaction between the wall and the polymer is observed. Thus the polymer size doesn't vary much in this regime. For $H_0 < 2$, there is slight repulsion between the wall and the polymer chain, the chain is constrained on the z-direction due to this repulsion. Combined with the excluded-volume effects within the chain, the chain expands on x- and y- directions and increase in size is observed. The size of the chain at strong confinement shows a power law relation with the confinement strength H_0. The power-law coefficient is -0.25, which corresponds to the theoretical prediction by Daoud and de Gennes[40].

We have also shown that our confinement system can accurately predict steady shear flow with no slip condition. Various of studies about the confinement influence on polymer dynamics have shown that single polymer chain migrates away from the wall in steady shear flow in weak confinement. We have observed from our simulations that the polymer chain migrates towards the wall and migrates back to the centerline at moderate and weak confinement. The chain not only extends but also tumbles and rotates in the flow, the higher the Wi, the higher chance the chain deviates from aligning to the flow. Hence the chain is subjected to imbalanced force in different parts and moves towards larger velocity, i.e., towards the wall. At the vicinity of the wall, the chain still has downward momentum, but the wall restricts the chain from moving downward, thus the chain collapses and forms a more compacted structure. The chain extends

and coils again due to the hydrodynamic force close to the wall. The repulsion between the wall and the polymer may push the chain back to the flow if the chain is in a more compacted configuration. If the chain is in a stretched configuration, it is entropically unfavorable, thus it is harder for a stretched the chain to migrates away from the wall. This implies that the higher Wi, the higher tendency the chain stays close to the wall. In weak confinement, the chain rotates, tumbles and migrates back to the flow before it reaches to the wall, the higher the Wi, the higher tumbling frequency, thus the higher chance it stays in the centerline of the flow. However, at very large Wi, tumbling frequency decreases and the chain has higher probability to stay in the extended configuration, thus it is prone to move towards the wall and stays close to the wall.

Chapter 6

Summary and future work

6.1 Introduction

Polymers are widely used in industrial and consumer products. Key to exploring their many useful properties is to understand the processes in which they are shaped. Polymer dynamics, which is complicated due to the hydrodynamic, entropic and stochastic forces experienced by the chains, have been shown to have profound influence on the macroscopic rheological properties of polymeric fluids. Recently, the emergence of nanofluidic devices[146, 147], has allowed the study of polymer dynamics at the single-molecule level: large molecules such as genomic double-stranded DNA can be stained with fluorescent dyes, so it can be directly observed under a microscope. However, not all polymers are large molecules. Most of the time, it is harder to conduct experiments on dilute polymer solutions and study the dynamics.

Recently, the advances in distributed computing and development of efficient algorithms have allowed for the use of multiscale models to predict flow behaviors of polymeric fluids. Continuum-level models can provide semi-quantitative predictions of the steady state in several different flows and can be used to obtain qualitative predictions of the critical conditions at which flow instabilities occur in prototypical curvilinear shear flows. Typical models that use to model shear thinning fluids include Giesekus, Phan-Thien and Tanner, and White-Metzner. While continuum-level models focus on the description of the macroscopic viscoelastic stress, they do not attempt to capture the details of the configurational dynamics. Brownian Dynamics

Simulations (BDS) are stochastic simulations that use detailed micromechanical models such as bead-rod, bead-spring or dumbbell models. These models have neglected the atomistic description that incorporates the chemical structure of the monomers and their spatial connectivity in terms of bond lengths and angles. Depending on the degree of coarse graining, a bead in these models represents a collection of atoms. These models have been shown to be informative in studying dynamics of polymer chain: by choosing different models, one can increase the internal degrees of freedom and explore the configurational dynamics in greater detail, or decrease the internal degrees of freedom and focus on the flow behaviors of the liquids. However, such models still have drawbacks. Most BDS represents solvents implicitly, i.e., solvent exists only through assumed potential of mean-force. This limits the application of using BDS to study the dynamics of polymers under different solvent conditions. Dissipative particle dynamics (DPD) is another kind of mesoscopic simulation method in which one simulates the motion of coarse-grained entities of mass, referred to as particles, subject to dissipative, random and conservative forces. DPD allows explicit solvent representations and have made great progress in studying the solvent quality influence on polymer dynamics. However, it is hard to calibrate DPD parameters, which lead to uncertainties in predicting molecular and rheological properties. On the other hand, all-atom simulations, give detailed atomistic descriptions on chemical structures of the monomer. While they have been widely used in studying the structure of proteins, such detailed representations are infeasible and unnecessary as far as configurational and rheological predictions for polymer systems are concerned.

In this thesis, we have selected a typical linear flexible polymer chain, and developed a coarse-grained molecular dynamics (CGMD) polymer model that can predict the structure, dynamic and rheology of polymeric liquids. We have shown that our model can explicitly

represent chemical, electrostatic or hydrophilic/hydrophobic interactions that are present the system. The results presenting in this thesis have shown that our CGMD model takes into account the hydrodynamic interactions (HI) and excluded-volume effects that are important in polymer solutions. The model can quantitatively predict the tumbling dynamics of single polymer chain as well as the shear thinning and normal stress of dilute and semidilute solution under steady shear flow. The explicit solvent-polymer interactions have allowed us to study the solvent quality influence on the dynamics and rheology of polymer liquids. Moreover, we have shown that our CGMD can predict the configurations and dynamics of single polymer chain under confinement without excessive computational complexity. The details will be discussed in the following sections.

6.2 Coarse-grained molecular dynamics (CGMD)

CGMD neglects detailed chemical structure inside each monomer, removes ultrahigh frequency motions inside molecules while preserving essential features inside the model. The first CGMD approach shows that typical chemical systems can be represented using hard-core repulsion. Typical CGMD techniques range from solvent-free models to explicit solvent representations. Marrink *et al.* [63] developed the MARTINI force field, which can be applied to a broad range of systems without reparameterize the model each time. The model uses a four-to-one mapping, i.e., on average four heavy molecules are aggregated to one interaction site. The non-bonded interactions are represented by Lennard-Jones potential while bonded interactions are represented by harmonic potentials. While MARTINI force field has a variety of applications ranging from lipid bilayers to carbohydrates, its application on polymers is very rare.

In this chapter, configuration dynamics and rheology of solutions of linear flexible polymers have been studied using coarse-grained molecular dynamics (CGMD) in presence of explicit solvent-polymer interactions. Equilibrium properties in solution such as radius of gyration, relaxation time and persistent length area accurately predicted by the simulations. The dynamics of a single polymer chain has been studied by using non-equilibrium molecular dynamics (NEMD). The simulations are capable of accurately predicting stretch-tumbling cycles of a single polymer chain subjected to steady uniform shear flow. Different configurations, i.e., extended, half-dumbbell, dumbbell, kinked, folded and coiled configurations, of a polymer chain have been observed in the simulations. Tumbling frequency has been found to increase and follow a power law relation with the increasing Weissenberg number. . The power law exponent has been found to approach 0.67 with the increasing chain length, which corresponds to experimental observations and predictions of stochastic dynamics theory/simulations. We have also analyzed the orientation distribution of the end-to-end vector, which is characterized by the orientation angle θ, defined as the angle between the projection of the end-to-end vector onto the flow-gradient plane and the flow direction. The mean orientation angle has been discovered to be slightly biased to positive θ values and the probability distribution function (PDF) of θ could be approximated by a shifted Gaussian for $Wi > 1$. Full width at half maximum (FWHM) of PDF of θ follows a power law relation with Wi, and the coefficient approaches to -1/3 with the increasing chain length, which is in good agreement with mesoscopic theories. Dihedral potential is shown to have no significant influence on the equilibrium properties and single chain dynamics of dilute PEO solution. This is because the persistent length is less than the length scale where dihedral potential affects the chain configuration. The dynamics of single, flexible

polymer chain is shown to be important to understand various macroscopic rheological phenomena.

In Chapter 2, we applied MARTINI force field and built linear flexible polymer chain model. We have validated the model against theoretical predictions and experimental observations. We have shown that with sufficiently long chain length, our model can faithfully predict the equilibrium behaviors of polymer chain as well as tumbling dynamics of the chain under steady shear flow.

6.3 Solvent quality influence on properties and dynamics of single polymer chain

Solvent quality has been shown to have great impact on equilibrium properties and dynamics in non-equilibrium conditions of single polymer chain. Previous studies have provided intuitive models on explaining the globule-coil transition of single polymer chain, however, these models do not show how solvent quality affects such transition. On the dynamics part, while a large variety of studies have been focused on the configuration dynamics of single polymer chain in theta solvent (explained in Chapter 2), few literature has discussed how solvent quality may affect dynamics. While advanced simulation techniques have allowed us to express solvent explicitly, most simulation methods (e.g., dissipative particle dynamics) require complicated parameterization and can only represent a particular system. Thus, developing a model that can be applied to study solvent quality influence without reparameterizing the model each time becomes critical.

In Chapter 3, we investigate the solvent quality influence on the dynamics of single polymer chain. We applied MARTINI force field, which uses Lennard-Jones (LJ) potential for all non-

bonded interactions, to build polymer-solvent system. The potential well of the LJ potential between polymer and solvent, ε_{ps}, is selected as the solvent quality tuning parameter. The polymer model is parameterized to mimic properties of PEO as described in Chapter 2. ε_{ps} is tuned to mimic the equilibrium properties (e.g., radius of gyration R_g, longest relaxation time τ_R) of single PEO chain in different solvent. The models are validated against Flory prediction of polymer size in different solvent systems. In Flory theory, besides the scaling exponent equaling 0.588 in good solvent as discussed in Chapter 2, in theta solvent and poor solvent, the scaling exponents are 0.5 and 0.33, respectively. Linear regression from our simulation data has shown the scaling exponent equals 0.58, 0.5 and 0.33 in good, theta and poor solvent, respectively. Thus, current parameterization can predict PEO's behavior in different solvent systems. Zimm model predicts that when hydrodynamic interaction (HI) is included, the polymer size scales with number of monomers N as $N^{3\nu}$, with ν the exponent predicted in Flory theory for the relations between polymer size and N. Our simulation has shown that the scaling exponents are 1.78, 1.51 and 1.01 in good, theta and poor solvent, which corresponds to Zimm model prediction and shows that our model includes HI.

We then discuss the solvent quality influence on the polymer size, characterized by R_g, and τ_R. We have shown that both R_g and τ_R remains constant when $\varepsilon_{ps} < \varepsilon_{pp}$, and gradually increases when $\varepsilon_{ps} > \varepsilon_{pp}$. This indicates that when the intra-chain interaction is larger than polymer solvent interaction ($\varepsilon_{ps} < \varepsilon_{pp}$), monomers adhere to each other due to the strong attraction, the size of the polymer may not vary much. When polymer-solvent interactions increase, the solvent molecules start to "pull" the chain, and chain relaxes and unknots to a loose blob. When ε_{ps} is close to theta-condition, the chain expands rapidly due to the attractions from

solvent molecules, and chain becomes a random coil. Moreover, linear regression between τ_R and ε_{ps} equals triple of the one between R_g and ε_{ps}, this may also indicate HI is considered.

When polymer chain is under steady shear, the hydrodynamic force stretches the chain while solvent fluctuations perturb the chain and make it tumble and coil, as discussed in Chapter 2. In theta solvent, when $Wi > 1$, the chain starts to stretch. In poor solvent, the chain acts as a dense globule, and the net attraction among polymer beads makes it harder for the hydrodynamic force to deform the chain. We have shown that the onset Wi at which the chain starts to stretch, Wi_0, follows a negative linear relationship with ε_{ps}, i.e., the better the solvent quality, the smaller the Wi_0, until it reaches 1, where the chain starts to stretch at theta solvent.

The configuration dynamics becomes more complicated when the chain is in poor solvent. At $Wi < Wi_0$, the chain cannot fully extend, but it is still subjected to rotational component of the shear flow thus rotates in the flow. At $Wi > Wi_0$, the chain may stretch, tumble, coil and stretch again, as discussed in Chapter 2. On the other hand, due to the repulsion between the polymer and the solvent, the chain may not tumble but collapse and coil directly from the stretched configuration. At very high Wi, the chain tends to align to the flow, thus the chance of collapsing directly from a stretched state gets higher. Based on the observation from the simulation, in addition to the tumbling mechanism, we have proposed a second mechanism, the collapse mechanism, where the polymer collapses to a globule without tumbling in a poor solvent. The higher the Wi, the higher chance we observe collapse mechanism. We have also plotted the probability distribution function (PDF) of the orientation angle of the chain. When polymer is in a poor solvent, we have discovered two peaks in PDF, one at the positive value and the other one close to zero. The one at positive value indicates the tumbling dynamics of the chain due to the chain rotation while the other one corresponds to the collapse dynamics. With

the increasing Wi, the peak at the positive value vanishes, indicating that collapse event dominates at high Wi. In the last part of Chapter 3, we calculate the tumbling frequency and shows that tumbling frequency follows a power law relationship with Wi at different solvent conditions, the exponent of which converges to the one predicted for the theta solvent.

In Chapter 3, we used the potential well ε_{ps} as the solvent quality tuning parameter and modeled PEO in different solvent systems. We validated the model against Flory theory and Zimm model prediction for the equilibrium properties of polymer chain. We have shown that the solvent quality affects the polymer size as well as the longest relaxation time of the polymer chain. In a steady shear flow, the Wi at which the chain starts to stretch follows a negative linear relationship with ε_{ps} until it converges one at theta solvent. We have also proposed a collapse mechanism where polymer collapses and forms a globule without tumbling when it is in a poor solvent. We have also shown that the tumbling frequency follows a power-law relation with Wi with the exponent converges to the one predicted for theta solvent.

6.4 Multi-chain system

The properties and dynamics of multi-chain system have a wide range of applications ranging from transporting biological cells to drag reduction in fluid flows. Theoretical and experimental studies have been focusing on how quantities change in the flow, e.g., based on the change of shear viscosity, determine if the polymer fluid performs shear thinning or shear thickening behavior. Continuum level simulations have allowed the predictions of rheological properties such as shear viscosity and normal stress become possible, however, they fail to predict the conformation changes of polymer chain under flows. Stochastic dynamics such as Brownian dynamics simulations (BDS) represents polymers using micromechanical models such

as bead-rod or bead-spring. Yet most of BDS represents solvent implicitly, making it harder to study the solvent quality influence on the rheological behaviors of polymer solution. Dissipative particle dynamics (DPD) allows explicit solvent representations, however, they require complicated parameterization thus can only represent a particular system.

In Chapter 4 we adapted MARTINI force field and built multi-chain systems for PEO in different solvent systems. We first study the concentration influence on the zero shear viscosity of PEO. We chose the parameters described in the previous two chapters and built systems of PEO in theta solvent. Critical concentration c^* is the one at which polymer chains start to interact with each other. For concentration C less than c^*, each polymer chain acts like random coil, the solution is defined as dilute solution. For $C > c^*$, chain starts to interact with each other, the solution at this regime is called semidilute solution. We calculated the zero shear viscosity η_0 using Green-Kubo relation and show that in dilute regime, a linear relationship can be discovered between η_0 and c, which is the normalized concentration defined as $c = C/c^*$. In semidilute regime, a power law relationship can be observed with power law exponent equals 1.94. These results correspond to the Zimm model prediction in dilute regime where hydrodynamic interactions are important and Rouse model prediction in semidilute regime.

When the polymer is in different solvent systems, different solvent-polymer interactions affect the conformations of the chain, as discussed in Chapter 3. In multi-chain system, such conformation differences affect the zero-shear viscosity of the solution. In poor solvents, due to the repulsion between solvent and chains, chains may aggregate together, thus phase separation is observed. In a good solvent, chains swell due to the attraction with the solvents, thus lead to a larger pervaded volume. Linear relationships between the zero-shear viscosity η_0 and normalized concentration c have been observed in dilute regime and power law relationships in semidilute

regime for all three conditions. In the dilute regime, linear regressions of all three conditions converge. In theta and good solvent, Zimm model applies. In poor solvent, for length scale larger than the aggregated clusters, HI is still important thus Zimm model is still applicable. In semidilute regime, the power law exponent decreases with improving solvent quality. de Gennes[32, 115] predicts that in good solvent, the scaling exponent is $1/(3\upsilon - 1)$ with $\upsilon = 0.588$. The prediction from our simulation leads to the exponent equals 1.50, which is slightly overpredicted from this theoretical value. However, experiments on DNA has shown that the exponent ranges from 1.50 to 1.90 depending on the solvent quality, thus we conclude our prediction is still in the reasonable range. In poor solvent, the aggregation of the chains lead to the increment of η_0 faster than that in theta and good solvents, which corresponds to experimental observations.

The dynamics of polymer chains under shear flow and corresponding rheological behaviors have a wide range of applications. PEO has been shown to perform shear thinning behaviors in steady shear flow. As mentioned above, few studies have been focused on using simulations to predict rheological behaviors of polymer solution. We have shown that our CG model can correctly predict the shear thinning and normal stress of PEO under steady shear. We also parameterized the simulation data to power-law model and Carreau - Yasuda model. In power-law model, we have shown that with the increasing concentration, shear thinning behavior becomes more profound. The power-law exponent is shown to increase in magnitude with increasing concentration. While power-law model allows us to approximate the behavior of the fluid at high shear rates, Carreau - Yasuda model takes into account η_0 and η_∞, the viscosity at infinite shear rate. Parameterization to Carreau - Yasuda model also shows a increasing in

magnitude of the coefficient n with the concentration c. The predictions of both models are shown to be consistent with theoretical and experimental observations.

As discussed in Chapter 3, when subjected to poor solvent, the chain will not extend until reaches to the onset Wi, Wi_0. This behavior is also observed in multi-chain systems: the Newtonian plateau is wider in a poor solvent then that in theta and good solvent. Moreover, the exponents of power-law regime in converge in different solvent systems. This implies that the shear thinning behavior is more related to the degree of extension of the chain rather than the solvent quality. We have also shown that our CG model can predict the normal stresses of polymer solutions in different solvent conditions. Both first and second normal stress coefficients are shown to decay faster in poor solvent that those in theta and good solvent.

In Chapter 4, we applied MARTINI force and built multi-chain systems of PEO solution. We have shown that in different solvent systems, zero shear viscosity follows a linear relationship with concentration in dilute regime and power law relations in semidilute regime. Linear regression of η_0 and c converge in all three different solvent conditions. In semidilute regime, power law exponent increases when the solvent quality gets poorer. When applied non-equilibrium molecular dynamics, our CGMD model is shown to be able to correctly predict shear thinning and normal stress in different solvent systems. Parameterizations to power-law model and Carreau-Yasuda are shown in good agreement with experimental data.

6.5 Single polymer under confined geometry

The dynamics and configurations of polymer fluids in confined geometries have been in great interest in industry. Such applications range from polymer processing to the development of novel microfluidic devices. For decades, various studies have been performed on this topic.

Equilibrium properties have been shown to be affected by the confinement. When subject to shear flow, various discoveries have been found. For example, polymer chain may migrate away from single wall at high shear[39]. When confined in a nano - channel, polymer chain migrates towards centerline at weak confinement and towards wall at strong confinement[47]. While all these studies are intuitive, due to the diversified behaviors of the polymer under shear and difficulties in observing the chain configurations, few studies have shown the migration mechanism of the chain under confinement.

Explained in the previous several chapters, coarse-grained molecular dynamics (CGMD) have been shown to preserve essential chemical and mechanical features without excessive computational complexity. In Chapter 5, we developed systems of single polymer chain under confinement using MARTINI force field. The confinement is modeled by confining the chain under two walls with a gap H normal to z-direction, which is defined as a slit-like confinement. Periodic boundary condition (PBC) is thus removed on z-direction so that the chain cannot move beyond the wall. Polymer-wall interaction is represented by Lennard-Jones (LJ) potential. In the current study, parameters are chosen in such a way to mimic a wall with almost no-wall interactions. The gap H is normalized by radius of gyration Rg_0 of the chain at no confinement condition, $H_0 = H/Rg_0$. We define a weak confinement if $H_0 > 4$, a strong confinement if $H_0 < 2$, and a moderate confinement if in between.

We first showed the average polymer-wall interaction V_{pw} under different degree of confinement. At weak confinement, V_{pw} is close to zero, indicating no polymer-wall interaction. V_{pw} starts to increase at moderate confinement and increase dramatically at strong confinement. This behavior is shown to affect the equilibrium size of polymer chain under confinement. At weak and moderate confinement, we have shown that no significant change has been found in

the size of the chain, characterized by the normalized radius of gyration, $Rg_N = Rg/Rg_0$. At strong confinement, Rg_N and H_0 has been shown to follow a power law relationship, with the power law coefficient equals -0.25, which is in good agreement with the theoretical prediction by Daoud and de Gennes[40].

The dynamics of a confined chain under shear has shown to be in great interest by both industry and academia. When polymer-wall and solvent-wall interaction is added to the simulation, it is necessary to reexamine the velocity profile of the system in a steady shear. We have shown that our system can accurately simulate a confined system in steady shear flow without slip.

From the simulation, we have observed that at strong confinement, i.e., $H_0 < 2$, no migration has been observed. The motion of the chain on z-direction is restricted, the chain stays in the centerline. Wi has no influence on the position of the chain. At moderate confinement, the chain shows migrating towards wall with increasing Wi. With the increasing degree of confinement, this tendency of migration towards wall decreases. This is understandable in that the motion of the chain on z-direction is increasingly constrained with the increasing degree of confinement. At weak confinement, migration towards centerline with increasing Wi is observed at moderate confinement. At very high confinement, migration towards wall is observed.

Based on the observations from our simulation, we then discussed the migration mechanism of the confined chain under shear. We believe the chain tends to migrate towards larger velocity regime in weak and moderate confinement, as long as the chain's motion on z-direction is not constrained. Since the chain tumbles and rotates in steady shear flow when $Wi > 1$ (see Chapter 2 and Chapter 3 for detail), when the chain is in a configuration that is normal to the wall, it has a momentum towards larger velocity regime. The larger the Wi, the higher the tumbling frequency

(see Chapter 2), thus the higher chance it is subjected to the momentum that drives it towards the larger velocity regime, i.e., towards wall. It is noticeable that in those experimental studies where polymer is observed to migrate away from wall, velocity is larger in the centerline then in the vicinity of the wall where the polymer was initially placed (e.g., experiments by Fang, *et al*.[43, 44]). Thus, we believe our result corresponds to experimental observations.

At the vicinity of the wall, the chain is subjected to both downward momentum and hydrodynamic drag force. Hence the chain rotates and forms a globule. Then the chain is "pushed" back by the wall due to weak repulsion generated when close to the wall, the chain migrates towards centerline.

At very high Wi, the velocity is extremely large at the vicinity of the wall. The chain is quickly stretched by the flow close to the wall. A stretched configuration is entropically unfavorable for the chain to move upward. Thus at high Wi, there is higher chance to find the chain close to the wall, i.e., it is harder for the chain to move back to the flow. This also explains the reason that at very high Wi, migration towards the wall is observed.

However, we have also observed that the chain tends to stay in the centerline in weak confinement. We believe that the chain tumbles and coils and thus rotates back to the flow before it reaches to the wall. The higher the Wi, the higher the tumbling frequency, thus the higher chance the chain migrates back to the flow. Previous studies (e.g., work by Kohale and Khare[145]) use concentration profile to characterize the positions of the chain. They discover that on average the chain tends to stay in the centerline. We believe that our simulations correspond to their discoveries.

In Chapter 5, we applied MARTINI force field and built a slit-like confined system of single PEO chain in theta solvent. We have shown that equilibrium configuration of the chain is

affected by the confinement. When subjected to steady shear flow, we have shown that polymer chain migrates towards large velocity regime. We have also proposed migration mechanisms of the chain under different degree of confinement.

6.6 Recommendations for future work

In this thesis, we have built a coarse-grained molecular dynamics (CGMD) polymer model and studied the structures, dynamics and rheology of polymer solution. We have shown that the model is capable of including hydrodynamic interactions, excluded volume effects and other physico-chemical interactions. The CGMD model is able to represent solvent-polymer interactions, solvent-wall interactions explicitly without requiring reparameterization each time. Nevertheless, there are still lots of unsolved problem need further investigation.

First, we have discussed the solvent quality influence on the equilibrium properties of single polymer chain. While we have shown that linear relationships between polymer size, longest relaxation time and solvent quality tuning parameter, further theoretical study is needed to explain the meaning of the coefficient. We have discussed the globule-stretch transition of single polymer chain subjected to steady shear in poor solvents and proposed a collapse mechanism in addition to the tumbling mechanism. Future studies can be made on quantify the collapse mechanism, e.g., determine a parameter to characterize how often collapse mechanism occurs in the flow (e.g., collapse frequency). Moreover, discussion can be made on the relation between flow characteristics, e.g., Wi and the collapse mechanism parameter. We have also shown that with the increasing Wi, collapse event starts to dominate. Ratio between collapse frequency versus tumbling frequency can be calculated and relation between flow characteristics and this ratio should be discussed. Further, solvent quality has been shown to affect coil-stretch

transition of polymer chain in elongational flow[96, 148]. Developing models on studying the solvent quality influence of chain dynamics in the elongational flow should also be considered.

Second, we have demonstrated that our CGMD model is able to predict rheological behaviors of polymer solution in dilute and semidilute regime. Further studies should be made on using CGMD to predict behaviors of polymers in concentrated solution. For shorter chain, entanglement may not be observed. However, for longer chains, polymers form constraints and networks, defined as entanglement, in concentrated solution and polymer melts. These constraints and networks limit the lateral motion of the chain. The confined region by neighboring polymer chains gives the polymer chain a tube-like region, and the polymer slides along this contour region through random walk. This motion is called by De Gennes reptation and was later developed into the tube model[149]. However, there are still certain discrepancies between the theoretical predictions and experiment results. For example, the tube model predicts a power law relation between molecular weight and zero-shear-rate viscosity with the exponent 3 for molecular weight higher than a critical one, while experimentally the exponent is 3.4[150]. Moreover, zero shear viscosity is predicted in theory to scales with concentration c as $c^{14/3}$ in the entanglement regime. Further, Figure 6.1 shows classification of polymer solutions in terms of concentration and molecular weight. It will be intuitive to use CGMD and provide rheological studies on polymers with different chain length.

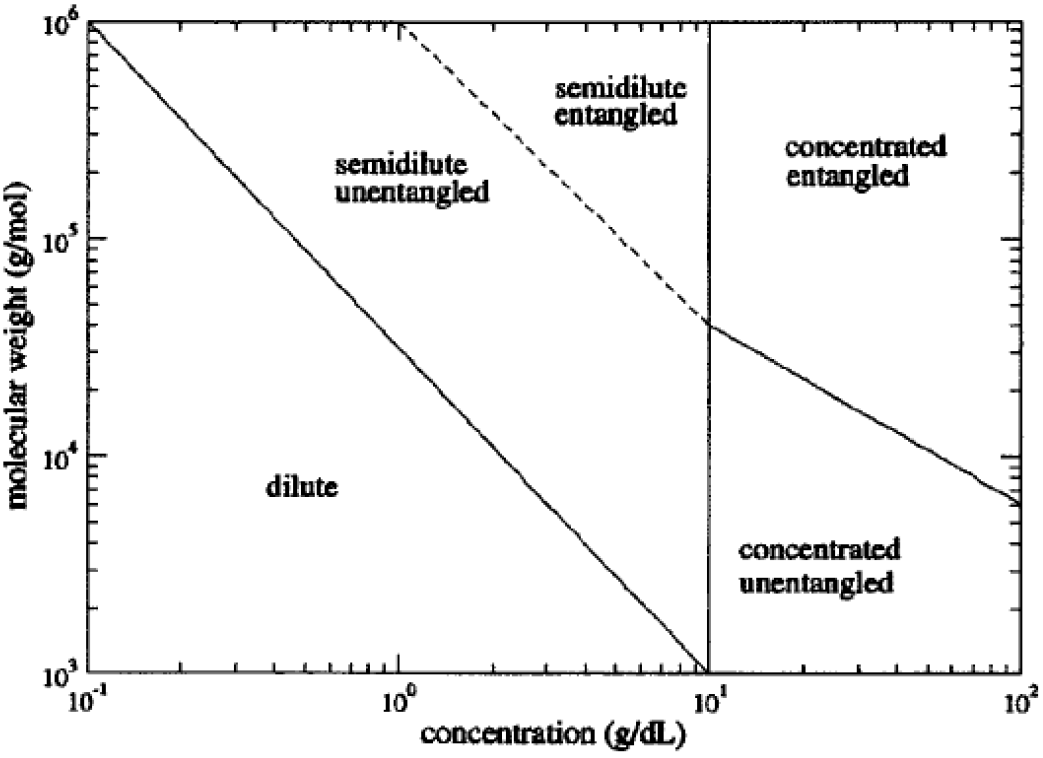

Figure 6.1: Classification of polymer solutions in terms of concentration and molecular weight[151].

Third, we have discussed solvent quality influence on rheological properties of polymer solutions. While we have provided quantitative details on solvent quality influence on the zero shear viscosity. Similar analysis should be conducted on the solvent quality influence on shear viscosity, first and second normal stress coefficients.

Fourth, we have shown that our CGMD model is capable of modeling polymer systems under confined geometry. We have discussed the influence of degree of confinement on equilibrium size of the polymer chain. It would be informative to also study the influence of confinement on other equilibrium properties such as relaxation time. The dynamics of confined

polymer chain under steady shear is fascinating. We have proposed a mechanism on the migration of the polymer chain under shear flow. However, theoretical investigation to support such mechanism is required. Moreover, as we have shown that in weak confinement, migration towards wall only occurs at the highest Wi, one question needed to be answered is that if there exists a critical $H_0 = H/Rg_0$ that separates the polymer's tendency to stay in the centerline and migrating towards wall. Lots of studies have been focusing on dynamics of single polymer chain in pressure-driven flow[34, 45, 46]. Applying CGMD and studying the behaviors of polymer chain in pressure-driven flow will also be informative. Rheological properties of polymer solutions are important in solving various problems in polymer processing. Thus, we would also recommend studies on how rheological properties of polymer solutions would change if the system is in confined geometry.

Last but not least, in this study, we choose polyethylene oxide (PEO) due to their wide range of applications ranging from drug delivery[152, 153] to protein crystallization[154, 155]. To fully develop the advantage of CGMD, similar studies on different polymers (e.g., branched polymers) should also be provided. In particular, it is shown that for linear flexible chains like PEO, contributions of dihedral angle potential is limited. However, for other polymers, such as semi-flexible polymers or ring-like polymers, the influence of dihedral angle potential may be significant. Thus, such studies should be provided.

REFERENCES

1. Smith, D. E.; Babcock, H. P.*, et al.*, Single-polymer dynamics in steady shear flow. *Science* **1999,** *283* (5408), 1724-1727.

2. Huang, C.-C.; Sutmann, G.*, et al.*, Tumbling of polymers in semidilute solution under shear flow. *EPL (Europhysics Letters)* **2011,** *93* (5), 54004.

3. Keffer, D.; Kim, J.*, et al.*, Dynamics of individual molecules of linear polyethylene liquids under shear: Atomistic simulation and comparison with a free-draining bead-rod chain. *Journal of Rheology* **2010,** *54* (2), 283-310.

4. Schroeder, C. M.; Teixeira, R. E.*, et al.*, Characteristic periodic motion of polymers in shear flow. *Physical review letters* **2005,** *95* (1), 018301.

5. Koopmans, R. J.; Molenaar, J., The "sharkskin effect" in polymer extrusion. *Polymer Engineering & Science* **1998,** *38* (1), 101-107.

6. Allal, A.; Lavernhe, A.*, et al.*, Relationships between molecular structure and sharkskin defect for linear polymers. *J Non-Newton Fluid* **2006,** *134* (1-3), 127-135.

7. Dimitropoulos, C. D.; Sureshkumar, R.*, et al.*, Direct numerical simulation of viscoelastic turbulent channel flow exhibiting drag reduction: effect of the variation of rheological parameters. *J Non-Newton Fluid* **1998,** *79* (2), 433-468.

8. Sureshkumar, R.; Beris, A. N.*, et al.*, Non-axisymmetric subcritical bifurcations in viscoelastic Taylor-Couette flow. *Proceedings of the Royal Society of London. Series A: Mathematical and Physical Sciences* **1994,** *447* (1929), 135-153.

9. Li, J. M.; Burghardt, W. R.*, et al.*, Flow birefringence and computational studies of a shear thinning polymer solution in axisymmetric stagnation flow. *J. Non-Newon. Fluid.* **1998,** *74* (1-3), 151-193.

10. Giesekus, H., A Simple Constitutive Equation for Polymer Fluids Based on the Concept of Deformation-Dependent Tensorial Mobility. *J Non-Newton Fluid* **1982,** *11* (1-2), 69-109.

11. Phan‐Thien, N., A nonlinear network viscoelastic model. *Journal of Rheology (1978-present)* **1978,** *22* (3), 259-283.

12. Tanner, R. I., *Engineering rheology*. Oxford University Press: 2000.

13. Xue, S. C.; Phanthien, N.*, et al.*, Numerical Study of Secondary Flows of Viscoelastic Fluid in Straight Pipes by an Implicit Finite-Volume Method. *J Non-Newton Fluid* **1995,** *59* (2-3), 191-213.

14. Joseph, D. D., *Fluid dynamics of viscoelastic liquids*. Springer-Verlag: New York, 1990; p xvii, 755 p.

15. Purnode, B.; Crochet, M. J., Polymer solution characterization with the FENE-P model. *J. Non-Newton Fluid.* **1998,** *77* (1-2), 1-20.

16. Sureshkumar, R.; Beris, A. N.*, et al.*, Direct numerical simulation of the turbulent channel flow of a polymer solution. *Phys. Fluids* **1997,** *9* (3), 743-755.

17. Doyle, P. S.; Shaqfeh, E. S. G.*, et al.*, Dynamic simulation of freely draining flexible polymers in steady linear flows. *J Fluid Mech* **1997,** *334*, 251-291.

18. Remmelgas, J.; Singh, P.*, et al.*, Computational studies of nonlinear elastic dumbbell models of Boger fluids in a cross-slot flow. *J Non-Newton Fluid* **1999,** *88* (1), 31-61.

19. Doyle, P. S.; Shaqfeh, E. S. G., Dynamic simulation of freely-draining, flexible bead-rod chains: Start-up of extensional and shear flow. *J Non-Newton Fluid* **1998,** *76* (1-3), 43-78.

20. Doyle, P. S.; Shaqfeh, E. S. G., Dynamic simulation of freely-draining, flexible bead-rod chains: Start-up of extensional and shear flow (vol 76, pg 43, 1998). *J Non-Newton Fluid* **2000,** *92* (2-3), 275-278.

21. Zwanzig, R., Theoretical basis for the Rouse‐Zimm model in polymer solution dynamics. *The Journal of Chemical Physics* **1974,** *60* (7), 2717-2720.

22. Fetsko, S. W.; Cummings, P. T., Brownian dynamics simulation of bead–spring chain models for dilute polymer solutions in elongational flow. *Journal of Rheology (1978-present)* **1995,** *39* (2), 285-299.

23. Larson, R.; Hu, H.*, et al.*, Brownian dynamics simulations of a DNA molecule in an extensional flow field. *Journal of Rheology* **1999,** *43*, 267.

24. Kroy, K.; Frey, E., Force-extension relation and plateau modulus for wormlike chains. *Physical review letters* **1996,** *77* (2), 306.

25. Cifre, J. G. H.; Barenbrug, T. M. A. O. M.*, et al.*, Brownian dynamics simulation of reversible polymer networks under shear using a non-interacting dumbbell model. *J Non-Newton Fluid* **2003,** *113* (2-3), 73-96.

26. Ottinger, H. C.; vandenBrule, B. H. A. A.*, et al.*, Brownian configuration fields and variance reduced CONNFFESSIT. *J Non-Newton Fluid* **1997,** *70* (3), 255-261.

27. Koppol, A. P.; Sureshkumar, R.*, et al.*, Anomalous pressure drop behaviour of mixed kinematics flows of viscoelastic polymer solutions: a multiscale simulation approach. *J Fluid Mech* **2009,** *631*, 231-253.

28. Hoogerbrugge, P. J.; Koelman, J. M. V. A., Simulating Microscopic Hydrodynamic Phenomena with Dissipative Particle Dynamics. *Europhys Lett* **1992,** *19* (3), 155-160.

29. Schlijper, A. G.; Hoogerbrugge, P. J.*, et al.*, Computer-Simulation of Dilute Polymer-Solutions with the Dissipative Particle Dynamics Method. *J Rheol* **1995,** *39* (3), 567-579.

30. Warren, P. B., Dissipative particle dynamics. *Curr Opin Colloid In* **1998,** *3* (6), 620-624.

31. Kong, Y.; Manke, C. W.*, et al.*, Effect of solvent quality on the conformation and relaxation of polymers via dissipative particle dynamics. *The Journal of chemical physics* **1997,** *107* (2), 592-602.

32. Rubinstein, M.; Colby, R., *Polymers Physics*. Oxford: 2003.

33. Hsieh, C. C.; Li, L.*, et al.*, Modeling hydrodynamic interaction in Brownian dynamics: simulations of extensional flows of dilute solutions of DNA and polystyrene. *J. Non-Newton Fluid.* **2003,** *113* (2-3), 147-191.

34. Jendrejack, R. M.; de Pablo, J. J.*, et al.*, Stochastic simulations of DNA in flow: Dynamics and the effects of hydrodynamic interactions. *J Chem Phys* **2002,** *116* (17), 7752-7759.

35. Kroger, M.; Alba-Perez, A.*, et al.*, Variance reduced Brownian simulation of a bead-spring chain under steady shear flow considering hydrodynamic interaction effects. *J Chem Phys* **2000,** *113* (11), 4767-4773.

36. Ermak, D. L.; Mccammon, J. A., Brownian Dynamics with Hydrodynamic Interactions. *J Chem Phys* **1978,** *69* (4), 1352-1360.

37. Prager, S.; Rotne, J., Variational Treatment of Hydrodynamic Interaction in Polymers. *B Am Phys Soc* **1968,** *13* (3), 370-&.

38. Rotne, J.; Prager, S., Variational Treatment of Hydrodynamic Interaction in Polymers. *J Chem Phys* **1969,** *50* (11), 4831-&.

39. Agarwal, U. S.; Dutta, A.*, et al.*, Migration of Macromolecules under Flow - the Physical Origin and Engineering Implications. *Chem Eng Sci* **1994,** *49* (11), 1693-1717.

40. Daoud, M.; De Gennes, P. G., Statistics of macromolecular solutions trapped in small pores. *Journal de Physique* **1977,** *38* (1), 85-93.

41. Teraoka, I., Polymer solutions in confining geometries. *Progress in polymer science* **1996,** *21* (1), 89-149.

42. Park, J.; Bricker, J. M.*, et al.*, Cross-stream migration in dilute solutions of rigid polymers undergoing rectilinear flow near a wall. *Phys Rev E* **2007,** *76* (4).

43. Fang, L.; Hsieh, C. C.*, et al.*, Molecular imaging of shear-induced polymer migration in dilute solutions near a surface. *Macromolecules* **2007,** *40* (23), 8490-8499.

44. Fang, L.; Hu, H.*, et al.*, DNA configurations and concentration in shearing flow near a glass surface in a microchannel. *J Rheol* **2005,** *49* (1), 127-138.

45. Seo, Y. H.; Park, O. O.*, et al.*, The behavior of velocity enhancement in microcapillary flows of flexible water-soluble polymers. *Journal of chemical engineering of Japan* **1996,** *29* (4), 611-619.

46. Jendrejack, R. M.; Schwartz, D. C.*, et al.*, Shear-induced migration in flowing polymer solutions: Simulation of long-chain DNA in microchannels. *The Journal of chemical physics* **2004,** *120* (5), 2513-2529.

47. Usta, O. B.; Butler, J. E.*, et al.*, Flow-induced migration of polymers in dilute solution. *Phys Fluids* **2006,** *18* (3).

48. Woo, N. J.; Shaqfeh, E. S. G.*, et al.*, Effect of confinement on dynamics and rheology of dilute DNA solutions. I. Entropic spring force under confinement and a numerical algorithm. *J Rheol* **2004,** *48* (2), 281-298.

49. Mackerell, A. D.; Banavali, N. K., All‐atom empirical force field for nucleic acids: II. Application to molecular dynamics simulations of DNA and RNA in solution. *J. Comput. Chem.* **2000,** *21* (2), 105-120.

50. MacKerell, A. D.; Bashford, D.*, et al.*, All-atom empirical potential for molecular modeling and dynamics studies of proteins. *J. Phys. Chem. B* **1998,** *102* (18), 3586-3616.

51. Weiner, S. J.; Kollman, P. A.*, et al.*, An All Atom Force-Field for Simulations of Proteins and Nucleic-Acids. *J. Comput. Chem.* **1986,** *7* (2), 230-252.

52. Smit, B.; Hilbers, P. A. J.*, et al.*, Computer-Simulations of a Water Oil Interface in the Presence of Micelles. *Nature* **1990,** *348* (6302), 624-625.

53. Goetz, R.; Lipowsky, R., Computer simulations of bilayer membranes: self-assembly and interfacial tension. *The Journal of chemical physics* **1998,** *108* (17), 7397-7409.

54. Lopez, C. F.; Moore, P. B.*, et al.*, Computer simulation studies of biomembranes using a coarse grain model. *Comput Phys Commun* **2002,** *147* (1-2), 1-6.

55. Marrink, S. J.; Lindahl, E.*, et al.*, Simulation of the spontaneous aggregation of phospholipids into bilayers. *Journal of the American Chemical Society* **2001,** *123* (35), 8638-8639.

56. Shelley, J. C.; Shelley, M. Y.*, et al.*, A coarse grain model for phospholipid simulations. *J Phys Chem B* **2001,** *105* (19), 4464-4470.

57. Brannigan, G.; Brown, F. L. H., Solvent-free simulations of fluid membrane bilayers. *J Chem Phys* **2004,** *120* (2), 1059-1071.

58. Farago, O., "Water-free" computer model for fluid bilayer membranes. *J Chem Phys* **2003,** *119* (1), 596-605.

59. Muller, M.; Katsov, K.*, et al.*, A new mechanism of model membrane fusion determined from Monte Carlo simulation. *Biophys J* **2003,** *85* (3), 1611-1623.

60. den Otter, W. K.; Briels, W. J., The bending rigidity of an amphiphilic bilayer from equilibrium and nonequilibrium molecular dynamics. *J Chem Phys* **2003,** *118* (10), 4712-4720.

61. Frink, L. J. D.; Frischknecht, A. L., Density functional theory approach for coarse-grained lipid bilayers. *Phys Rev E* **2005,** *72* (4).

62. Stevens, M. J., Coarse-grained simulations of lipid bilayers. *J Chem Phys* **2004,** *121* (23), 11942-11948.

63. Marrink, S. J.; Risselada, H. J.*, et al.*, The MARTINI force field: coarse grained model for biomolecular simulations. *J. Phys. Chem B* **2007,** *111* (27), 7812-7824.

64. Faller, R.; Marrink, S. J., Simulation of domain formation in DLPC-DSPC mixed bilayers. *Langmuir* **2004,** *20* (18), 7686-7693.

65. Monticelli, L.; Kandasamy, S. K.*, et al.*, The MARTINI coarse-grained force field: Extension to proteins. *J. Chem. Theory Comput.* **2008,** *4* (5), 819-834.

66. Lopez, C. A.; Rzepiela, A. J.*, et al.*, Martini Coarse-Grained Force Field: Extension to Carbohydrates. *J. Chem. Theory Comput.* **2009,** *5* (12), 3195-3210.

67. Gautieri, A.; Russo, A.*, et al.*, Coarse-Grained Model of Collagen Molecules Using an Extended MARTINI Force Field. *J. Chem. Theory Comput.* **2010,** *6* (4), 1210-1218.

68. Sangwai, A. V.; Sureshkumar, R., Coarse-Grained Molecular Dynamics Simulations of the Sphere to Rod Transition in Surfactant Micelles. *Langmuir* **2011,** *27* (11), 6628-6638.

69. Sangwai, A. V.; Sureshkumar, R., Binary Interactions and Salt-Induced Coalescence of Spherical Micelles of Cationic Surfactants from Molecular Dynamics Simulations. *Langmuir* **2012,** *28* (2), 1127-1135.

70. Nangia, S.; Sureshkumar, R., Effects of Nanoparticle Charge and Shape Anisotropy on Translocation through Cell Membranes. *Langmuir* **2012,** *28* (51), 17666-17671.

71. DeSalvo, S. C.; Liu, Y.*, et al.* In *Probing Mechanisms of Bacterial Infection through Molecular Dynamics Simulations*, Bioengineering Conference (NEBEC), 2013 39th Annual Northeast, IEEE: 2013; pp 41-42.

72. Sambasivam, A.; Sangwai, A. V.*, et al.*, Dynamics and Scission of Rodlike Cationic Surfactant Micelles in Shear Flow. *Phys. Rev. Lett.* **2015,** *114* (15).

73. LeDuc, P.; Haber, C.*, et al.*, Dynamics of individual flexible polymers in a shear flow. *Nature* **1999,** *399* (6736), 564-566.

74. Schroeder, C. M.; Teixeira, R. E.*, et al.*, Characteristic periodic motion of polymers in shear flow. *Phys Rev Lett* **2005,** *95* (1), 018301.

75. Schroeder, C. M.; Teixeira, R. E.*, et al.*, Dynamics of DNA in the flow-gradient plane of steady shear flow: Observations and simulations. *Macromolecules* **2005,** *38* (5), 1967-1978.

76. Venkataramani, V.; Sureshkumar, R.*, et al.*, Coarse-grained modeling of macromolecular solutions using a configuration-based approach. *J Rheol* **2008,** *52* (5), 1143-1177.

77. Schroeder, C. M.; Teixeira, R. E.*, et al.*, Characteristic periodic motion of polymers in shear flow. *Phys. Rev. Lett.* **2005,** *95* (1).

78. Lee, H.; de Vries, A. H.*, et al.*, A coarse-grained model for polyethylene oxide and polyethylene glycol: conformation and hydrodynamics. *J. Chem. Phys. B* **2009,** *113* (40), 13186-13194.

79. Darre, L.; Machado, M. R.*, et al.*, Coarse-grained models of water. *Wires Comput Mol Sci* **2012,** *2* (6), 921-930.

80. Pronk, S.; Páll, S.*, et al.*, GROMACS 4.5: a high-throughput and highly parallel open source molecular simulation toolkit. *Bioinformatics* **2013,** *29* (7), 845-854.

81. Polverari, M.; van deVen, T. G. M., Dilute aqueous poly(ethylene oxide) solutions: Clusters and single molecules in thermodynamic equilibrium. *J. Phys. Chem.* **1996,** *100* (32), 13687-13695.

82. Flory, P. J., Thermodynamics of high polymer solutions. *The Journal of chemical physics* **1942,** *10* (1), 51-61.

83. Zimm, B. H., Dynamics of polymer molecules in dilute solution: viscoelasticity, flow birefringence and dielectric loss. *The journal of chemical physics* **1956,** *24* (2), 269-278.

84. Hezaveh, S.; Samanta, S.*, et al.*, Molecular dynamics simulation study of solvent effects on conformation and dynamics of polyethylene oxide and polypropylene oxide chains in water and in common organic solvents. *J. Chem. Phys* **2012,** *136* (12), 124901.

85. Lee, H.; Venable, R. M.*, et al.*, Molecular dynamics studies of polyethylene oxide and polyethylene glycol: Hydrodynamic radius and shape anisotropy. *Biophys. J.* **2008,** *95* (4), 1590-1599.

86. Huang, C. C.; Sutmann, G.*, et al.*, Tumbling of polymers in semidilute solution under shear flow. *Europhys. Lett.* **2011,** *93* (5).

87. Kim, J. M.; Edwards, B. J.*, et al.*, Dynamics of individual molecules of linear polyethylene liquids under shear: Atomistic simulation and comparison with a free-draining bead-rod chain. *J. Rheol.* **2010,** *54* (2), 283-310.

88. Winkler, R. G., Semiflexible polymers in shear flow. *Phys. Rev. Lett.* **2006,** *97* (12), 128301.

89. Gerashchenko, S.; Steinberg, V., Statistics of tumbling of a single polymer molecule in shear flow. *Physical review letters* **2006,** *96* (3), 038304.

90. Jose, P. P.; Szamel, G., Single-chain dynamics in a semidilute polymer solution under steady shear. *J Chem Phys* **2008,** *128* (22).

91. De Gennes, P. G., Kinetics of collapse for a flexible coil. *Journal de Physique Lettres* **1985,** *46* (14), 639-642.

92. Dawson, K. A.; Gorelov, A. V.*, et al.*, Formation of mesoglobules from phase separation in dilute polymer solutions: a study in experiment, theory, and applications. *Physica A* **1997,** *244* (1-4), 68-80.

93. Kuznetsov, Y. A.; Timoshenko, E. G.*, et al.*, Kinetics at the Collapse Transition of Homopolymers and Random Copolymers. *J Chem Phys* **1995,** *103* (11), 4807-4818.

94. Timoshenko, E. G.; Kuznetsov, Y. A.*, et al.*, Kinetics at the Collapse Transition Gaussian Self-Consistent Approach. *J Chem Phys* **1995,** *102* (4), 1816-1823.

95. Birshtein, T. M.; Pryamitsyn, V. A., Coil Globule Type Transitions in Polymers .2. Theory of Coil Globule Transition in Linear Macromolecules. *Macromolecules* **1991,** *24* (7), 1554-1560.

96. Radhakrishnan, R.; Underhill, P. T., Impact of Solvent Quality on the Hysteresis in the Coil–Stretch Transition of Flexible Polymers in Good Solvents. *Macromolecules* **2012,** *46* (2), 548-554.

97. Somani, S.; Shaqfeh, E. S. G.*, et al.*, Effect of Solvent Quality on the Coil-Stretch Transition. *Macromolecules* **2010,** *43* (24), 10679-10691.

98. Lee, E. C.; Muller, S. J., Flow light scattering studies of polymer coil conformation in solutions under shear: effect of solvent quality. *Polymer* **1999,** *40* (10), 2501-2510.

99. Alexander-Katz, A.; Netz, R. R., Dynamics and instabilities of collapsed polymers in shear flow. *Macromolecules* **2008,** *41* (9), 3363-3374.

100. Pan, G.; Manke, C. W., Effects of solvent quality on the dynamics of polymer solutions simulated by dissipative particle dynamics. *J Rheol* **2002,** *46* (5), 1221-1237.

101. Schlijper, A. G.; Hoogerbrugge, P. J.*, et al.*, Computer simulation of dilute polymer solutions with the dissipative particle dynamics method. *Journal of Rheology (1978-present)* **1995,** *39* (3), 567-579.

102. Spenley, N. A., Scaling laws for polymers in dissipative particle dynamics. *Europhys Lett* **2000,** *49* (4), 534-540.

103. Opps, S. B.; Polson, J. M.*, et al.*, Discontinuous molecular dynamics simulation study of polymer collapse. *J Chem Phys* **2006,** *125* (19).

104. Darré, L.; Machado, M. R.*, et al.*, Coarse‐grained models of water. *WIREs Comput Mol Sci* **2012,** *2* (6), 921-930.

105. Tóthová, J.; Lisý, V., Relaxation Times of Flexible Polymer Chains in Solution from Non- Conventional Viscosity Measurements. *Open Macromolecules Journal* **2010,** *4* (1), 26-31.

106. Baysal, B. M.; Karasz, F. E., Coil‐Globule Collapse in Flexible Macromolecules. *Macromolecular theory and simulations* **2003,** *12* (9), 627-646.

107. Buguin, A.; BrochardWyart, F.*, et al.*, Collapse of a flexible coil in a poor solvent. *Comptes rendus de l academie des sciences serie ii fascicule b-mecanique physique chimie astronomie* **1996,** *322* (10), 741-746.

108. Kobayashi, H.; Yamamoto, R., Tumbling motion of a single chain in shear flow: A crossover from Brownian to non-Brownian behavior. *Phys Rev E* **2010,** *81* (4).

109. Nevins, D.; Spera, F. J., Accurate computation of shear viscosity from equilibrium molecular dynamics simulations. *Molecular Simulation* **2007,** *33* (15), 1261-1266.

110. Hoover, W. G.; Evans, D. J.*, et al.*, Lennard-Jones triple-point bulk and shear viscosities. Green-Kubo theory, Hamiltonian mechanics, and nonequilibrium molecular dynamics. *Physical Review A* **1980,** *22* (4), 1690.

111. Hida, T., *Brownian motion*. Springer: 1980.

112. Dalal, I. S.; Hoda, N.*, et al.*, Multiple regimes of deformation in shearing flow of isolated polymers. *J Rheol* **2012,** *56* (2), 305-332.

113. Usabiaga, F. B.; Delgado-Buscalioni, R., Characteristic Times of Polymer Tumbling Under Shear Flow. *Macromolecular Theory and Simulations* **2011,** *20* (7), 466-471.

114. Ellis, R. J.; Minton, A. P., Cell biology - Join the crowd. *Nature* **2003,** *425* (6953), 27-28.

115. Gennes, P.-G. d., *Scaling concepts in polymer physics*. Cornell University Press: Ithaca, N.Y., 1979; p 324 p.

116. Doi, M.; Edwards, S. F., *The theory of polymer dynamics*. Clarendon Press ;
Oxford University Press: Oxford Oxfordshire

New York, 1987; p xiii, 391 p.

117. Khokhlov, A. R., *Statistical physics of macromolecules*. Amer Inst of Physics: 1994.

118. Takahashi, Y.; Isono, Y.*, et al.*, Zero-Shear Viscosity of Linear Polymer-Solutions over a Wide-Range of Concentration. *Macromolecules* **1985,** *18* (5), 1002-1008.

119. Gandhi, K. S.; Williams, M. C., Solvent Effects on Viscosity of Moderately Concentrated Polymer Solutions. *J Polym Sci Pol Sym* **1971,** (35), 211-&.

120. Kulicke, W. M.; Kniewske, R., The Shear Viscosity Dependence on Concentration, Molecular-Weight, and Shear Rate of Polystyrene Solutions. *Rheol Acta* **1984,** *23* (1), 75-83.

121. Koopmans, R. J.; Molenaar, J., The "sharkskin effect" in polymer extrusion. *Polym. Eng. Sci.* **1998,** *38* (1), 101-107.

122. Bird, R. B., *Dynamics of polymeric liquids*. 2nd ed.; Wiley: New York, 1987.

123. Heo, Y.; Larson, R. G., The scaling of zero-shear viscosities of semidilute polymer solutions with concentration. *J. Rheol.* **2005,** *49* (5), 1117-1128.

124. Likhtman, A. E.; Sukumaran, S. K.*, et al.*, Linear viscoelasticity from molecular dynamics simulation of entangled polymers. *Macromolecules* **2007,** *40* (18), 6748-6757.

125. Baig, C.; Mavrantzas, V. G.*, et al.*, Flow Effects on Melt Structure and Entanglement Network of Linear Polymers: Results from a Nonequilibrium Molecular Dynamics Simulation Study of a Polyethylene Melt in Steady Shear. *Macromolecules* **2010,** *43* (16), 6886-6902.

126. Chen, T.; Smit, B.*, et al.*, Are pressure fluctuation-based equilibrium methods really worse than nonequilibrium methods for calculating viscosities? *J. Chem. Phys.* **2009,** *131* (24).

127. Ebagninin, K. W.; Benchabane, A.*, et al.*, Rheological characterization of poly(ethylene oxide) solutions of different molecular weights. *J. Colloid. Interf. Sci.* **2009,** *336* (1), 360-367.

128. Rubinstein, M.; Colby, R. H., *Polymer physics*. Oxford University Press: Oxford ; New York, 2003; p xi, 440 p.

129. Pan, S.; Nguyen, D. A.*, et al.*, Universal solvent quality crossover of the zero shear rate viscosity of semidilute DNA solutions. *J Rheol* **2014,** *58* (2), 339-368.

130. Jain, A.; Dunweg, B.*, et al.*, Dynamic Crossover Scaling in Polymer Solutions. *Phys Rev Lett* **2012,** *109* (8).

131. Cho, K. S.; Song, K. W.*, et al.*, Scaling relations in nonlinear viscoelastic behavior of aqueous PEO solutions under large amplitude oscillatory shear flow. *J. Rheol.* **2010,** *54* (1), 27-63.

132. Fredrickson, C. K.; Fan, Z. H., Macro-to-micro interfaces for microfluidic devices. *Lab on a Chip* **2004,** *4* (6), 526-533.

133. Odom, T. W.; Thalladi, V. R.*, et al.*, Generation of 30-50 nm structures using easily fabricated, composite PDMS masks. *Journal of the American Chemical Society* **2002,** *124* (41), 12112-12113.

134. Reisner, W.; Pedersen, J. N.*, et al.*, DNA confinement in nanochannels: physics and biological applications. *Reports on Progress in Physics* **2012,** *75* (10), 106601.

135. Kreuter, J.; Alyautdin, R. N.*, et al.*, Passage of peptides through the blood-brain barrier with colloidal polymer particles (nanoparticles). *Brain research* **1995,** *674* (1), 171-174.

136. Torchilin, V. P., Targeted pharmaceutical nanocarriers for cancer therapy and imaging. *The AAPS journal* **2007,** *9* (2), E128-E147.

137. Hsieh, C. C.; Doyle, P. S., Studying confined polymers using single-molecule DNA experiments. *Korea-Aust Rheol J* **2008,** *20* (3), 127-142.

138. Hernandez-Ortiz, J. P.; Ma, H. B.*, et al.*, Cross-stream-line migration in confined flowing polymer solutions: Theory and simulation. *Phys Fluids* **2006,** *18* (12).

139. Zheng, J.; Yeung, E. S., Anomalous radial migration of single DNA molecules in capillary electrophoresis. *Analytical chemistry* **2002,** *74* (17), 4536-4547.

140. Mavrantzas, V. G.; Beris, A. N., A hierarchical model for surface effects on chain conformation and rheology of polymer solutions. I. General formulation. *J Chem Phys* **1999,** *110* (1), 616-627.

141. Mavrantzas, V. G.; Beris, A. N., A hierarchical model for surface effects on chain conformation and rheology of polymer solutions. II. Application to a neutral surface. *J Chem Phys* **1999,** *110* (1), 628-638.

142. Ma, H.; Graham, M. D., Theory of shear-induced migration in dilute polymer solutions near solid boundaries. *Physics of Fluids (1994-present)* **2005,** *17* (8), 083103.

143. Graham, M. D., Fluid Dynamics of Dissolved Polymer Molecules in Confined Geometries. *Annu Rev Fluid Mech* **2011,** *43*, 273-298.

144. Depablo, J. J.; Ottinger, H. C.*, et al.*, Hydrodynamic Changes of the Depletion Layer of Dilute Polymer-Solutions near a Wall. *Aiche J* **1992,** *38* (2), 273-283.

145. Kohale, S. C.; Khare, R., Cross stream chain migration in nanofluidic channels: Effects of chain length, channel height, and chain concentration. *J Chem Phys* **2009,** *130* (10).

146. Dimalanta, E. T.; Lim, A.*, et al.*, A microfluidic system for large DNA molecule arrays. *Analytical Chemistry* **2004,** *76* (18), 5293-5301.

147. Jo, K.; Dhingra, D. M.*, et al.*, A single-molecule barcoding system using nanoslits for DNA analysis. *P Natl Acad Sci USA* **2007,** *104* (8), 2673-2678.

148. Somani, S.; Shaqfeh, E. S. G.*, et al.*, Effect of Solvent Quality on the Coil– Stretch Transition. *Macromolecules* **2010,** *43* (24), 10679-10691.

149. Larson, R. G., The structure and rheology of complex fluids. In *Topics in chemical engineering* [Online] Oxford University Press: New York, 1999.

150. Berry, G.; Fox, T., *The viscosity of polymers and their concentrated solutions*. Springer: 1968.

151. Graessley, W. W., Polymer chain dimensions and the dependence of viscoelastic properties on concentration, molecular weight and solvent power. *Polymer* **1980,** *21* (3), 258-262.

152. Imura, Y.; Nishida, M.*, et al.*, Action mechanism of PEGylated magainin 2 analogue peptide. *Bba-Biomembranes* **2007,** *1768* (10), 2578-2585.

153. Nishida, M.; Imura, Y.*, et al.*, Interaction of a magainin-PGLa hybrid peptide with membranes: Insight into the mechanism of synergism. *Biochemistry-Us* **2007,** *46* (49), 14284-14290.

154. Cudney, B.; Patel, S.*, et al.*, Screening and Optimization Strategies for Macromolecular Crystal-Growth. *Acta Crystallogr D* **1994,** *50*, 414-4123.

155. Mcpherson, A., Crystallization of Macromolecules - General-Principles. *Method Enzymol* **1985,** *114*, 112-120.

Curriculum Vitae

Yutian Yang

Education

Ph.D. in Chemical Engineering, Syracuse University, June 2015

B.S. in Applied Chemistry, Shanghai Jiao Tong University

Publication

Yutian Yang, Radhakrishna Sureshkumar, "Coarse-Grained Molecular Dynamics Simulations of Viscoelastic Polymer Solutions" (in preparation)

Yutian Yang, Radhakrishna Sureshkumar, "Effect of solvent quality on dynamics and rheology of dilute and semi-dilute polymer solutions" (in preparation)

Award and Honors

Syracuse University Graduate Fellowship	2013
Nunan Travel Grant	2014
Graduate Student Organization Travel Grant	2014

Professional Affiliation

American Institute of Chemical Engineers (AIChE)

Society of Rheology (SOR)